Université de Montréal

Préparation, étude de l'orientation et caractérisation physico-chimique de films polymères comportant des fluorophores

par
Amine Fourati

Département de chimie
Faculté des Arts et des Sciences

Thèse présentée à la Faculté des études supérieures et postdoctorales
en vue de l'obtention du grade de doctorat
en chimie

Décembre 2012

Université de Montréal
Faculté des études supérieures et postdoctorales

Cette thèse intitulée :

Préparation, étude de l'orientation et caractérisation physico-chimique de films polymères comportant des fluorophores

Présentée par :
Amine Fourati

a été évaluée par un jury composé des personnes suivantes :

Julian X. Zhu, président-rapporteur
C. Géraldine Bazuin, directeur de recherche
Robert E. Prud'homme, co-directeur
Michel Lafleur, membre du jury
Jean Duhamel, examinateur externe
et un représentant du doyen de la FAS

Résumé

Les propriétés intrinsèques, photophysiques, électrochimiques et cristallographiques des molécules fluorescentes 4,4'-bis(2-benzoxazolyle)stilbène (BBS) et 2,5-bis(5-*tert*-butyl-2-benzoxazolyle)thiophène (BBT) ont été étudiées en solution et dans les polymères semi-cristallins : poly(butylène succinate) (PBS) et polylactide (PLA). Les deux fluorophores sont caractérisés par de hauts rendements quantiques absolus de fluorescence. Toutefois, une désactivation de la fluorescence peut se produire par croisement intersystème vers l'état triplet pour le BBT, et par photoisomérisation *trans-cis* pour le BBS. La cinétique de ce dernier processus dépend de la concentration, résultant en un pur isomère *cis* photo-induit à faibles concentrations, qui est accompagné à des concentrations élevées par l'apparition d'un composé acide après photo-clivage suivi d'une oxydation.

Cette étude a révélé des changements spectroscopiques prononcés suite à l'augmentation de la concentration des fluorophores, en particulier à l'état solide, spécifiques à l'agrégation des molécules à l'état fondamental pour le BBT et à la formation d'excimères pour le BBS, permettant ainsi de corréler les propriétés fluorescentes avec les caractéristiques du monocristal pour chaque fluorophore. En outre, le passage d'une dispersion moléculaire à une séparation de phases dans le cas du BBS est accompagné d'un changement de couleur du bleu au vert, qui est sensible à la déformation, à la température et au temps, affectant les rendements quantiques absolus de fluorescence et fournissant une large opportunité à la création d'une grande variété de polymères intelligents indicateurs capables d'auto-évaluation. D'autre part, la solubilité élevée du BBT dans les solvants courants, combinée à ses propriétés optoélectroniques élevées, en font un candidat en tant que référence universelle de fluorescence et matériau intelligent à la fois pour les études de polymères et en solution.

Similairement aux mélanges comprenant des polymères miscibles, l'orientation du PBS augmente après ajout d'une molécule fluorescente, dont les monomères ont tendance à être orientés dans des films étirés, contrairement aux excimères ou agrégats.

Mots-clés : Fluorescence, Orientation, Matériaux indicateurs, Polyesters, Fluorophores, Caractérisation, Mécanisme de désactivation.

Abstract

The intrinsic, photophysical, electrochemical and crystallographic properties of the fluorescent molecules 4,4'-bis(2-benzoxazolyl)stilbene (BBS) and 2,5-bis(5-*tert*-butyl-2-benzoxazolyl)thiophene (BBT) have been investigated in solution as well as in semi-crystalline poly(butylene succinate) (PBS) and polylactide (PLA). Both fluorophores were found to be characterized by high fluorescence absolute quantum yields. However, fluorescence quenching was found to occur by intersystem crossing to the triplet state for BBT, and by *trans*-*cis* photoisomerization for BBS. The latter process was kinetically concentration-dependent, resulting in a pure photoinduced *cis*-isomer at low concentrations, which is accompanied at high concentrations by the appearance of an acidic compound after photocleavage followed by oxidation.

This study revealed pronounced spectroscopic changes upon an increase of the fluorophore concentration, especially in the solid-state, specific to aggregation of ground state molecules for BBT or excimer formation for BBS, thus correlating the fluorescent features with the single crystal characteristics for each fluorophore. Moreover, the transformation from molecular dispersion to phase separation, occurring for BBS, is accompanied by a significant colour change from blue to green, which is sensitive to deformation, time and temperature, thus affecting the absolute fluorescence quantum yields and providing a broad opportunity for the creation of a wide variety of smart polymers with self-assessing capabilities. On the other hand, the BBT's high solubility in common solvents combined with its measured enhanced optoelectronic properties make it a candidate as a universal fluorophore reference and smart material for both polymeric and solution studies.

Similarly to blends comprising miscible polymers, the PBS orientation was found to increase by adding a fluorescent molecule, whose monomers tend to be oriented in stretched films, contrary to excimers or aggregates.

Keywords: Fluorescence, Orientation, Indicating materials, Polyesters, Fluorophores, Characterization, Quenching mechanism.

Table des matières

Liste des tableaux

Liste des figures

Liste des abréviations

A_0	absorbance de l'échantillon non étiré
Å	angström
A	absorbance
A_p	absorbance polarisée parallèle
A_s	absorbance polarisée perpendiculaire
B_1, B_2	facteurs pré-exponentiels
BBA	4-(1,3-benzoxazol-2-yle)acid benzoïque
BBS	4,4'-bis(2-benzoxazolyle)stilbène
BBT	2,5-bis(5-*tert*-butyl-benzoxazol-2-yle)thiophène
BCMDB	1,4-bis(R-cyano-4-méthoxystyryl)-2,5-diméthoxybenzène
C	concentration molaire
CHD	1,3-cyclohexadiène
CI	conversion interne
CIF	"crystallographic information file" : acronyme anglais de format de fichier texte en cristallographie
CIS	croisement intersystème
ΔA	différence dichroïque
ΔE	écart énergétique
ΔH_m	enthalpie de fusion
ΔH_m^0	enthalpie de fusion d'un cristal parfait
D_{diff}	coefficient de diffusion
DFT	"density functional theory" : acronyme anglais de théorie de la fonctionnelle de la densité
DMF	diméthylformamide
DOSY	"diffusion ordered spectroscopy" : acronyme anglais de spectroscopie de diffusion ordonnée
DRX	diffraction des rayons X
DSC	"differential scanning calorimetry" : acronyme de calorimétrie différentielle à balayage
$\vec{E}$	vecteur électrique du rayonnement incident

EA	"electron affinity" : acronyme anglais d'affinité électronique
Éch	échantillon
E_g	"energy gap" : acronyme anglais d'écart énergétique
E_g^{el}	"electrochemical energy-gap" : acronyme anglais d'écart énergétique électrochimique
E_{pa}, E_{ox}	potentiel d'oxydation
E_{pc}, E_{red}	potentiel de réduction
$E_{//}$	émission polarisée parallèle
$E_{\perp}$	émission polarisée perpendiculaire
EtOH	éthanol
FDA	"US Food and Drug Administration" : acronyme anglais d'agence fédérale américaine des produits alimentaires et médicamenteux
fl	fluorescence
FQRNT	fonds québécois de la recherche sur la nature et les technologies
FRET	"Förster resonance energy transfer" : acronyme anglais de transfert d'énergie par résonance de type Förster
FT-IR	"Fourier transform infrared spectroscopy" : acronyme anglais de spectroscopie infrarouge à transformée de Fourier
HOMO	"highest occupied molecular orbital" : acronyme anglais d'orbitale moléculaire la plus haute occupée
I	intensité d'émission ou d'absorption de l'échantillon
I_0	intensité de la référence
I_2	intensité du $2^{ème}$ pic
I_3	intensité du $3^{ème}$ pic
IC	"internal conversion" : acronyme anglais de conversion interne
I_E	intensité de l'excimère
I_M	intensité du monomère
IP	"ionization potential" : acronyme de potentiel d'ionisation
IR	infrarouge
ISC	"intersystem crossing" : acronyme anglais de croisement intersystème

IUPAC	"International Union of Pure and Applied Chemistry" : acronyme anglais d'union internationale de chimie pure et appliquée
J_{HH}	constante de couplage
k_B	constant de Boltzmann
kcal	kilocalories
kN	kiloNewton
l	longueur du trajet optique
L	litre
L_f	longueur finale
LFP	"laser flash photolysis" : acronyme anglais de photolyse par impulsion laser
L_i	longueur initiale
LLDPE	polyéthylène linéaire à basse densité
LUMO	"lowest unoccupied molecular orbital" : acronyme anglais d'orbitale moléculaire la plus basse vacante
M	molécule à l'état fondamental
$\overrightarrow{M}$	moment de transition
M*	molécule à l'état excité
MeOH	méthanol
MM*	excimère
µM	micromolaire
mM	millimolaire
mol	mole
ms	milliseconde
N	indice de réfraction
Nd-YAG	"neodymium-doped yttrium aluminium garnet" : acronyme de l'anglais de grenat d'yttrium-aluminium dopé au néodyme
NMR	"nuclear magnetic resonance" : acronyme anglais de résonance magnétique nucléaire
NSERC	"Natural Sciences and Engineering Research Council of Canada" : acronyme anglais du Conseil de recherches en

	sciences naturelles et en génie du Canada
$<P_2>$, $<P_4>$	polynômes de Legendre
PBS	poly(1,4-butylène succinate)
PE	polyéthylène
PIL	photolyse par impulsion laser
PLA	polylactide
PM-IRSAS	"polarization modulation infrared structural absorbance spectroscopy" : acronyme de spectroscopie infrarouge avec modulation de la polarisation
ppm	partie par million
PPO	polyoxide de phénylène
PS	polystyrène
PVME	poly(vinyl méthyl éther)
r	"hydrodynamic radius" : acronyme anglais de rayon hydrodynamique
R	rapport dichroïque
Réf	actinomètre
RMN	résonance magnétique nucléaire
rpm	"revolutions per minute" : acronyme anglais de tours par minute
RT	"room temperature" : acronyme anglais de température ambiante
S_0	état fondamental
S_1	état excité singulet
S	"apparent order parameter" : acronyme anglais de paramètre d'ordre apparent
SCE	"saturated calomel electrode" : acronyme anglais d'électrode au calomel saturé
T_1	état triplet
T	température
TCE	1,1,2,2-tétrachloroéthane
T_g	température de transition vitreuse
THF	tétrahydrofuranne
TMS	tétraméthylsilane

TTI	"time-temperature indicator" : acronyme anglais d'indicateur temps-température
UV	ultraviolet
W	watt
wt	"weight" : acronyme anglais de poids
XRD	"X-ray diffraction" : acronyme anglais de diffraction des rayons X
α	angle entre le moment de transition et la chaîne principale
γ	rapport gyromagnétique
ε	coefficient d'extinction molaire
η	viscosité
λ	longueur d'onde ou taux d'étirement local
τ	temps de vie
$\langle\tau\rangle$	temps de vie moyen
Φ	rendement quantique
Φ_{CI}, Φ_{IC}	rendement quantique de conversion interne
Φ_{CIS}, Φ_{ISC}	rendement quantique de croisement intersystème
Φ_{fl}	rendement quantique de fluorescence
$\Phi_{fl,Éch}$	rendement quantique de fluorescence de l'échantillon
χ	taux de cristallinité

À ma mère, mon père et mon épouse.

À mon oncle, le défunt Tahar Fourati.
Que Dieu ait pitié de son âme.

Remerciements

Pour commencer, je tiens à remercier mes directeurs de thèse, les professeurs C. Géraldine Bazuin et Robert E. Prud'homme, qui m'ont énormément appris durant ces cinq années et encouragé à poursuivre mes projets tout en me poussant toujours vers l'originalité et en m'illuminant avec leurs observations aussi judicieuses qu'éclairées. Je leur suis également reconnaissant de m'avoir donné la liberté de tester les hypothèses que j'émettais, me permettant de développer mon autonomie et mon intérêt pour la recherche, et surtout pour la découverte. J'ai beaucoup apprécié la diversité, la qualité et l'originalité de leurs projets.

Un grand merci également aux collaborateurs, Pr. Will G. Skene et Pr. Christian Pellerin, pour leurs disponibilités, leurs conseils et pour m'avoir permis d'utiliser les instruments scientifiques de leurs laboratoires. Merci aussi au Pr. Karen Waldron pour avoir toujours cru en mes capacités intellectuelles et pédagogiques en m'offrant l'opportunité d'être à la fois auxiliaire d'enseignement et chargé de cours à maintes reprises.

Je souhaiterais également exprimer ma profonde gratitude à mon pays, la Tunisie, auquel je souhaite les plus beaux jours dans la démocratie post-révolution, pour l'octroi d'une bourse d'excellence, et à l'Université de Montréal pour la bourse FESP.

Merci au département de chimie en général, et à son personnel de soutien en particulier, pour m'avoir gentiment transmis leur savoir sur les différents instruments de recherche et pour les divers services d'analyses prodigués. Je cite Stéphane Dufresne, ancien étudiant en Ph.D. du groupe Skene, Dr. Thierry Maris pour la diffraction des rayons X, Sylvain Essiembre pour la calorimétrie différentielle à balayage, Dr. Cédric Malveau pour la spectroscopie de résonance magnétique nucléaire, Patricia Moraille pour la microscopie à force atomique, Dr. Sepehr Ravati du centre de recherche sur les polymères

et les composites et Dr. Gaétan Caron pour sa bonne humeur et les discussions fructueuses que nous avons eues, studieuses ou pas.

Merci aussi au Dr. Ouajdi Felfoul, de l'École polytechnique de Montréal, pour son amitié et sincérité, qui me sont très chères, et pour m'avoir aimablement commandé et fourni les articles et livres non disponibles à l'université de Montréal.

Je voudrais remercier les membres du jury de mon comité de thèse de me faire l'honneur d'avoir accepté l'évaluation attentive de mon travail et de me faire part de leurs commentaires justes qui ne pourront que contribuer à l'amélioration du présent manuscrit.

Un immense merci de tout cœur à mes parents, Moncef Fourati et Haifa Essid, pour leur soutien moral tout au long de ces années passées loin d'eux, pour leur amour infini même à distance et pour m'avoir toujours encouragé à persévérer dans la voie de l'excellence, dans les meilleurs, comme dans les moins bons moments. Je remercie également mes grands-parents, Ameur Fourati et Khedija Essid, pour m'avoir inculpé les valeurs du travail sérieux, sans oublier mes frère et sœurs, Ghassen, Amal et Ghada, ainsi que son époux Med Ali et ma nièce préférée Nesrine, dont j'ai eu l'immense plaisir de m'occuper durant sa naissance avant mon départ au Canada, mais qui a si rapidement grandi en mon absence. Je ne manquerais pas non plus de dire un grand merci à mes beaux-parents qui m'ont continuellement soutenu au cours de cette aventure.

Enfin, je remercie du fond du cœur, la dernière et certainement pas la moindre, ma chère et tendre épouse, Insaf Salem Fourati, pour son amour inconditionnel, sa présence et son soutien quotidien, et pour m'avoir épaulé tout au long de ce processus. Je la remercie également d'avoir été mon plus grand soutien psychologique mais aussi pour tout son apport intellectuel, et lui souhaite le meilleur des mondes dans la poursuite de sa thèse.

CHAPITRE I : Introduction

I.1. Introduction générale

Selon Galilée, le fondateur de la physique moderne, "l'univers est écrit en langue mathématique et ses caractères sont le triangle, le cercle et autres figures géométriques, sans lesquelles il est humainement impossible d'en comprendre un mot". Dans le même ordre d'idées, la science, tout comme l'ingénierie, se base sur des lois qui régissent l'ordre et le fonctionnement, faisant ainsi passer le scientifique, en général, et le chimiste en particulier, d'un observateur à un inventeur, avec des avancées majeures concomitantes en science et en technologie, conduisant à l'amélioration de la qualité de vie de l'homme. Les nouvelles technologies ont, cependant, entraîné l'apparition de nouveaux problèmes engendrés par la pollution environnementale, les méfaits de l'utilisation de produits chimiques sur l'agriculture et la nourriture, l'utilisation de substances radioactives et hautement toxiques dans le domaine de l'armurerie, etc. De ce fait, un paradoxe s'est établi entre les avantages apportés par les nouvelles technologies et les inconvénients engendrés principalement par la pollution de l'environnement et l'utilisation accrue des ressources, dont le renouvellement demeure plus lent. La meilleure solution plausible, mais difficile voire impossible à réaliser, consisterait à adopter des technologies avancées et à s'appuyer sur des procédés novateurs afin d'améliorer la qualité de la vie quotidienne de l'être humain tout en préservant la qualité de l'environnement. En effet, le respect de l'environnement est un point capital dans un contexte de développement durable, ce qui pousse l'innovateur tout comme le consommateur à préserver les ressources fossiles et à réduire la pollution de la terre. Par conséquent, la fabrication de produits industriels doit se baser sur des ressources renouvelables ou biodégradables.

Parmi ces technologies novatrices, on peut citer les sondes moléculaires qui s'appuient sur l'incorporation de molécules fluorescentes dans une matrice polymère afin de fournir une information spécifique suite à l'application d'un stimuli. Elles permettent ainsi l'amélioration du quotidien de l'être humain tout en limitant les répercussions sur

l'environnement et en se basant sur des produits écologiques et biodégradables, voire même alimentaires et conformes à l'US Food and Drug Administration (FDA).

I.2.Sondes moléculaires

Différents composés présentent un comportement thermochromique ou mécanochromique avec, respectivement, une sensibilité à la température et à la déformation, tels que les polydiacétylènes,[1-8] un élastomère tribloc portant des unités carbazole,[9] un polyuréthane thermoplastique avec des unités azobenzène[10] et d'autres matériaux non polymères.[11-14] Cependant, le coût de ces composés est prohibitif et il est difficile de les intégrer à d'autres matériaux. En conséquence, différents colorants aptes à former des excimères (fluorophores) ont été utilisés afin de préparer des matériaux (polymères) pouvant servir comme sondes, tels que les pérylènes,[15] l'oligo(p-phénylène vinylène)[16] et le 4,4'-bis(2-benzoxazolyle)stilbène (BBS).[17]

Ce sont les groupes de Weder et de Pucci qui ont le plus étudié les sondes polymère-colorant. Les premières sondes polymères ont été préparées par le groupe de Weder en incorporant de petites quantités de divers colorants, tels que le 1,4-bis(α-cyano-4-méthoxystyryl)-2,5-diméthoxybenzène dans du polyéthylène (PE),[16,18,19] le 1,4-bis-(α-cyano-styryl)-benzène dans du poly(éthylène téréphtalate)[20,21] et l'oligo(phenylène vinylène) dans divers polymères.[22-25] D'autre part, Pucci et son groupe ont étudié des sondes mettant en jeu le BBS dispersé dans divers polymères[26,2717,28-30] ou des sondes à base de pérylène dans le polyéthylène[31-33] et le poly(vinyl alcool).[34]

Les sondes moléculaires polymères renfermant des fluorophores présentent un changement permanent de fluorescence à la suite d'un changement de conformation moléculaire du fluorophore, faisant passer le système d'une composition saturée en monomères à une autre basée sur des espèces excitées : les excimères. Ce changement de couleur permet de répondre à différents stimuli externes tels que la température,[20-22,35-44] la déformation mécanique,[8,10-12,18,19,25,45-52] les produits chimiques,[53-55] la lumière,[56-58] la pression,[59] l'humidité[60] et d'autres,[61,62] aboutissant ainsi à une multitude d'applications innovatrices.[63,64] Ces sondes moléculaires polymères pourraient également conduire à de

nouvelles applications telles que la détection de polluants d'origines industrielle, agricole ou naturelle, le suivi des chaînes agroalimentaires, les analyses médicales d'urgence, etc.

Le thermochromisme dans les polymères a attiré plus d'attention dans la littérature que le mécanochromisme.[35-43,65] Les matériaux thermochromiques sont caractérisés par des changements de couleur irréversibles à la suite d'une exposition à des températures supérieures à un certain seuil, indiquant ainsi l'exposition antérieure du matériau à une température excessive.

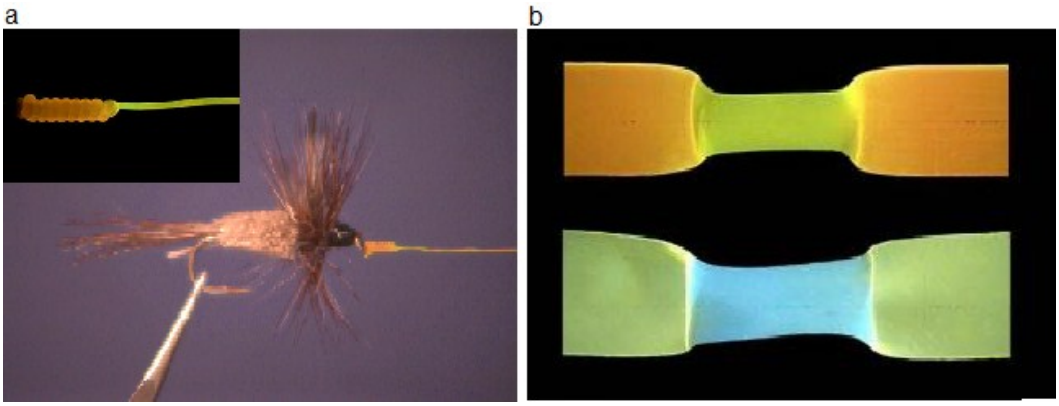

Figure I.1. Exemples de sondes mécanochromiques se basant sur un changement de couleur induit par la formation d'excimères : a) utilisation pour la pêche d'un matériau à base de polyéthylène linéaire à basse densité (LLDPE) et de 1,4-bis(R-cyano-4-méthoxystyryl)-2,5-diméthoxybenzène (BCMDB) afin de détecter la morsure d'un poisson à l'hameçon ;[66] b) LLDPE renfermant 0.18 % p/p de BCMDB (haut) et 0.20 % p/p de 1,4-bis(R-cyano-4-méthoxystyryl)benzène (bas) après déformation à 500% à température ambiante.[19]

D'autre part, la déformation mécanique d'un polymère peut conduire à la dispersion des molécules agrégées de colorant incorporées dans la matrice hôte, provoquant ainsi la formation d'un mélange moléculaire.[67] Ce phénomène a pu être exploité en combinaison avec les propriétés d'émission propres aux excimères ou aux monomères afin de créer des matériaux avec des sondes mécanochromiques intégrées, telles que celles illustrées à la Figure I.1.[16]

I.3.Excimères

I.3.1. Définition des excimères

Les excimères sont des complexes formés par une paire de molécules organiques conjuguées, l'une étant dans un état électronique excité et l'autre dans l'état fondamental.[68-74,68,75,76] Ils sont caractérisés par des temps de vie très courts, de l'ordre des nanosecondes, et des propriétés fluorescentes différentes de celles d'une molécule simple. Le passage de molécules isolées de colorant, appelées monomères, à des excimères entraîne un changement de couleur, tout comme le passage inverse.

Les excimères permettent d'extraire des informations sur les polymères et, plus précisément, sur leur architecture,[73] leur conformation en solution,[77-80] leur morphologie,[81,82] la miscibilité des mélanges polymères[83-86] et la distribution des sites de dopant.[15] La concentration joue un rôle important sur leur formation pour des molécules comme le pyrène dans divers polymères.[75,87-89]

I.3.2. Formation des excimères

La formation des excimères résulte du rapprochement des molécules isolées de colorant. La Figure I.2 montre une représentation schématique de l'énergie potentielle d'une paire de molécules à l'état fondamental (M+M), à l'état singulet excité (M+M*) et formant un excimère (MM*) en fonction de la distance intermoléculaire. L'énergie potentielle de l'état fondamental et de l'état excité est la résultante d'un potentiel attractif de van der Waals à longue échelle, qui est négligée à faibles distances intermoléculaires, et d'un potentiel répulsif à courte échelle. À une distance infinie où il n'y a pas d'interactions moléculaires, l'énergie potentielle de l'état fondamental est nulle au contraire de l'état singulet excité. Par contre, à une distance très faible, le potentiel répulsif prend le dessus sur le potentiel attractif empêchant la formation d'excimère. Par conséquent, cette dernière dépend étroitement de la variation de l'énergie potentielle en fonction de la distance intermoléculaire. Il n'y a donc formation d'excimères (MM*) que quand les molécules individuelles (M et M*) se rapprochent à une distance bien précise, de l'ordre de 3─4

Å,[70,71] induisant généralement une structure sous forme de sandwich, favorisée par des interactions π-π intermoléculaires entre les noyaux aromatiques[16,75] ainsi que par une concentration élevée de monomères.

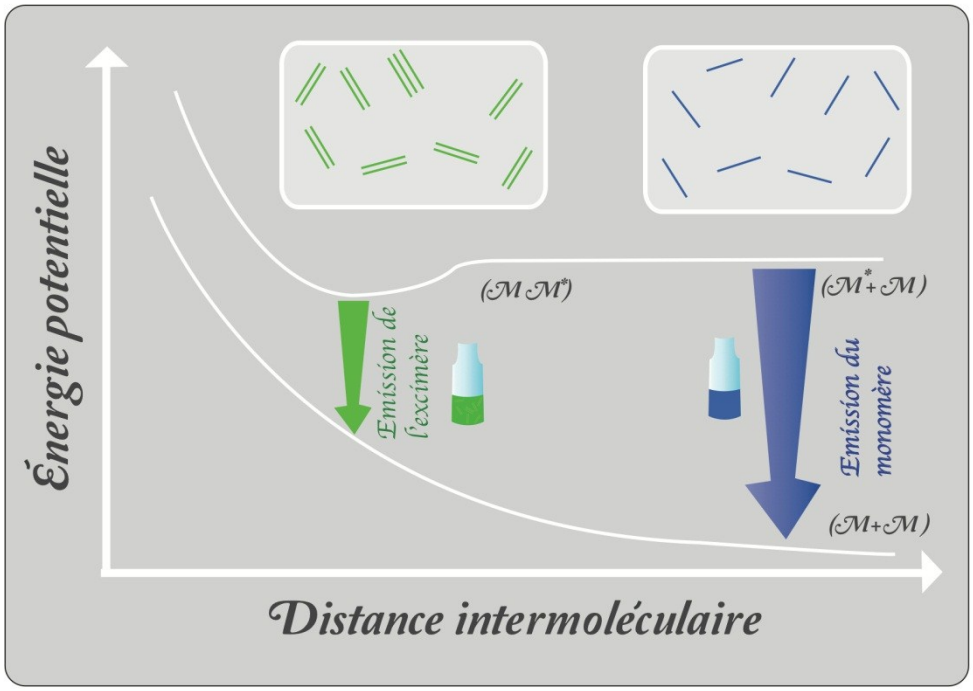

Figure I.2. Représentation schématique inspirée de Birks[72] des niveaux énergétiques des états excité et fondamental des excimères et des monomères. M : molécule à l'état fondamental ; M* : molécule à l'état excité ; MM* : excimère.

Selon la Figure I.2, un excimère est caractérisé par une énergie potentielle plus faible que celle des monomères le constituant, ce qui lui confère une émission à des longueurs d'onde supérieures à celles de ses composants séparés ainsi que de plus longs temps de vie.[16,71] Il est à signaler que la désactivation d'un excimère se fait, tout comme pour une molécule isolée, via des processus radiatifs (fluorescence et phosphorescence) ou non radiatifs (conversion interne et croisement intersystème)[72] et que ses propriétés optiques peuvent également être suivies par spectroscopie de fluorescence.

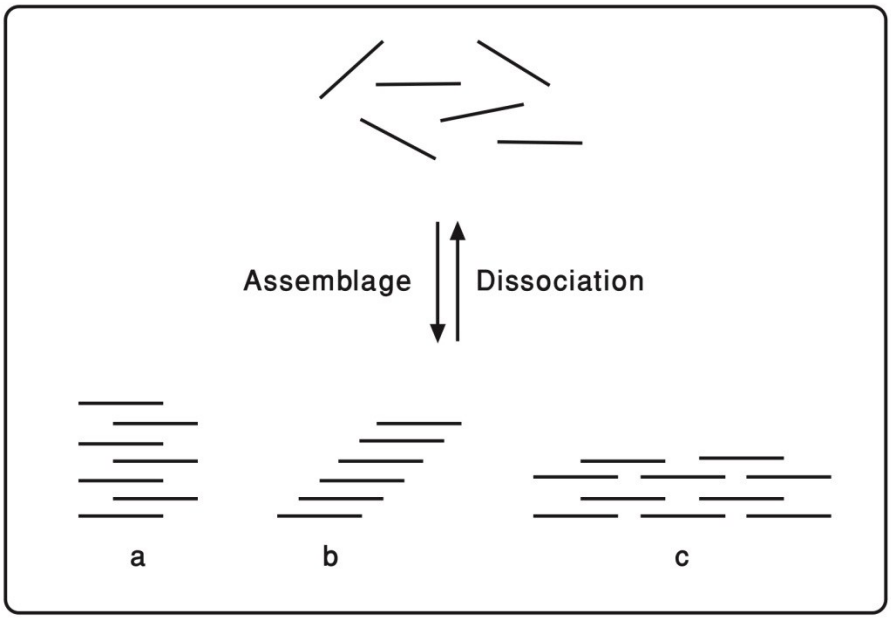

Figure I.3. Représentation schématique des différents arrangements pouvant avoir lieu entre des molécules de colorant empilées grâce à des interactions π-π : sous forme a) d'échelle, b) d'escalier ou c) de briques.[43]

La Figure I.3 montre que dans le cas de molécules de colorant empilées grâce à des interactions π-π, différents arrangements peuvent avoir lieu, dont la disposition sous forme d'échelle, d'escalier ou de briques.[90]

I.3.3. Caractéristiques moléculaires favorisant la formation d'excimères

Différents polymères aromatiques,[72] tels que le polystyrène[91] et le polyéthylène téréphtalate,[92] ainsi que des molécules organiques aromatiques conjuguées bien connues, telles que le stilbène,[93] le benzène,[94] le p-xylène,[95] le naphtalène[96] et le pérylène[15] ont l'aptitude de former des excimères. Cependant, l'exemple le plus classique est le pyrène,[97] qui passe en solution d'une structure vibronique bien résolue, caractéristique des monomères,[70] à un spectre d'émission dominé par une large bande non structurée et décalée vers le rouge, spécifique aux excimères, à des concentrations supérieures à 10^{-3} mol/L.[98] L'intensité de la bande d'excimères devient de plus en plus élevée au fur et à mesure que la probabilité qu'une molécule à l'état excité rencontre une seconde molécule à l'état

fondamental devienne élevée. La Figure I.4 montre la molécule d'anthracène,[99] qui peut former des excimères sous forme de sandwich[98] si non substituée (Figure I.4.a) ou des photodimères[100] en cas de substitution (Figure I.4.b).

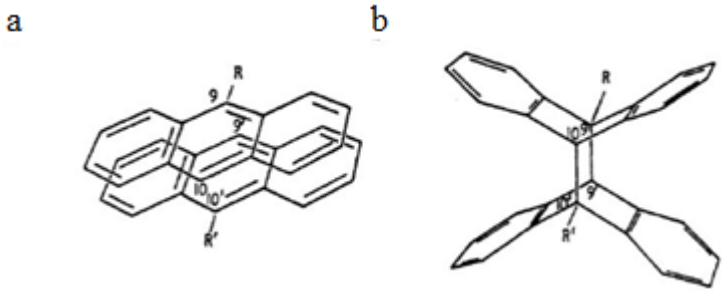

Figure I.4. La molécule d'anthracène a) sous forme d'excimère (R = H) ou b) sous forme de photodimère (R = CH_3, CN, Cl).[37]

I.4.Fluorophores et polymères utilisés

Pour la réalisation de ce projet, deux fluorophores ont été utilisés, à savoir le 4,4′-bis(2-benzoxazolyle)stilbène (BBS) et le 2,5-bis(5-*tert*-butyl-benzoxazol-2-yle)thiophène (BBT), qui sont des molécules conjuguées ayant des propriétés optiques similaires et une fluorescence intrinsèque importante. Ils ont des températures de fusion et de dégradation élevées, leur permettant de résister à la température de traitement (comme dans le cas de la préparation de mélanges polymère-fluorophore) et faisant d'eux des produits satisfaisant l'U.S. Food and Drug Administration (FDA). De plus, ils sont dotés d'une excellente dispersibilité dans les polymères fondus, favorisant leur utilisation en tant qu'additifs dans les matériaux d'emballage des denrées alimentaires. D'autre part, ils sont caractérisés par des structures moléculaires différentes : une forme de banane pour le BBT et une forme de bâtonnet pour le BBS. Cette dernière permet la formation d'excimères entraînant un changement de couleur suite au réarrangement moléculaire à partir des monomères et favorise son utilisation en tant que sondes moléculaires dans des matériaux intelligents. Cependant, aucune investigation approfondie des conditions favorisant la formation d'excimères n'a été réalisée auparavant.

Malgré les avantages énumérés ci-dessus, BBS présente également des inconvénients. En effet, il n'est pas soluble dans les solvants peu toxiques et bon marché, ce qui restreint son utilité. De plus, étant un dérivé du stilbène qui est connu pour subir une conversion entre les isomères *trans* et *cis*, il serait intéressant d'investiguer l'aptitude de BBS à photoisomériser, qui pourrait également être un désavantage à son utilisation surtout en cas d'isomérisation irréversible, diminuant ainsi la stabilité du produit. Contrairement au BBS, BBT n'est pas capable de photoisomériser et présente une solubilité étendue dans une multitude de solvants. Il a également été utilisé en tant que transporteur d'électrons, apte à former des complexes transitoires donneur-accepteur avec des matériaux transporteurs de trous. De ce fait, il serait utile d'étudier les propriétés photophysiques, en général, et les mécanismes de désactivation, en particulier, de ces deux fluorophores en se basant sur des rendements quantiques absolus de fluorescence et non relatifs par rapport à un actinomètre, comme précédemment rapportés dans la littérature. Le but serait d'avoir une idée précise sur les processus de dissipation de l'énergie de leurs états excités qui peuvent être responsables de la diminution de leur fluorescence. Cette thèse rapporte également les propriétés optiques, électrochimiques et cristallographiques de BBS et de BBT à l'état solide et en solution afin de mieux comprendre les conditions favorisant la formation d'excimères et d'étudier l'effet de leurs formes sur ce réarrangement moléculaire et sur la détection de stimuli. Cette étude permet ainsi de mieux comprendre leur utilité tout en mettant l'accent sur leurs limites afin d'élargir leurs domaines d'applications et de faciliter la sélection future de molécules fluorescentes destinées à être utilisées comme sondes moléculaires. D'autre part, l'incorporation de ces molécules aromatiques fluorescentes (BBS et BBT) dans une matrice polymère (PBS) permettrait de conduire, pour la première fois, une analyse quantitative de l'orientation de ces fluoropohores dans une matrice polymère, en plus d'élucider l'effet du taux de déformation du film et de la concentration des fluorophores sur l'orientation des chaînes polymères.

L'accumulation des déchets plastiques et l'augmentation du prix du pétrole ces dernières années a conduit au développement de polymères biodégradables produits à partir de ressources renouvelables, en comparaison avec les polymères dérivant du pétrole et nocifs pour l'environnement. Parmi ceux-ci, on peut citer le polylactide (PLA) et le

poly(1,4-butylène succinate) (PBS), qui sont les matériaux plastiques écologiques[101,102] choisis pour la conduite de cette étude. Ils ont principalement été utilisés pour la préparation de films destinés à la fabrication de sacs à provisions.[103]. Étant des polymères aliphatiques, PLA et PBS présentent une bonne biodégradabilité, permettant leur décomposition en dioxyde de carbone et en eau dans la nature.[104] PLA est obtenu à partir de la fermentation du glucose et d'une polymérisation à ouverture de cycle du dimère lactide.[105] D'autre part, PBS est produit à partir de l'acide succinique, qui découle des sucres, et du 1,4-butanediol, qui est obtenu par réduction du premier monomère, ce qui en fait un polymère entièrement bio.[105-107] Il est caractérisé par des propriétés mécaniques et une ductilité qui en font un remplaçant intéressant pour les polyoléfines. Dans cette thèse, ces deux polyesters, PBS et PLA, servent principalement de matériau hôte pour les fluorophores parce qu'ils permettent une bonne dispersion des molécules invitées dans le but de préparer des matériaux intelligents.

Dans le cas d'un polymère semi-cristallin (PBS ou PLA), la phase amorphe inter-lamellaire est constituée de chaînes partagées entre les phases cristalline et amorphe, de chaînes mal repliées, de chaînes formant de longues boucles, ainsi que de bouts de chaînes. Lorsqu'ajoutées au PBS ou au PLA, les molécules de colorants (BBS ou BBT) se dispersent uniquement dans leur phase amorphe et non dans leur phase cristalline, tel que décrit par la Figure I.5. Il est à signaler que la forme cristalline la plus stable suppose que les chaînes soient étendues, bien que le repliement des chaînes soit favorisé cinétiquement.[108]

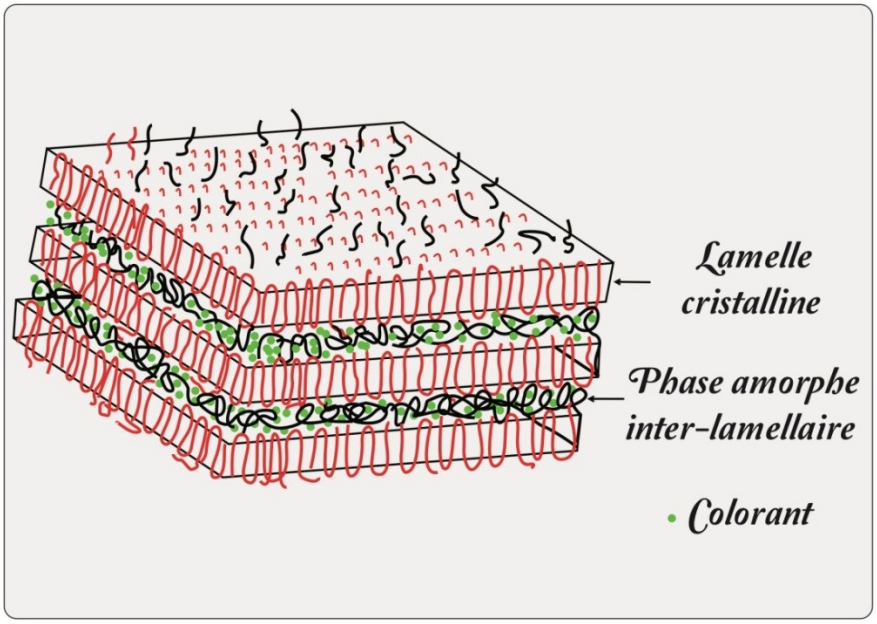

Figure I.5. Schéma d'insertion des molécules de colorant dans la phase amorphe du polymère.

I.5. Orientation des polymères et des petites molécules à l'état solide

I.5.1. Orientation des polymères

L'orientation des polymères est un phénomène d'une grande importance théorique et technique. Elle désigne l'alignement au niveau moléculaire des chaînes polymères par rapport à une direction macroscopique de référence.[109]

Les polymères semi-cristallins sont formés d'une partie amorphe désordonnée et d'une partie cristalline, qui présente des chaînes ordonnées, ce qui confère au matériau cristallin de meilleures propriétés mécaniques par rapport aux polymères amorphes.[110,111] Les polymères caractérisés par une structure régulière primaire peuvent adopter une structure secondaire ordonnée et, ensuite, cristalliser afin de former des sphérolites, qui croissent à partir d'un centre et se propagent dans toutes les directions afin d'occuper tout l'espace vide. Ces sphérolites sont constitués de lamelles d'une épaisseur uniforme de l'ordre de 100 Å, formant un arrangement polycristallin constitué de cristallites radiales séparées par la phase amorphe et produites par des molécules repliées.[112] La Figure I.6

montre que dans cette structure complexe, la phase amorphe est répartie entre les lamelles (rejet de la phase amorphe lors de la cristallisation) et entre les sphérolites.

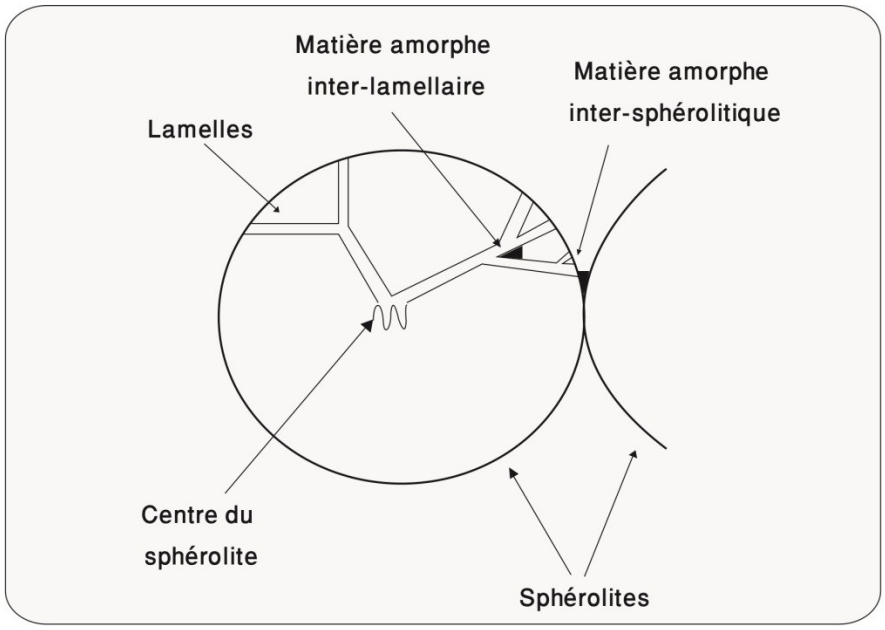

Figure I.6. Représentation schématique de la structure d'un polymère cristallisé à partir de l'état fondu.

L'orientation peut être induite par des forces générées par des champs électriques, magnétiques ou mécaniques. Le moyen le plus courant d'induire une orientation dans un échantillon polymère est l'application d'une force mécanique permettant l'étirement du polymère et entraînant l'orientation de ses chaînes dans la direction de l'élongation.

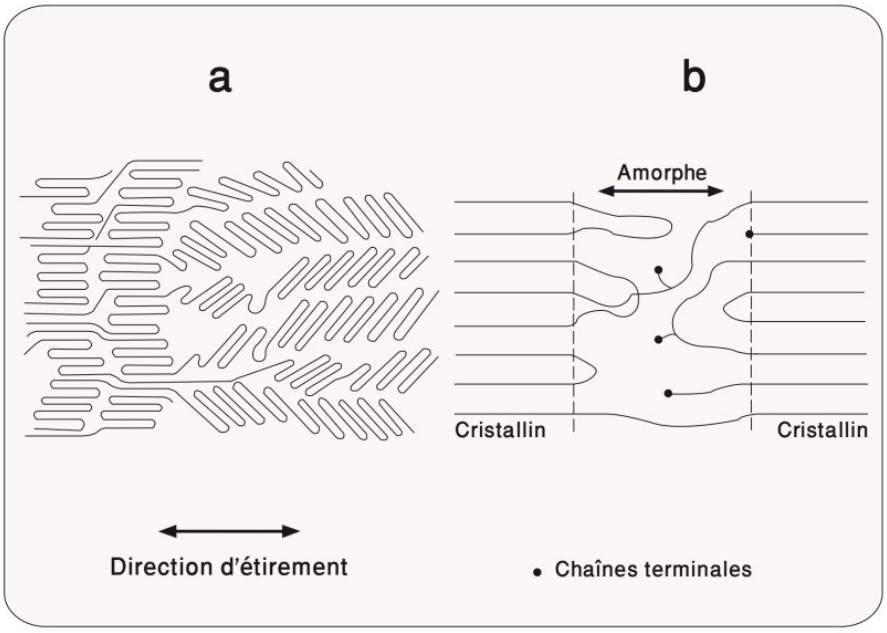

Figure I.7. Représentation schématique a) du réarrangement lamellaire pendant l'étirement et b) des couches amorphes et cristallines après étirement.[151]

La Figure I.7 montre qu'un réarrangement lamellaire se produit au sein du sphérolite d'origine pendant l'étirement. En effet, les lamelles disposées de façon ordonnée et non perpendiculaire à la direction de déformation ont tendance à s'orienter selon la direction d'étirement, entraînant la formation de microlamelles. Celles-ci sont constituées de régions cristallines et amorphes alternées, qui sont généralement connectées par des molécules d'attache suite au déploiement des chaînes durant le processus de déformation.[113]

Le repliement régulier des macromolécules dans les cristallites ainsi que la faible quantité de liaisons interlamellaires favorisent l'étirement des polymères.[114-116] La cassure des liaisons faibles de van der Waals, qui relient les chaînes enchevêtrées du polymère, ainsi que la déformation des chaînes de liaison, qui vont se faufiler à travers les enchevêtrements, ont également été évoquées afin d'expliquer l'augmentation de l'orientation en fonction de l'étirement.[117,118] D'autre part, l'orientation des cristallites est directement affectée par la vitesse de la déformation mécanique. En effet, une orientation plus efficace des cristallites est obtenue à des vitesses d'étirement élevées puisque les

chaînes amorphes n'ont pas le temps de relaxer et restent immobilisées à l'état étiré après déformation mécanique.[119]

I.5.2. Conséquences de l'étirement des films polymères sur les petites molécules

La zone où les petites molécules, en général, et les fluorophores en particulier, se trouvent suite au réarrangement structurel, engendré par la déformation mécanique, a été souvent étudiée. La valeur très élevée de l'énergie d'activation de la diffusion de molécules dans le cristal polymère (> 24 kJ/mol) ne permet pas aux molécules de pénétrer dans les cristaux du polymère semi-cristallin en raison d'une cinétique de diffusion trop lente. Toutefois, ces petites molécules peuvent se situer à la surface des cristallites de polymère,[120] et plus généralement dans trois sites potentiels dans le cas d'un polymère semi-cristallin non orienté et dans quatre sites dans le cas d'une matrice orientée, tel que décrit par la Figure I.8.[121,122]

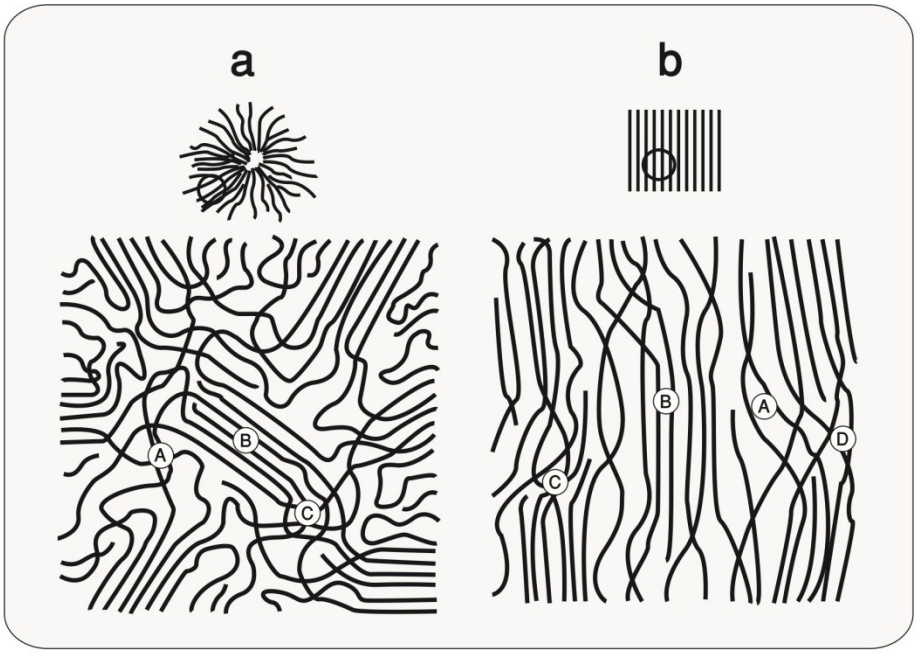

Figure I.8. Emplacement suggéré des petites molécules dans un polymère semi-cristallin non orienté (a) et dans une matrice orientée (b) : phase amorphe (A), surface latérale du cristal (B), surface des chaînes repliées (C) et phase amorphe interlamellaire (D).[121,122]

Avant déformation, les petites molécules sont dispersées majoritairement entre la phase amorphe (A) et la surface des chaînes repliées (C), et minoritairement à la surface latérale du cristal (B). Après déformation, les petites molécules peuvent se trouver dans les endroits précédemment cités, auxquels s'ajoute un site supplémentaire à savoir la phase amorphe inter-lamellaire (D), qui contient des chaînes partiellement orientées. Par conséquent, les molécules de colorant ne peuvent s'orienter que si elles se trouvent sur les sites d'adsorption présents sur la surface latérale des cristallites (B) ou plus rarement à l'intérieur de la phase amorphe inter-fibrillaire (D), alors que l'orientation des molécules se trouvant dans les sites A et C reste inchangée.

I.6.Techniques d'analyse

I.6.1. Spectroscopie de fluorescence

Dans le cas d'une molécule fluorescente, l'absorption de la lumière d'une longueur d'onde donnée est suivie du retour de l'état singulet excité vers l'état fondamental sans changement de spin des électrons. Ce retour peut avoir lieu principalement via un processus radiatif par émission de fluorescence à des longueurs d'onde plus élevées que celles de la lumière absorbée ou via un processus non radiatif, qui a lieu par croisement intersystème (CIS) ou conversion interne (CI), tels que par vibrations de liaison ou collisions avec des molécules de solvant. Ces différentes voies de désactivation de l'état excité sont schématiquement décrites à la Figure I.9 à travers un diagramme de Perrin-Jablonski,[123,124] dans lequel les états vibrationnels les plus bas des différents états électroniques sont représentés par des lignes épaisses alors que les lignes minces représentent leurs états vibrationnels plus élevés que zéro. D'autre part, les flèches droites caractérisent les processus d'absorption, de fluorescence ou de phosphorescence, alors que les flèches ondulées sont spécifiques à la relaxation vibrationnelle, à la conversion interne ou au croisement intersystème.

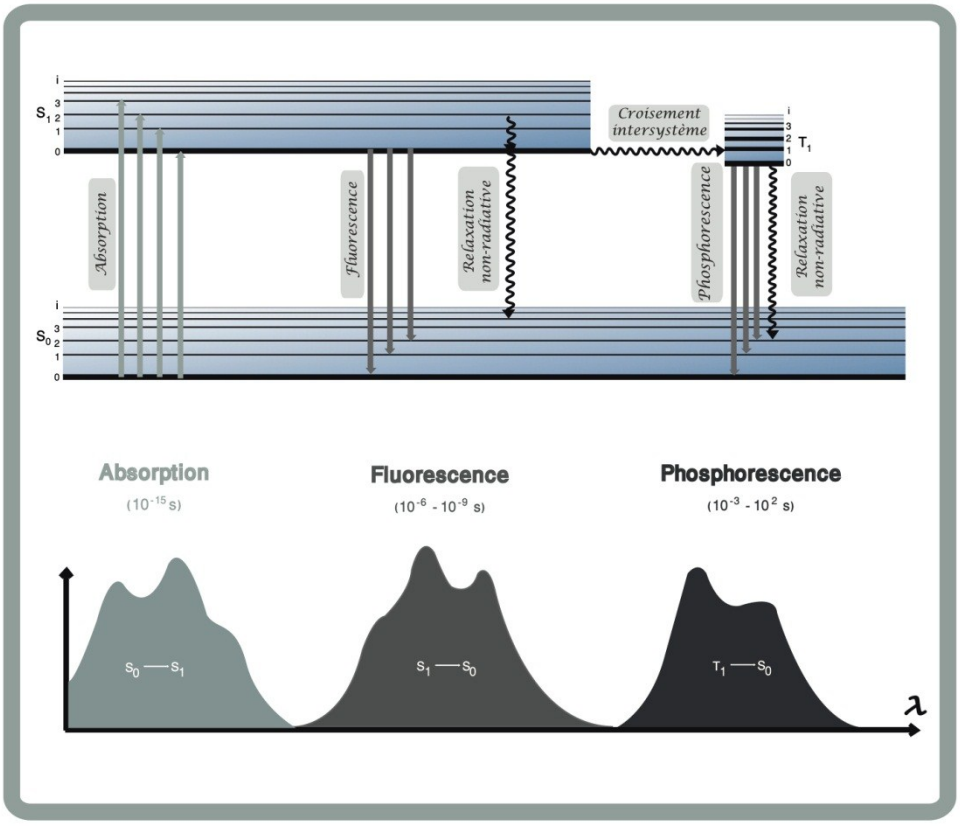

Figure I.9. Représentation schématique du diagramme de Perrin-Jablonski décrivant les différents types de processus pouvant avoir lieu dans le cas d'une molécule luminescente avec une illustration des positions relatives de l'absorbance, de la fluorescence et de la phosphorescence. S_0 et S_1 désignent, respectivement, l'état fondamental singulet et le premier état singulet excité, T_1 étant le premier état triplet. Pour chacun de ces états, plusieurs états vibrationnels notés 0, 1, 2, i existent. Les temps caractéristiques évoqués sont des ordres de grandeur, qui peuvent fortement varier d'un fluorophore à un autre.

La Figure I.9 montre également les temps typiques nécessaires pour chacun des processus énumérés ci-dessus avec une durée de vie beaucoup plus longue pour la phosphorescence (10^{-6} ─ 1 s) par rapport à la fluorescence (10^{-10} ─ 10^{-7} s). Cependant, la phosphorescence demeure moins probable que la fluorescence étant donné qu'elle implique une transition interdite entre deux états de multiplicité différente, dû au fait que le système doit changer d'état de spin lors de son passage de l'état triplet vers l'état fondamental. Cette transition électronique est considérée en violation avec les principes d'exclusion de Pauli, ce qui rend difficile le retour de l'électron vers l'état singulet fondamental.

La spectroscopie de fluorescence est l'outil adéquat permettant le suivi du passage des monomères vers les excimères. Elle a été utilisée dans cette thèse afin de caractériser les propriétés spectroscopiques des fluorophores en solution et à l'état solide en fonction de la concentration des chromophores ou de l'étirement des films polymères. Elle a également été utilisée pour la mesure des temps de vie des différentes espèces (monomères et excimères) ainsi que des rendements quantiques de fluorescence.

Le rendement quantique de fluorescence, Φ_{fl}, est le rapport entre le nombre de photons émis et le nombre de photons absorbés. Le calcul du rendement quantique de fluorescence était fait auparavant par actinométrie, qui consiste à utiliser des molécules de référence, de rendement quantique de fluorescence connu, appelées actinomètres.[125-127] Le rendement quantique de fluorescence de l'échantillon, $\Phi_{fl,Éch}$, peut ainsi être calculé selon l'Équation I.1 :

$$\Phi_{fl,Éch} = \Phi_{fl,Réf} \frac{A_{Réf} \, x \, Aire_{Éch} \, x \, N^2_{Éch}}{A_{Éch} \, x \, Aire_{Réf} \, x \, N^2_{Réf}} \qquad \textbf{(I.1)}$$

où A indique la valeur d'absorption à la longueur d'onde d'excitation, Aire l'aire sous la courbe de fluorescence et N l'indice de réfraction du solvant utilisé pour l'actinomètre, Réf, et l'échantillon, Éch. Le problème avec cette méthode d'actinométrie est que même si elle peut être utilisée pour une large gamme de fluorophores en solution dans divers solvants, elle demeure limitée puisqu'elle exige l'utilisation d'une molécule de référence possédant des rendements quantiques ainsi que des valeurs d'absorbance et d'émission similaires, à ± 5%, pour les deux molécules (actinomètre et échantillon) à la longueur d'onde d'excitation. Par conséquent, afin de calculer des valeurs absolues et bien plus précises que celles obtenues par actinométrie relative, les rendements quantiques de fluorescence (Φ_{fl}) calculés dans cette thèse ont été mesurés avec une sphère d'intégration, qui est revêtue d'un matériau réfléchissant ($BaSO_4$), permettant de refléter pratiquement toute la lumière émise par fluorescence dans la sphère vers le détecteur de fluorescence. Dans ce cas, le calcul du rendement quantique de fluorescence d'un fluorophore, $\Phi_{fl,Éch}$, est fait selon l'Équation I.2 :

$$\Phi_{\boldsymbol{fl,\acute{E}ch}} = \frac{\int \acute{E}\boldsymbol{mission}_{\acute{E}\boldsymbol{ch}}}{\int \boldsymbol{Diffusion}_{\boldsymbol{Bl}} - \int \boldsymbol{Diffusion}_{\acute{E}\boldsymbol{ch}}} \quad \textbf{(I.2)}$$

où $\int \acute{E}mission_{\acute{E}ch}$ est la quantité de lumière émise, alors que la quantité de lumière absorbée par l'échantillon est mesurée par la différence entre la diffusion du blanc, $\int Diffusion_{Bl}$, et de l'échantillon, $\int Diffusion_{\acute{E}ch}$. Bien que la sphère d'intégration permette une mesure directe, efficace et absolue du rendement quantique, son utilisation demeure limitée aux échantillons dotés d'un rendement quantique de fluorescence élevé, $\Phi_{fl} > 0{,}05$.

Tel qu'illustré par le diagramme de Perrin-Jablonski de la Figure I.9, l'état singulet excité peut aussi subir une désactivation non radiative, soit par CI, à travers des processus vibrationnels, de flexion ou d'étirement, soit par CIS, suite au passage d'un électron de l'état singulet vers l'état triplet le plus bas (T_1), entraînant un changement du spin de l'électron et un passage de la multiplicité d'un à trois.

I.6.2. Spectroscopie infrarouge

L'orientation moléculaire d'un polymère peut être quantifiée par dichroïsme linéaire infrarouge via le rapport dichroïque d'absorbance entre deux spectres : l'un mesuré avec une lumière polarisée parallèlement (A_p) et l'autre avec une lumière polarisée perpendiculairement (A_s) à la direction d'étirement. La fonction d'orientation $<P_2>$ est déduite à partir de ce rapport dichroïque, calculé selon l'Équation I.3, et de l'angle α entre le moment de transition et la chaîne principale, tel que décrit par l'Équation I.4.

$$\boldsymbol{R = A_p / A_s} \quad \textbf{(I.3)}$$

$$\langle \boldsymbol{P_2} \rangle = \frac{\boldsymbol{2}}{\langle \boldsymbol{3cos^2\alpha - 1} \rangle} \frac{\boldsymbol{R-1}}{\boldsymbol{R+2}} \quad \textbf{(I.4)}$$

Une orientation parfaite est caractérisée par un $<P_2>$ égal à l'unité, alors qu'une absence d'orientation est définie par un $<P_2>$ nul. Lors de la mesure des spectres polarisés, le polariseur est tourné afin d'enregistrer les spectres parallèlement et perpendiculairement à l'axe d'orientation du film.

Une autre méthode de spectroscopie en transmission a été employée, à savoir la spectroscopie infrarouge avec modulation de la polarisation (PM-IRSAS),[128,129] qui consiste à utiliser un modulateur photoélastique afin de moduler très rapidement la polarisation du faisceau infrarouge entre 0 et 90°, permettant ainsi d'enregistrer les spectres de polarisation parallèle et perpendiculaire pratiquement en même temps et conférant une très grande précision à la mesure du dichroïsme linéaire. Le second moment du polynôme de Legendre $<P_2>$ est alors mesuré conformément à l'Équation I.5 :[128]

$$\langle \boldsymbol{P_2} \rangle = \frac{-2\sqrt{\lambda}\ \Delta \boldsymbol{A}}{3\ \boldsymbol{A_0}} \qquad \textbf{(I.5)}$$

où A_0 est l'absorbance de l'échantillon non étiré, ΔA la différence dichroïque et $\sqrt{\lambda}$ un terme correctif tenant compte de la diminution de la largeur et de l'épaisseur du film analysé, et pouvant être négligé aux très faibles élongations.

Diverses techniques peuvent être utilisées pour mesurer l'orientation uniaxe des polymères semi-cristallins, telles que la biréfringence, la spectroscopie Raman, la diffraction des rayons X et la spectroscopie infrarouge (IR). La biréfringence aboutit au calcul d'un $<P_2>$ moyen, qui ne permet pas d'attribuer une orientation spécifique à chacun des différents constituants d'un mélange et ne peut donc pas être considérée comme une méthode adaptée à l'étude de l'orientation d'un film polymère renfermant des molécules de fluorophore. La spectroscopie Raman est quant à elle une méthode puissante permettant le calcul du $<P_2>$ et du $<P_4>$, mais demeure également inadéquate pour la conduite de cette étude puisque les matériaux utilisés sont fortement fluorescents, ce qui a tendance à masquer l'effet Raman, en plus d'offrir une bibliothèque de spectres moins complète et une sensibilité moins élevée que celles de la spectroscopie infrarouge. Vu la faible concentration des fluorophores dans les films polymères, la diffraction des rayons X

permettrait l'étude exclusive de l'orientation du polymère et non des petites molécules dispersées dedans. De plus, ces mesures tiennent en compte uniquement de la partie cristalline du polymère et non de sa partie amorphe. Elles aboutissent, par conséquent, à des valeurs de $<P_2>$ supérieures à celles déterminées par spectroscopie IR, qui fournit une orientation moyenne globale du polymère tenant compte des phases cristalline et amorphe. D'autre part, la spectroscopie infrarouge peut être considérée comme une méthode de choix puisqu'elle joint la rapidité, la sensibilité et la facilité d'échantillonnage, permettant ainsi l'étude simultanée de l'orientation moléculaire des polymères et des petites molécules à travers l'absorption d'un rayonnement infrarouge tout en discriminant l'orientation des phases amorphe et cristalline dans un polymère semi-cristallin.

Par conséquent, dans cette thèse, la spectroscopie IR a été utilisée pour étudier l'orientation uniaxe à la fois de PBS et des fluorophores qui y sont dispersés. Les bandes spécifiques des diverses composantes obtenues en même temps permettent d'obtenir un $<P_2>$ spécifique à chaque molécule. Cette approche donne l'information avec un nombre limité d'expériences, ce qui permet d'économiser en matière, en coût et en temps de mesure. Dans le cas d'un chevauchement entre les pics spécifiques à la matrice polymère et aux fluorophores, la spectroscopie de fluorescence polarisée demeure une méthode intéressante et complémentaire afin de suivre le comportement des molécules fluorescentes.

I.6.3. Spectroscopie de fluorescence polarisée

La spectroscopie de fluorescence polarisée permet l'étude de l'orientation des molécules fluorescentes, que ce soit des fluorophores ou des polymères fluorescents. Le suivi du dichroïsme et de l'orientation des molécules fluorescentes peut être réalisé sur des films polymères étirés renfermant des fluorophores en excitant les échantillons avec une lumière non polarisée et en mesurant l'émission polarisée parallèlement (//) et perpendiculairement (⊥) à la direction d'étirement, tel que décrit par la Figure I.10.

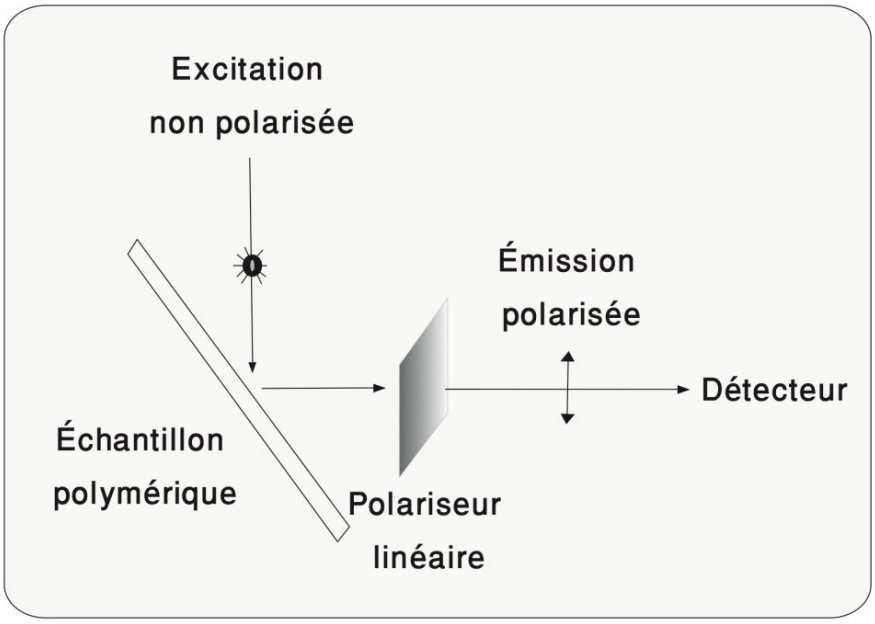

Figure I.10. Représentation schématique de l'appareillage pour les mesures de fluorescence en lumière polarisée.

L'orientation a été évaluée quantitativement par fluorescence polarisée en calculant le rapport dichroïque (R), selon l'Équation I.6, des intensités des émissions parallèle ($E_{//}$) et perpendiculaire ($E_{\perp}$) à l'axe d'étirement, permettant ainsi d'aboutir au paramètre d'ordre S,[130] défini par l'Équation I.7 :

$$\boldsymbol{R = E_{//}/E_{\perp}} \qquad \textbf{(I.6)}$$

$$\boldsymbol{S = \frac{(R-1)}{(R+2)}} \qquad \textbf{(I.7)}$$

Dans les mélanges polymères renfermant une petite molécule, on s'attend à ce que cette dernière adopte l'orientation du polymère hôte dans lequel elle est dispersée suivant le régime de déformation affine.[131] Cependant, en raison de la complexité structurale moléculaire, la Figure I.11 montre que le dipôle de transition d'une molécule comme le BBS n'est pas nécessairement parallèle à son axe moléculaire, aboutissant à un angle β entre les deux, de sorte qu'après étirement, le colorant n'est pas nécessairement aligné suivant l'axe d'étirement, résultant en un angle α entre ce dernier et l'axe de la molécule. Ainsi, un angle de décalage total γ est formé comme étant la somme des angles α et β, affectant directement la valeur du rapport dichroïque.

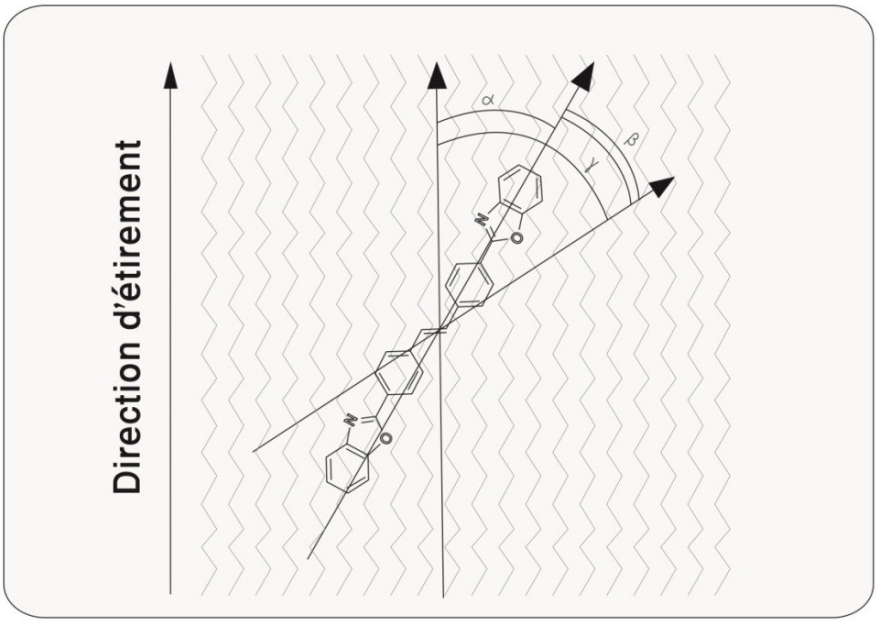

Figure I.11. Orientation d'une molécule de colorant (BBS) par rapport à l'orientation des chaînes polymères.

Un changement du moment de transition ($\vec{M}$) d'une molécule se produit suite à l'excitation de ses électrons lors du processus d'émission. Lorsque les unités structurelles sont disposées de manière anisotrope dans la matrice polymère, un phénomène de dichroïsme se produit affectant l'orientation moléculaire et entraînant une dépendance

directe entre l'émission (E) ou l'absorbance (A) et la direction du vecteur électrique ($\vec{E}$) du rayonnement incident.

Dans cette thèse, grâce aux rendements quantiques de fluorescence élevés (>10%) de BBS et de BBT, leur orientation uniaxe, lorsque dispersés dans les films polymères (PBS), a été investiguée par spectroscopie de fluorescence en lumière polarisée, qui représente une méthode de choix. Pour des molécules de colorant dotées de faibles rendements quantiques (<1%), la spectroscopie UV-visible polarisée serait plus adéquate.

I.6.4. Voltampérométrie cyclique

La voltampérométrie cyclique est souvent utilisée afin d'étudier les propriétés électrochimiques des molécules en observant l'évolution du courant en fonction du potentiel entre une électrode de travail et une électrode auxiliaire. Les niveaux énergétiques HOMO et LUMO sont par la suite déduits à partir des potentiels d'oxydation et de réduction obtenus en étalonnant avec un standard. Les molécules dont les processus d'oxydation et/ou de réduction sont réversibles sont généralement considérées comme attrayantes pour diverses applications en électronique. Dans le cas de processus parfaitement réversibles, la molécule devrait présenter un voltampérogramme, tel que décrit par la Figure I.12, dans laquelle E_{pa} et E_{pc} décrivent, respectivement, le potentiel d'oxydation et de réduction de la molécule étudiée relativement à l'électrode de référence.

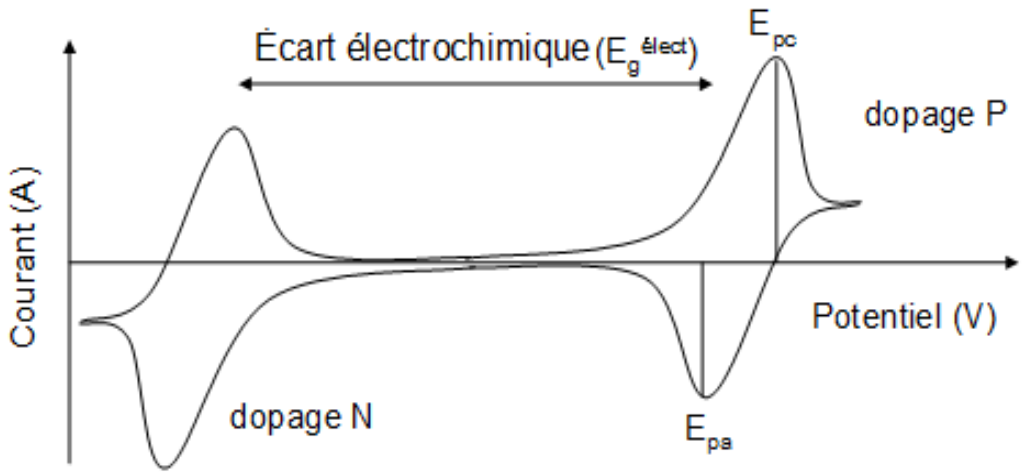

Figure I.12. Voltampérogramme caractéristique d'une molécule présentant des processus d'oxydation et de réduction parfaitement réversibles.

Les potentiels d'oxydation et de réduction varient d'une molécule à une autre, en fonction des groupements fonctionnels. En effet, les substituants électrodonneurs ont tendance à abaisser la bande de valence (HOMO), alors que les substituants électroaccepteurs vont plutôt augmenter la bande de conduction (LUMO). D'autre part, des paramètres tels que la concentration d'une molécule, le changement de conformation induit par chauffage ou l'état dans lequel elle se trouve agissent également sur ses propriétés. C'est le cas des polymères dont les propriétés changent dépendamment s'ils se trouvent en solution ou à l'état solide.[132,133] À l'état solide, la structure des fluorophores est généralement stabilisée par la formation d'excimères ou d'interactions π, abaissant ainsi les distances de bande de façon considérable.

La voltampérométrie cyclique a été utilisée dans cette étude afin d'élucider les propriétés électrochimiques de BBS et de BBT, et d'étudier la réversibilité de leurs processus d'oxydation et de réduction.

I.7.Objectifs et portée de la présente thèse

Les deux fluorophores choisis, BBS et BBT, ont été souvent utilisés dans la littérature. Cependant, peu d'études ont porté sur leurs propriétés optiques et aucune étude

complète n'a été effectuée sur leurs propriétés intrinsèques. Les chapitres 2, 3 et 4 visent, de ce fait, une investigation détaillée des propriétés optiques, photophysiques, électrochimiques et cristallographiques des chromophores BBS et BBT à l'état solide et en solution en vue de sonder leurs limites d'utilisation. Cette étude permet de déterminer, entre autres, les interactions intermoléculaires et les conditions à l'origine de la formation ou de l'absence d'excimères. Elle permet également d'élucider les différentes voies de désactivation de l'état singulet excité. Pour ce faire, diverses techniques de caractérisation sont utilisées, telles que la spectroscopie de fluorescence, de phosphorescence, de résonance magnétique nucléaire et UV-visible, la photolyse par impulsion laser et la diffraction des rayons X. Notre but est de combiner les propriétés mécaniques des polymères aux propriétés optiques des fluorophores afin de permettre la préparation ultérieure de dispositifs nécessitant de telles caractéristiques, à l'instar des sondes polymères de déformation ou de température. Cette étude permet, en plus, de proposer une nouvelle molécule en tant que remplaçant pour les fluorophores conventionnels, en plus de mettre l'accent sur le faible potentiel d'oxydation et la faible différence d'énergie entre la bande de valence et la bande de conduction (E_g) des fluorophores utilisés.

Le cinquième chapitre vise l'étude par spectroscopie infrarouge polarisée en modes dynamique et statique de l'orientation du polymère, PBS, et des deux petites molécules dispersées dedans, BBS et BBT. Peu d'études se sont intéressées à l'orientation d'une petite molécule dichroïque dans des matrices macromoléculaires orientées,[134-139] et encore moins se sont focalisées sur l'effet de l'ajout d'une petite molécule sur l'orientation de la macromolécule de départ. Cette étude vise ainsi à corréler les orientations du polymère et des chromophores, et de comprendre l'effet de la déformation mécanique sur la dynamique de l'orientation des chromophores. L'effet de l'orientation des chromophores après étirement est élucidé en fonction du comportement du polymère par spectroscopie infrarouge. Par la suite, une investigation complémentaire par spectroscopie de fluorescence polarisée permet de confirmer les résultats préliminaires obtenus par spectroscopie infrarouge, en plus de pouvoir suivre séparément l'orientation des molécules isolées et des agrégats de colorant.

Le sixième chapitre de la présente thèse vise à poursuivre les études sur la préparation de sondes polymères, entamées par les groupes de Pucci et de Weder, afin de comprendre leur fonctionnement en fonction de différents paramètres environnementaux dans le PBS déjà étudié et d'élargir ces résultats à un autre polyester, à savoir le PLA. Le but de ce chapitre est d'investiguer la variation des rendements quantiques et des temps de vie des films polymère-petite molécule en fonction de la concentration du colorant, afin de déduire le type d'arrangement moléculaire des fluorophores tout en étudiant les propriétés photophysiques des films préparés, ce qui permettra de développer une compréhension prédictive des relations structure-propriétés dans ce type de système. Ce chapitre vise également à suivre les propriétés fluorescentes des différents mélanges polymères en fonction du temps et de la température afin d'évaluer leur aptitude à être utilisés comme sondes moléculaires tout en suivant un facteur mal exploité précédemment, à savoir le taux de cristallinité du mélange polymère, pour essayer d'expliquer la tendance de séparation de phase entraînant la formation d'excimères.

I.8. Références des articles

Les références complètes des différents articles constituant cette thèse ainsi que leur situation au moment du dépôt et la contribution des différents auteurs sont énoncées ci-dessous.

I. M. Amine Fourati, Thierry Maris, W. G. Skene, C. Géraldine Bazuin and Robert E. Prud'homme. Photophysical, Electrochemical and Crystallographic Investigations of the Fluorophore 2,5-Bis(5-*tert*-butyl-benzoxazol-2-yl)thiophene. Article (papier complet) publié dans Journal of Physical Chemistry B. J. Phys. Chem. B 2011, 115, 12362-12369.
J'ai préparé tous les échantillons (solutions, films, poudre et monocristaux) et effectué toutes les manipulations de caractérisation excepté la diffraction des rayons X et les calculs DFT, réalisés, respectivement, par Dr. Thierry Maris et Pr. W. G. Skene. J'ai également rédigé l'article.

II. M. Amine Fourati, W. G. Skene, C. Géraldine Bazuin and Robert E. Prud'homme. Photophysical and Electrochemical Investigations of the Fluorescent Probe, 4,4'-Bis(2-Benzoxazolyl)Stilbene. Article (papier complet) publié dans Journal of Physical Chemistry A. J. Phys. Chem. A, 2013, ASAP, DOI: 10.1021/jp312598c. Les diverses préparations et manipulations ont été effectuées par l'auteur de ces lignes excepté les expériences de DRX et de DOSY. Les calculs DFT ont été réalisés par Pr. W. G. Skene, qui m'a également permis l'accès à ses instruments. J'ai également analysé toutes les données et rédigé l'article.

III. M. Amine Fourati, Thierry Maris, C. Géraldine Bazuin and Robert E. Prud'homme. (E)-4,4'-Bis(1,3-benzoxazol-2-yl)-stilbene at 150 and 375 K. Article (papier court) publié dans Acta Crystallographica C. Acta Cryst. 2010, C66, o11-o14. La préparation des monocristaux ainsi que la rédaction de l'article ont été réalisées par l'auteur de cette thèse. La diffraction des rayons X a été effectuée par Thierry Maris.

IV. M. Amine Fourati, Christian Pellerin, C. Géraldine Bazuin and Robert E. Prud'homme. Infrared and Fluorescence Spectroscopy Investigation of the Orientation of Two Fluorophores in Stretched Polymer Films. Article (papier complet) publié dans Polymer 2013, 54, 730-736. La préparation des films polymères et la caractérisation ainsi que la rédaction de l'article sont le fruit de mon travail. Pr. Christian Pellerin m'a permis l'utilisation de ses instruments et a participé à l'interprétation des résultats.

V. M. Amine Fourati, C. Géraldine Bazuin and Robert E. Prud'homme. Self-Assembly of Molecular Probes as the Source of Time-Temperature Probes in Polyesters. Article (papier complet) prêt à être soumis. J'ai effectué toutes les manipulations de préparation et de caractérisation, et rédigé l'article.

I.9.Références

(1) Batchelder, D. N.; Bloor, D. *J. Phys. C: Solid State Phys.* **1978**, *11*, L629.

(2) Burns, A. R.; Carpick, R. W.; Sasaki, D. Y.; Shelnutt, J. A.; Haddad, R. *Trib. Let.* **2001**, *10*, 89.

(3) Burns, A. R.; Houston, J. E.; Carpick, R. W.; Michalske, T. A. *Langmuir* **1999**, *15*, 2922.

(4) Carpick, R. W.; Sasaki, D. Y.; Burns, A. R. *Trib. Let.* **2000**, *7*, 79.

(5) Carpick, R. W.; Sasaki, D. Y.; Burns, A. R. *Langmuir* **2000**, *16*, 1270.

(6) Carpick, R. W.; Sasaki, D. Y.; Marcus, M. S.; Eriksson, M. A.; Burns, A. R. *J. Phys. Condens. Matter.* **2004**, *16*, R679.

(7) Tomioka, Y.; Tanaka, N.; Imazeki, S. *J. Chem. Phys.* **1989**, *91*, 5694.

(8) Lee, S. B.; Koepsel, R. R.; Russell, A. J. *Nano Lett.* **2005**, *5*, 2202.

(9) Spanggaard, H.; Jorgensen, M.; Almdal, K. *Macromolecules* **2003**, *36*, 1701.

(10) Kim, S. J.; Reneker, D. H. *Polym. Bull.* **1993**, *31*, 367.

(11) Hubner, J.; Chen, L.; Liu, Y.; Schanze, K.; Ifju, R.; Nicolosi, J.; El-Ratal, W. *Exp. Mech.* **2005**, *45*, 137.

(12) Hubner, J. P.; Ifju, P. G.; Schanze, K. S.; Jiang, S.; Liu, Y.; El-Ratal, W. *AIAA Journal* **2004**, *42*, 1662.

(13) Todres, Z. V. *J. Chem. Res.* **2004**, *2*, 89.

(14) Rohrig, U. F.; Troppmann, U.; Frank, I. *Chem. Phys.* **2003**, *289*, 381.

(15) Naciri, J.; Weiss, R. G. *Macromolecules* **1989**, *22*, 3928.

(16) Lowe, C.; Weder, C. *Adv. Mater.* **2002**, *14*, 1625.

(17) Pucci, A.; Bertoldo, M.; Bronco, S. *Macromol. Rapid Commun.* **2005**, *26*, 1043.

(18) Crenshaw, B. R.; Burnworth, M.; Khariwala, D.; Hiltner, A.; Mather, P. T.; Simha, R.; Weder, C. *Macromolecules* **2007**, *40*, 2400.

(19) Crenshaw, B. R.; Weder, C. *Chem. Mater.* **2003**, *15*, 4717.

(20) Kinami, M.; Crenshaw, B. R.; Weder, C. *Chem. Mater.* **2006**, *18*, 946.

(21) Kunzelman, J.; Crenshaw, B. R.; Kinami, M.; Weder, C. *Macromol. Rapid Comm.* **2006**, *27*, 1981.

(22) Crenshaw, B. R.; Weder, C. *Adv. Mater.* **2005**, *17*, 1471.

(23) Lott, J.; Weder, C. *Macromol. Chem. Phys.* **2010**, *211*, 28.

(24) Kunzelman, J.; Chung, T.; Matherx, P. T.; Weder, C. *J. Mater. Chem.* **2008**, *18*, 1082.

(25) Crenshaw, B. R.; Weder, C. *Macromolecules* **2006**, *39*, 9581.

(26) Pucci, A.; Di Cuia, F.; Signori, F.; Ruggeri, G. *J. Mater. Chem.* **2007**, *17*, 783.

(27) Pucci, A.; Signori, F.; Bizzarri, R.; Bronco, S.; Ruggeri, G.; Ciardelli, F. *J. Mater. Chem.* **2010**, *20*, 5843.

(28) Pucci, A.; Cappelli, C.; Bronco, S.; Ruggeri, G. *J. Phys. Chem. B* **2006**, *110*, 3127.

(29) Pucci, A.; Ruggeri, G.; Bronco, S.; Bertoldo, M.; Cappelli, C.; Ciardelli, F. *Prog. Org. Coat.* **2007**, *58*, 105.

(30) Donati, F.; Pucci, A.; Boggioni, L.; Tritto, I.; Ruggeri, G. *Macromol. Chem. Phys.* **2009**, *210*, 728.

(31) Pucci, A.; Donati, F.; Ruggeri, G.; Ciardelli, F. *e-Polymers*, 2009; *58*.

(32) Donati, F.; Pucci, A.; Cappelli, C.; Mennucci, B.; Ruggeri, G. *J. Phys. Chem. B* **2008**, *112*, 3668.

(33) Pucci, A.; Ruggeri, G.; Bronco, S.; Signori, F.; Donati, F.; Bernabò, M.; Ciardelli, F. *Prog. Org. Coat.* **2011**, *72*, 21.

(34) Donati, F.; Pucci, A.; Ruggeri, G. *Phys. Chem. Chem. Phys.* **2009**, *11*, 6276.

(35) Balamurugan, S. S.; Bantchev, G. B.; Yang, Y. M.; McCarley, R. L. *Angew. Chem. Int. Ed.* **2005**, *44*, 4872.

(36) Beck, J. B.; Rowan, S. J. *J. Am. Chem. Soc.* **2003**, *125*, 13922.

(37) Chandrasekharan, N.; Kelly, L. A. *J. Am. Chem. Soc.* **2001**, *123*, 9898.

(38) Ellison, C. J.; Torkelson, J. M. *J. Polym. Sci., Part B: Polym. Phys.* **2002**, *40*, 2745.

(39) Leclerc, M. *Adv. Mater.* **1999**, *11*, 1491.

(40) Seeboth, A.; Lötzsch, D. *Encyclopedia of Polymer Science and Technology*; 3rd ed.; Wiley-Interscience: New York, 2003, *12*, 143.

(41) Uchiyama, S.; Matsumura, Y.; de Silva, A. P.; Iwai, K. *Anal. Chem.* **2003**, *75*, 5926.

(42) van den Berg, O.; Sengers, W. G. F.; Jager, W. F.; Picken, S. J.; Wuebbenhorst, M. *Macromolecules* **2004**, *37*, 2460.

(43) Wang, Y.; Archambault, N.; Marold, A.; Weng, L.; Lucht, B. L.; Euler, W. B. *Macromolecules* **2004**, *37*, 5415.

(44) Crenshaw, B. R.; Kunzelman, J.; Sing, C. E.; Ander, C.; Weder, C. *Macromol. Chem. Phys. Chem.* **2007**, *208*, 572.

(45) Edrington, A. C.; Urbas, A. M.; DeRege, P.; Chen, C. X.; Swager, T. M.; Hadjichristidis, N.; Xenidou, M.; Fetters, L. J.; Joannopoulos, J. D.; Fink, Y.; Thomas, E. L. *Adv. Mater.* **2001**, *13*, 421.

(46) Foulger, S. H.; Jiang, P.; Ying, Y. R.; Lattam, A. C.; Smith, D. W.; Ballato, J. *Adv. Mater.* **2001**, *13*, 1898.

(47) Foulger, S. H.; Jiang, P.; Lattam, A. C.; Smith, D. W.; Ballato, J. *Langmuir* **2001**, *17*, 6023.

(48) Lawrence, J. R.; Shim, G. H.; Jiang, P.; Han, M. G.; Ying, Y. R.; Foulger, S. H. *Adv. Mater.* **2005**, *17*, 2344.

(49) Lu, Y. F.; Yang, Y.; Sellinger, A.; Lu, M. C.; Huang, J. M.; Fan, H. Y.; Haddad, R.; Lopez, G.; Burns, A. R.; Sasaki, D. Y.; Shelnutt, J.; Brinker, C. J. *Nature* **2001**, *410*, 913.

(50) Nallicheri, R. A.; Rubner, M. F. *Macromolecules* **1991**, *24*, 517.

(51) Rubner, M. F. *Macromolecules* **1986**, *19*, 2114.

(52) Rubner, M. F. *Macromolecules* **1986**, *19*, 2129.

(53) Albert, K. J.; Lewis, N. S.; Schauer, C. L.; Sotzing, G. A.; Stitzel, S. E.; Vaid, T. P.; Walt, D. R. *Chem. Rev.* **2000**, *100*, 2595.

(54) McQuade, D. T.; Pullen, A. E.; Swager, T. M. *Chem. Rev.* **2000**, *100*, 2537.

(55) Potyrailo, R. A. *Angew. Chem. Int. Ed.* **2006**, *45*, 702.

(56) Natansohn, A.; Rochon, P. *Chem. Rev.* **2002**, *102*, 4139.

(57) Shibaev, V.; Bobrovsky, A.; Boiko, N. *J. Photochem. Photobiol., A* **2003**, *155*, 3.

(58) Wigglesworth, T. J.; Myles, A. J.; Branda, N. R. *Eur. J. Org. Chem.* **2005**, 1233.

(59) Kunzelman, J.; Kinami, M.; Crenshaw, B. R.; Protasiewicz, J. D.; Weder, C. *Adv. Mater.* **2008**, *20*, 119.

(60) Kunzelman, J.; Crenshaw, B. R.; Weder, C. *J. Mat. Chem.* **2007**, *17*, 2989.

(61) Argun, A. A.; Aubert, P. H.; Thompson, B. C.; Schwendeman, I.; Gaupp, C. L.; Hwang, J.; Pinto, N. J.; Tanner, D. B.; MacDiarmid, A. G.; Reynolds, J. R. *Chem. Mater.* **2004**, *16*, 4401.

(62) Mortimer, R. J.; Dyer, A. L.; Reynolds, J. R. *Displays* **2006**, *27*, 2.

(63) Bamfield, P., *Chromic Phenomena*; RSC: Cambridge, **2001**.

(64) Jenekhe, S. A.; Kiserow, D. J. *Chromogenic Phenomena in Polymers: Tunable Optical Properties.* ACS Symposium Series: Washington, **2005**.

(65) Crano, J. C.; Guglielmetti, R. J., *Organic Photochromic and Thermochromic Compounds: Physicochemical Studies, Biological Applications and Thermochromism*; Springer: New York, **1999**.

(66) Freemantle, M. *Chem. Eng. News*, **2003**, *22*, 10.

(67) Trabesinger, W.; Renn, A.; Hecht, B.; Wild, U. P.; Montali, A.; Smith, P.; Weder, C. *J. Phys. Chem. B* **2000**, *104*, 5221.

(68) Förster, T.; Kasper, K. *Z. Physik. Chem. N. F.* **1954**, *1*, 275.

(69) Förster, T.; Kasper, K. *Z. Elektrochem. Angew. Physik. Chem.* **1955**, *59*, 976.

(70) Birks, J. B. *Photophysics of Aromatic Molecules*; Wiley-Interscience: Chichester, **1970**.

(71) Gilbert, A.; Baggott, J. *Essentials of Molecular Photochemistry*; Blackwell Science: Oxford, **1991**.

(72) Birks, J. B. *Rep. Prog. Phys.* **1975**, *38*, 903.

(73) Guillet, J. *Polymer Photophysics and Photochemistry*; Cambridge University Press: Cambridge, **1985**.

(74) Valeur, B. *Molecular Fluorescence: Principles and Applications*; Wiley-VCH: New York, **2002**.

(75) Spies, C.; Gehrke, R. *J. Phys. Chem. A* **2002**, *106*, 5348.

(76) van Hutten, P. F.; Krasnikov, V. V.; Brouwer, H. J.; Hadziioannou, G. *Chem. Phys.* **1999**, *241*, 139.

(77) Fitzgibbon, P. D.; Frank, C. W. *Macromolecules* **1981**, *14*, 1650.

(78) Turro, N. J.; Arora, K. S. *Polymer* **1986**, *27*, 783.

(79) Oyama, H. T.; Tang, W. T.; Frank, C. W. *Macromolecules* **1987**, *20*, 474.

(80) Wang, Y.; Morawetz, H. *Macromolecules* **1989**, *22*, 164.

(81) Zimerman, O. E.; Weiss, R. G. *J. Phys. Chem. A* **1998**, *102*, 5364.

(82) Vigil, M. R.; Bravo, J.; Baselga, J.; Yamaki, S. B.; Atvars, T. D. Z. *Curr. Org. Chem.* **2003**, *7*, 197.

(83) Gashgari, M. A.; Frank, C. W. *Macromolecules* **1981**, *14*, 1558.

(84) Semerak, S. N.; Frank, C. W. *Macromolecules* **1981**, *14*, 443.

(85) Gelles, R.; Frank, C. W. *Macromolecules* **1982**, *15*, 1486.

(86) Semerak, S. N.; Frank, C. W. *Macromolecules* **1984**, *17*, 1148.

(87) Johnson, G. E. *Macromolecules* **1980**, *13*, 839.

(88) Avis, P.; Porter, G. *J. Chem. Soc., Faraday Trans. 2* **1974**, *70*, 1057.

(89) Szadkowska-Nicze, M.; Wolszczak, M.; Kroh, J.; Mayer, J. *J. Photochem. Photobiol., A* **1993**, *75*, 125.

(90) Mishra, A.; Behera, R. K.; Behera, P. K.; Mishra, B. K.; Behera, G. B. *Chem. Rev.* **2000**, *100*, 1973.

(91) Phillips, D.; Roberts, A. J.; Soutar, I. *Macromolecules* **1983**, *16*, 1593.

(92) Chen, L. S.; Jin, X. G.; Du, J. H.; Qian, R. Y. *Makromol. Chem.* **1991**, *192*, 1399.

(93) Lewis, F. D.; Wu, T. F.; Burch, E. L.; Bassani, D. M.; Yang, J. S.; Schneider, S.; Jager, W.; Letsinger, R. L. *J. Am. Chem. Soc.* **1995**, *117*, 8785.

(94) Amicangelo, J. C. *J. Phys. Chem. A* **2005**, *109*, 9174.

(95) Birks, J. B.; Braga, C. L.; Lumb, M. D. *Proc. R. Soc. London, Ser. A* **1965**, *283*, 83.

(96) Kazzaz, A. A.; Munro, I. H. *Proc. Phys. Soc.* **1966**, *87*, 329.

(97) Birks, J. B.; Dyson, D. J.; Munro, I. H. *Proc. R. Soc. London, Ser. A* **1963**, *275*, 575.

(98) Birks, J. B.; Christophorou, L. G. *Spectrochim. Acta* **1963**, *19*, 401.

(99) Itoh, M.; Fuke, K.; Kobayashi, S. *J. Chem. Phys.* **1980**, *72*, 1417.

(100) Chandross, E. A. *J. Phys. Chem.* **1965**, *43*, 4175.

(101) Ichikawa, Y.; Mizukoshi, T. *Adv. Polym. Sci.* **2012**, *245*, 285.

(102) Fujimaki, T. *Polym. Degrad. Stabil.* **1998**, *59*, 209.

(103) Ishioka, R.; Kitakuni, E.; Ichikawa, Y. *Biopolymers* **2002**, *4*, 275.

(104) Oishi, A.; Zhang, M.; Nakayama, K.; Masuda, T.; Taguchi, Y. *Polym. J.* **2006**, *38*, 710.

(105) Jacquel, N.; Freyermouth, F.; Fenouillot, F.; Rousseau, A.; Pascault, J. P.; Fuertes, P.; Saint-Loup, R. *J. Polym. Sci., Part A: Polym. Chem.* **2011**, *49*, 5301.

(106) Deshpande, R.; Buwa, V. V.; Rode, C. V.; Chaudhari, R. V.; Mills, P. L. *Catal. Commun.* **2002**, *3*, 269.

(107) Minh, D.; Besson, M.; Pinel, C.; Fuertes, P.; Petitjean, C. *Top. Catal.* **2010**, *53*.

(108) Avenas, P. *Colloque de physique* **1978**, *39*, C2-37.

(109) Ward, I. M. *Structure and Properties of Oriented Polymers*; Chapman & Hall: London, **1997**.

(110) Bassett, D. C. *Macromol. Symp.* **2004**, *214*, 5.

(111) Keller, A.; Kolnaar, J. *Prog. Colloid Polym. Sci.* **1993**, *92*, 81.

(112) Kobayashi, K. *Polymer single Crystals*; Wiley: New York, **1963**.

(113) Peterlin, A. *Polym. Eng. Sci.* **1977**, *17*, 183.

(114) Fakirov, S. *Oriented Polymer Materials*; Hüthig & Wepf Zug: Oxford, **1986**.

(115) Kryszewski, M.; Uznanski, P. *Mol. Cryst. Liq. Cryst.* **1993**, *230*, 77.

(116) Uznanski, P.; Kryszewski, M.; Thulstrup, E. W. *Polish J. Chem.* **1993**, *67*, 949.

(117) Savitskii, A. V.; Petrov, A. V. *Vjsokomol. Soedin. A* **1985**, *27*, 1438.

(118) Smith, P. I.; Lemstra, P. J. *Colloid Polym. Sci.* **1980**, *258*, 891.

(119) Yalcin, B.; Cakmak, M. *J. Polym. Sci. Pol. Phys.* **2005**, *43*, 724.

(120) Konwerska-Hrabowska, J. *J. Mol. Struct.* **1978**, *45*, 95.

(121) Jang, Y. T.; Phillips, P. J.; Thulstrup, E. W. *Chem. Phis. Lett.* **1982**, *93*, 66.

(122) Parikh, D.; Phillips, P. J. *J. Chem. Phys.* **1985**, *83*, 1948.

(123) Lakowicz, J. R., *Principles of Fluorescence Spectroscopy*; Springer: New York, **2006**.

(124) Jablonski, A. *Z. Phys.* **1935**, *94*, 139.

(125) Burdette, S. C.; Walkup, G. K.; Spingler, B.; Tsien, R. Y.; Lippard, S. J. *J. Am. Chem. Soc.* **2001**, *123*, 7831.

(126) Rusalov, M. V.; Druzhinin, S. I.; Uzhinov, B. M. *J. Fluoresc.* **2004**, *14*, 193.

(127) Schäfer, F. P.; Drexhage, K. H. *Dye Lasers*; Springer-Verlag: Berlin, **1977**.

(128) Buffeteau, T.; Desbat, B.; Pézolet, M.; Turlet, J. M. *J. Chem. Phys.* **1993**, *90*, 1467.

(129) Liang, Y.; Mauran, D.; Prud'homme, R. E.; Pellerin, C. *Appl. Spectrosc.* **2008**, *62*, 941.

(130) Jang, Y. T.; Phillips, P. J.; Thulstrup, E. W. *Chem. Phys. Lett.* **1982**, *93*, 66.

(131) Mark, H. F. *Encyclopedia of Polymer Science and Engineering*; John Wiley & Sons: New York, **1985**.

(132) Pina, J.; Seixas de Melo, J.; Burrows, H. D.; Bilge, A.; Farrell, T.; Forster, M.; Scherf, U. *J. Phys. Chem. B*. **2006**, *110* 15100.

(133) Zhang, X.; Johnson, J. P.; Kampf, J. W.; Matzger, A. J. *Chem. Mater.* **2006**, *18* 3470.

(134) Jagt, H.; Dirix, Y.; Hikmet, R.; Bastiaansen, C. *Adv. Mater.* **1998**, *10*, 934.

(135) Dirix, Y.; Bastiaansen, C.; Caseri, W.; Smith, P. *Mater. Res. Soc. Symp. Proc.* **1999**, *559*, 147.

(136) Tirelli, N.; Amabile, S.; Cellai, C.; Pucci, A.; Regoli, L.; Ruggeri, G.; Ciardelli, F. *Macromolecules* **2001**, *34*, 2129.

(137) Montali, A.; Bastiaansen, C.; Smith, P.; Weder, C. *Nature* **1998**, *392*, 261.

(138) Dirix, Y.; Trevoort, T.; Bastiaansen, C. *Macromolecules* **1997**, *30*, 2175.

(139) Pucci, A.; Moretto, L.; Ruggeri, G.; Ciardelli, F. *e-Polymers*, **2002**; *15*.

CHAPITRE II: Photophysical, Electrochemical and Crystallographic Investigations of the Fluorophore 2,5-Bis(5-*tert*-butyl-benzoxazol-2-yl)thiophene*

Abstract

The photophysics of 2,5-bis(5-*tert*-butyl-benzoxazol-2-yl)thiophene (BBT) were investigated for assessing its limitations for use as a universal fluorophore and as a viable sensor for both polymeric and solution studies. This is of importance given the limitations of currently used materials. BBT's steady-state and time-resolved fluorescence were additionally investigated to correlate its solid-state features, observed by fluorescence spectroscopy when mixed in poly(1,4-butylene succinate) (PBS) films, with its single crystal characteristics. The conjugated fluorophore was found to be highly fluorescent, with absolute quantum yields of (Φ_{fl}) $\geq$ 0.60. The Φ_{fl} values were high, regardless of solvent polarity and proticity and whether alone or in polymeric films. The major competitive fluorescence quenching pathway was found to occur by intersystem crossing to the triplet state. This was confirmed by laser flash photolysis in which the BBT triplet absorbed at 500 nm. The triplet transient was confirmed by quenching studies with 1,3-cyclohexadiene. Meanwhile, nonradiative deactivation of BBT's singlet excited state by internal conversion was found to be negligible. In solution and especially when distributed in semicrystalline PBS, BBT exhibits spectral changes and a bathochromic shift as a function of concentration due to aggregation of ground state molecules, which is present even at low BBT concentrations. Consistent monoexponential lifetimes on the order of ~2 ns were observed regardless of solvent and independent of both the excitation wavelength and concentration.

---

*Fourati, M. A., Maris, T., Skene, W. G., Bazuin, C. G. and Prud'homme, R. E., *J. Phys. Chem. B* **2011**, *115*, 12362-12369. 10.1021/jp207136K.

The constant excited state kinetics confirms the absence of a singlet excited state deactivation by excimer formation. The electrochemistry of BBT demonstrated that it is irreversibly oxidized and the resulting radical cation is unstable. Conversely, the cathodic process, resulting in the radical anion, is reversible, confirming its n-doping character. Crystallographic studies revealed that the planes described by the benzoxazolyl moieties are twisted from the plane described by the central thiophene. Several weak C–H···π and π-π intermolecular interactions were also observed. BBT's high solubility in common solvents combined with its measured enhanced opto-electronic properties make it a candidate as a universal fluorophore reference and smart material for both polymeric and solution studies.

II.1. Introduction

4,4'-Bis(2-benzoxazolyl)stilbene (BBS) has interesting optical properties that have led to its use as photoactive switches[1,2] and as an optical brightener for textiles,[3] in detergents and other materials.[4] These properties have also made it ideal for use in smart materials by probing temperature and deformation in polymer films,[5-7] upon formation or breaking of BBS excimers, respectively, leading to a color change under UV illumination. Despite these spectroscopic advantages, a major drawback of BBS is its limited solubility in only high-boiling chlorinated solvents, specifically hot tetrachloroethane. Moreover, such solvents are both toxic and expensive, which restricts the usefulness of BBS. The stillbenoid structure of the latter further provides an efficient fluorescence quenching mode possible by *E-Z* photoisomerization.[8] This excited state quenching process results in low fluorescence quantum yields in solution and further limits the usefulness of BBS in certain fields. Therefore, a fluorophore exhibiting solubility in a broad range of solvents with consistent high fluorescence yields that does not suffer from the limitations of BBS is required.

In contrast to BBS, 2,5-bis(5-tert-butyl-benzoxazol-2-yl)thiophene (BBT) is soluble in a wide range of organic solvents. Moreover, BBT cannot photoisomerize, which can increase the chances for an intrinsic fluorescence in solution. It also absorbs and emits in

the visible owing to its extended π-conjugation. As a result of its collective optical properties that can be visibly tracked by the naked eye concomitant to its solubility in a broad range of process compatible solvents, BBT has found many optical applications. These include the use as an optical brightener,[9] whitening agent in many polymers and textiles[10] in addition to uses in various opto-electronic applications.[11-21] BBT further shows excellent heat stability and it can be used to improve the color of various plastics.

The similar optical properties of BBT and BBS, but the much wider solubility range of BBT, combined with its inherent fluorescence, make BBT a potential replacement of BBS. Yet, depsite BBT's use in various applications because of its spectroscopic and thermal properties, no extended opto-electrochemical studies have been undertaken. In particular, it would be beneficial to probe the photophysics of BBT and examine its solvent dependent fluorescence. Such studies are pivotal for determining the fluorescence limitations of BBT and for its use as a universal fluorophore. Here, we report the opto-electrochemical and extensive photophysical properties of BBT, including its crystallographic data. Our purpose is to study in depth the BBT characteristics to correlate its solid-state properties, observed by fluorescence spectroscopy when mixed in poly(1,4-butylene succinate) (PBS) films, with its single crystal features. These features motivate a characterization as well as an investigation of the BBT photophysical properties to study the possibility of using BBT as a potential substitute of BBS.

II.2. Experimental Section

Materials

4,4'-Bis(2-benzoxazolyl)stilbene (97%, melting point > 300 °C) and 2,5-bis(5-*tert*-butyl-benzoxazol-2-yl)thiophene (99%, melting point ~ 200 °C) were purchased from Aldrich Chemicals and used without further purification.

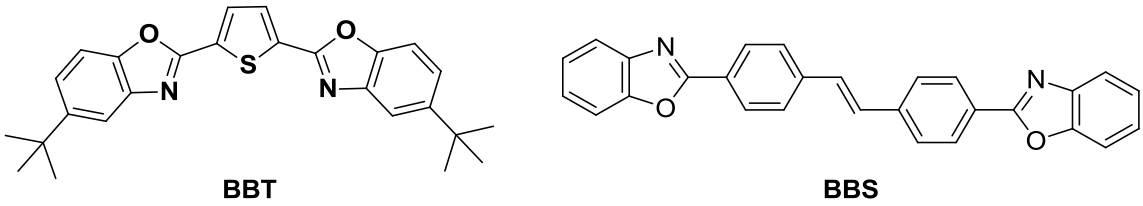

Chart II.1. Structures of 2,5-bis(5-*tert*-butyl-benzoxazol-2-yl)thiophene (BBT) and 4,4'-bis(2-benzoxazolyl)stilbene (BBS).

Poly(1,4-butylene succinate) (PBS) ("Bionolle 1001") was graciously supplied by Showa Highpolymer Company (Japan). PBS is a semi-crystalline polymer, used primarily for the manufacturing of films and packaging, and is degradable in compost or activated sludge. It is characterized by a glass transition temperature of -34 °C and a melting temperature of 113 °C.

Film Preparation

PBS-BBT films were prepared by melt-processing in a DDRV501/DIGI-SYS Plasti-Corder Brabender mixer by mixing ~20 g of PBS and 0.02 to 2 wt % of BBT at 200 °C, at 50 rpm, for 10 min. The obtained material was compressed and molded between two aluminum foils in a Carver Laboratory Press at 200 °C, under a pressure of 5 tons. The samples were then introduced in a cold press and were left to cool slowly to room temperature before removal from the press, under a pressure of 2 tons. Films with thicknesses of 60─120 μm were obtained.

Spectroscopic Measurements

Absorption measurements were done on a Varian Cary-500 UV-visible spectrometer, and the solvent absorption spectra were subtracted from the spectra of the analyzed samples. Fluorescence emission spectra were recorded at ambient temperature in 10 mm cuvettes exciting at the corresponding absorption maximum with an Edinburgh Instruments FLS-920 combined steady-state and time-resolved fluorometer. Both the front-face and 90^{o} geometries were used for solution fluorescence studies. Meanwhile, the front-face geometry was exclusively used for both polymeric films and powder (prepared by

using a press for KBr pellets to get compacted pastilles). The fluorescence lifetimes were measured according to standard time-correlated single photon counting methods with the FLS-920 by fitting with a monoexponential decay function. The calculated values have an experimental error of ~10%. Fluorescence quantum yields were used to quantify the efficiency of the emission process by taking the ratio of photons absorbed to photons emitted through fluorescence at a particular wavelength in the same period of time. Absolute fluorescence quantum yields were measured using an integrating sphere that was calibrated with basic ethanolic fluorescein. These were done by integrating over the entire emission spectrum from baseline to baseline, as previously studied.[22] Phosphorescence emission spectra were recorded at 77 K in a solid matrix of 4:1 ethanol/methanol using a Cary Eclipse phosphorescence spectrophotometer.

Peak decomposition was carried out with the Origin Pro8 software by increasing gradually the number of peaks until obtaining a peak sum similar to the studied spectrum. HOMO and LUMO molecular orbitals were calculated semi-empirically using DFT methods available in Spartan 06 with the 6-31g* basis set. The bond angles, distances, torsions, and other parameters used for the theoretical calculations were experimentally derived from the X-ray data for BBT.

Laser Flash Photolysis (LFP)

The triplet–triplet absorption spectra were measured in anhydrous acetonitrile using a Luzchem mini-LFP system, excited at 355 nm from the third harmonic of a Continuum Nd-YAG Sure-lite laser using a 175 W xenon lamp. An average of 15 shots per wavelength was used for generating the transient absorption spectrum. The samples were dissolved in anhydrous acetonitrile in static quartz cuvettes and assured to have an absorbance of < 0.4. All samples were purged with nitrogen for at least 20 min before LFP analyses.

Crystallographic Study

BBT light green plate crystals suitable for X-ray diffraction analysis were obtained by slow evaporation from a saturated 1,2-dichlorobenzene solution. The single crystal study

was carried out by using a Bruker Microstar diffractometer with a rotating anode generator producing CuK_α radiation, a kappa goniometer and a CCD Platinum 135 detector.

H atoms were positioned geometrically and refined with a riding model, with C—H distances of 0.95 Å and Uiso (H) values constrained to be 1.2 times Ueq of the carrier atom.

II.3. Results and Discussion

Absorbance and Emission Studies

Solution absorbance studies of both BBS and BBT were first done in order to determine the appropriate excitation wavelength for fluorescence studies.

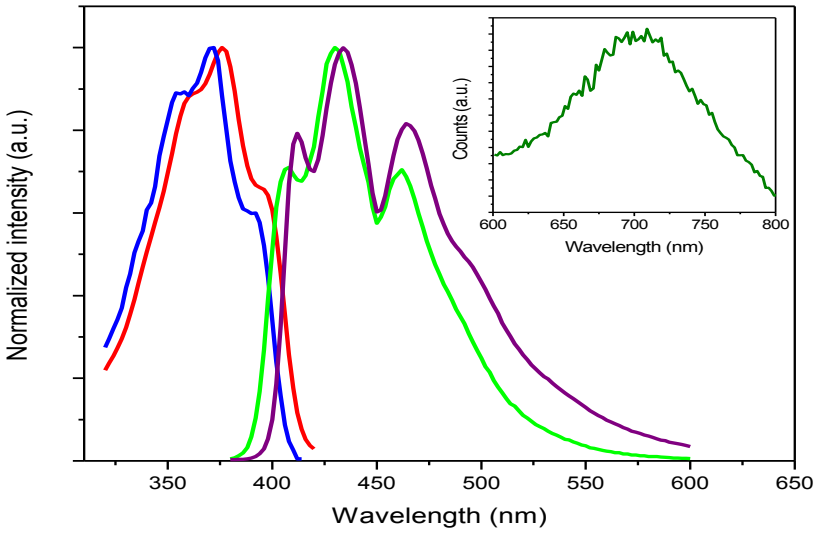

Figure II.1. Normalized BBT and BBS absorption and emission spectra in tetrachloroethane: blue, BBT absorption; red, BBS absorption; green, BBT emission at λ_{exc} = 378 nm; purple, BBS emission at λ_{exc} = 374 nm. Inset: BBT phosphorescence emission in a 4:1 ethanol/methanol matrix at 77 K.

According to Figure II.1, both well-known fluorophores, BBS and BBT, are characterized by virtually identical features. Indeed, the absorption spectra exhibit three well-defined peaks at 354, 374 and 392 nm for BBS and at 358, 378 and 398 nm for BBT. The emission spectra also show three well-defined vibronic peaks located at 412, 434 and

464 nm for BBS and at 408, 430 and 462 nm for BBT. It can be seen that the fluorescence spectra are a symmetric image of the absorption spectra (Kasha's law).[23] It should be noted that there was no distinct change in absorption peaks for both compounds in tetrachloroethane with increasing concentration. Moreover, both fluorophores are highly conjugated and exhibit a high fluorescence. The BBS dye is visually yellow, while BBT is green, which enables its use as color indicator. This comparison between BBS and BBT, showing their similarity, indicates that it might be possible, from a spectroscopic point of view, to replace BBS by BBT. An advantage of BBT is its high solubility in standard organic solvents, in constrast to BBS that is only sparingly soluble in hot tetrachloroethane and other high-boiling chlorinated solvents.

Fluorescence Investigation

To study the BBT characteristics in comparison with BBS, its photophysical properties were measured in a series of 12 solvents of varying polarity for investigating their effect on the BBT ground and excited states. Slight bathochromic shifts have been observed in all solvents with a shift in absorbance of 8 nm between acetonitrile and 1,2-dichlorobenzene, and a shift in fluorescence of 14 nm upon increasing polarity from cyclohexane to tetrachloroethane (Table II.1). A rough estimate of the energy gap (E_g = 3.1 eV) is derived from the onset of the absorption in the red region of the spectrum. The absolute energy difference between the ground (HOMO) and excited (LUMO) states can be calculated from the intercept of the normalized absorption and emission spectra. According to the spectroscopically measured values, the energy gaps are unaffected by the solvent polarity and concentration. Quantum yields of the order of 0.6─0.7 were measured for BBT concentrations ranging up to 6 wt % in PBS films. The fluorescence yield was found to be invariable either with freshly prepared PBS-BBT-2 wt % films or films stretched to a local strain of either 190 or 230%. The consistent emission yields for relaxed and stretched films imply the absence of any molecular rearrangement induced by the polymer deformation. This is probably due to the banana shape of the BBT molecule, encouraged by the 2,5-disubstitution of the central thiophene aromatic ring, and mainly to the terminal *t*-butyl

groups, which weaken the π-π intermolecular interactions and avoid the formation of BBT excimers. Unlike BBT, BBS neighbouring molecules can easily form π-π and C-H···π intermolecular interactions[24] that facilitate the formation of BBS excimers and thus their use as molecular probes in polymeric smart materials, based on a color change that remains unfortunately absent for BBT even by increasing the fluorophore concentration.

Table II.1. BBT spectroscopic data measured in different solvents at $\lambda_{exc} = \lambda_{ab}$

	ε_{max} [a] (M^{-1} cm^{-1})	λ_{ab} [b] (nm)	λ_{fl} [c] (nm)	Φ_{fl} [d]			
[BBT] (mM)				0.002	0.02	0.2	2
1,2-Dichlorobenzene	33000	379	437			0.96	0.93
Acetonitrile	20000	371	432	0.76	0.74	0.73	
Butanol	42000	375	434	1	0.87	0.83	0.83
Ethanol	35000	373	434	1	0.82	0.78	
EtOH/MeOH 4:1	26000	373	434		0.75	0.77	
Methyl cyclohexane	37000	373	426	0.66	0.66	0.58	0.54
DMF	35000	374	434	0.87	0.83	0.82	0.80
Cyclohexane	52000	372	426	0.80		0.68	
Benzene	27000	377	434	0.82	0.84	0.80	0.75
Toluene	38000	376	434	1	0.93	0.87	0.81
Tetrachloroethane	31000	378	440	1	0.97	0.91	0.88
THF	35000	374	432	0.78	0.77	0.75	0.68

[a]Molar absorptivity. [b]Maximum absorption. [c]Maximum fluorescence. [d]Absolute quantum yields were calculated with an integrating sphere.

Quantum yield measurements are usually done by relative actinometry. An actinometer is a chemical system that undergoes a light-induced reaction at a certain wavelength for which the quantum yield is accurately known.[25] The limitation of this method is that the reference must both absorb and emit within the same wavelength as the compound to be measured, in addition to having approximately the same emission yield. Moreover, the absolute quantum yield of the reference must be accurately known for a given solvent. The cumulative experimental errors for relative actinometry lead to quantum yields that can be known to within 80% accuracy at best.[26] Absolute and accurate quantum yields can, however, be obtained with an integrating sphere.[27] Given that previously

reported BBT emission yields were done by relative actinometry in a limited number of solvents, we measured its absolute quantum yields in twelve different solvents.

It is evident from Table II.1 that BBT fluoresces strongly and is independent of solvent polarity and proticity, which may allow its use as a suitable replacement for conventional fluorophores such as BBS. Moreover, BBT's thermal stability, which excludes complications due to dark reactions, its direct spectrophotometric analysis as well as its commercial availability,[25] in addition to its high fluorescence quantum yields whatever its state, make it a suitable reference for actinometric fluorescence studies. These collective properties make BBT an attractive universal fluorophore and sensor probe. For solutions having a quantum yield of 1, deactivation occurs only by fluorescence but the measured quantum yields are less than unity in most solvents, implying the presence of deactivation modes other than fluorescence. Additional spectroscopic modes were subsequently investigated in order to assign the competing fluorescence deactivation modes and for ensuring that these would not eventually suppress the desired fluorescence under specific conditions.

Temperature-dependent fluorescent studies were subsequently undertaken in order to assign the competing excited state deactivation processes responsible for the observed fluorescence below unity (vide supra). At 77 K, deactivation modes by bond rotations are normally suppressed and internal conversion (IC) deactivation can therefore be calculated at this temperature according to $\Phi_{IC} \approx \Phi_{fl}$ (77 K) $- \Phi_{fl}$ (RT). We observed that the fluorescence quantum yield increased by 9%, from 0.75 to 0.82, in ethanol/methanol matrix at 77 K relative to that at room temperature. The observed increase confirms that deactivation by IC occurs, albeit only a minor energy dissipation pathway, probably via the thiophene–oxazole bond.

Solution, Solid-State, and Powder Fluorescence

The photophysical properties of BBT led us to study its optical and fluorescent properties in solution and in a polymer matrix, i.e., in poly(1,4-butylene succinate) (PBS). Like many other polymers, PBS is processed at temperatures well below the degradation

temperature of BBT (> 300 °C). Figure II.2 shows the fluorescence spectra of BBT at various concentrations in THF, or when incorporated into PBS as well as a powder. The fluorescence spectra of the lowest BBT concentration, in solution (2 μM) or into PBS (0.02 wt %), are characteristic of a well-defined vibronic structure, attributed to radiative transitions 0–0, 0–1, and 0–2 for BBT monomers. Intensity changes occur upon increasing the BBT concentration, since the first vibronic peak decreases considerably to become a shoulder and further disappears upon increasing the BBT concentration from 2×10^{-3} to 2 mM in THF or from 0.02 to 0.2 wt % or higher in PBS. A bathochromic shift also occurs for both the second, from 429 (at 0.02 wt %) to 448 nm (at 6 wt %), and third peaks, from 461 (at 0.02 wt %) to 476 nm (at 6 wt %), by increasing the BBT concentration (Figure II.2) while the first peak, after shifting from 406 to 412 nm, can no longer be followed. These two peaks are representative of relatively weak interactions when compared with the first peak. These emission spectral changes were observed whatever the proticity or polarity of the solvent (tested in all of the solvents listed in Table II.1) and regardless of the state (solution or solid). Therefore, the change in the intensity of the lowest-wavelength peak at 462 nm is not a consequence of solvent–solute interactions, as is frequently observed in protic solvents. Moreover, since the absorption spectrum remains unchanged even at high BBT concentrations, the disappearance of the high energy vibronic peak at 407 nm is not due to intermolecular interactions.

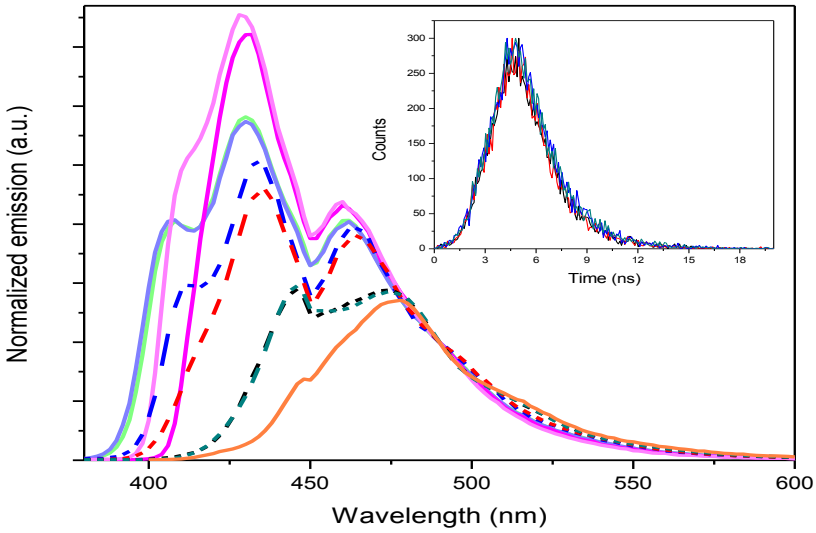

Figure II.2. Normalized BBT fluorescence spectra at λ_{exc} = 378 nm and at various BBT concentrations in THF (light green, 2 µM; blue-purple, 0.02 mM; magenta, 0.2 mM; light pink, 2 mM), when dispersed in polybutylene succinate films (blue, 0.02 wt %; red, 0.2 wt %; black, 2 wt %; dark cyan, 6 wt %) and as a powder (orange). Inset: BBT fluorescence kinetics monitored at 412 (black line), 432 (red line), 460 (blue line) and 500 nm (green line) in THF at ambient temperature at a concentration of 0.15 mM taking into account the IRF.

BBT has been widely used as an electron-transporting material interacting with a hole-transporting material, such as a polymer like poly(*N*-vinyl carbazole) (PVK) or a small molecule like *N*,*N'*-diphenyl-*N*,*N'*-bis(3-methylphenyl)-[1,1'-biphenyl]-4,4'-diamine.[13,18,19] This results in a transient donor–acceptor complex between the excited state of the donor (BBT) and the ground state of the acceptor.[28] The broad emission peak at ~ 500 nm might at first sight be attributed to such a transient complex. Both concentration-dependent emission and bimolecular lifetimes are expected for such a BBT excimer. However, the emission at 500 nm is present even at low concentrations, and it has a unimolecular lifetime. The measured lifetime of 1.7 ns is further comparable to that reported previously,[140] specific to BBT monomers. Interestingly, the measured unimolecular lifetime was also independent of the excitation wavelength and concentration (see Supporting

Information). The lifetime of each vibronic peak was also identical and independent of concentration (inset Figure II.2).

To ensure that the observed concentration dependent spectral trend was not a result of an artifact or from inner filter effects, the emission measurements in solution were additionally done using the front-face geometry. These undesired effects are significantly reduced with this geometry.[30] Consistent fluorescence between both the right-angle and front-face (see Supporting Information) excitation–emission geometries were observed and confirm that the concentration-dependent emission shifts are true effects. This was further corroborated with consistent bathochromic fluorescence shifts observed in both thin film and solid state that were also measured with the front-face geometry. Although the emission spectra were found to be independent of excitation wavelength, the excitation spectra were similar to the absorbance spectra. This suggests that the measured spectroscopic properties are those of the fluorophore and not from an artifact.

High quantum yields were also observed, regardless of concentration. These were calculated using an integrating sphere and by integrating over the entire range of the emission wavelengths relative to the scattering of the pure solvent.[22] The concentration-dependent spectral changes are similar to those observed for interchain π-stacking of conjugated polymers in thin films.[16,31] Although the concentration-dependent emission shifts of BBT are real, an inner filter effect cannot be entirely dismissed. This is in part because of the unknown effect of light scattering from BBT aggregates in PBS films. The collective spectroscopic data nonetheless suggest that the observed concentration-dependent spectral changes result from intermolecular interactions.

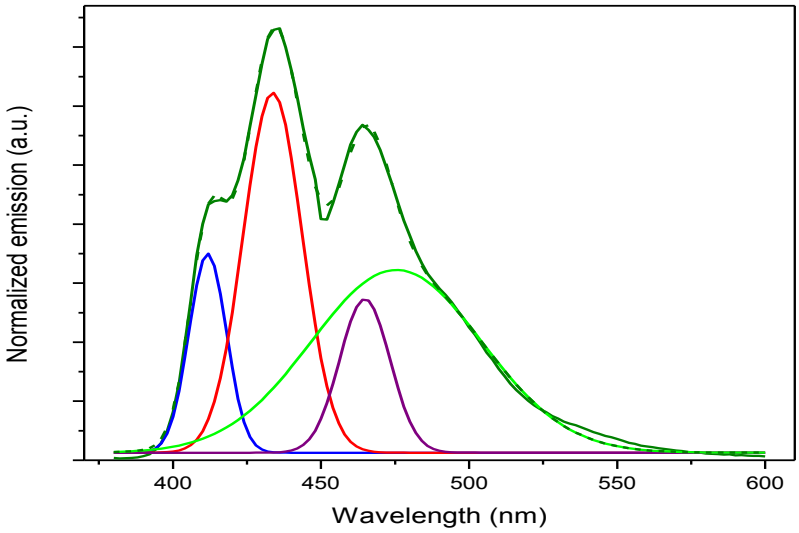

Figure II.3. Multipeak fitting of the fluorescence spectrum of PBS-BBT-0.02 wt % at λ_{exc} = 378 nm: olive, emission; blue, peak 1; red, peak 2; purple, peak 3; green, peak 4 ; - - -, peak sum.

To better understand the concentration dependent fluorescence, the PBS-BBT-0.02 wt % emission spectrum was decomposed and the relative distribution of the different peaks was calculated. As seen in Figure II.3, the emission spectrum can be decomposed into four discrete peaks. The three high-energy peaks are assigned to BBT monomers, whereas the lower energy one is ascribed to BBT aggregates; the aggregate band was found in the powder, in solution and in polymeric samples, whatever the BBT concentration. From its relative area, it is found that the aggregate component is small at the lowest concentration but increases by increasing the BBT concentration, suggesting that the number of molecules influencing each other increases, involving a widening of this band to become a continuum. Indeed, the aggregate band is a consequence of the proximity of the orbitals of the different molecules inducing a splitting of the HOMO and LUMO energy levels.[32]

A similar emission at 516 nm is observed in the powder fluorescence spectrum and is attributed to BBT aggregates from the stacking of neighboring molecules (vide infra). In addition, the red-shifted spectrum of the powder, compared with the solution spectra,

exhibits a shoulder at 448 nm and a well-defined peak at 478 nm, both belonging to the BBT monomers. BBT therefore exhibits both concentration and solution/PBS spectral shifts, confirming that it has local concentration probelike properties. No distinct fluorescence quenching has been observed within the concentration range in the polymeric state, confirming that PBS is an excellent host material to hold dye molecules such as BBT. On the other side, it is noteworthy that BBT is more easily dispersed in solution than in PBS, where the molecules are forced to come into contact with each other due to the PBS high crystallinity. Therefore, the emission spectra from low concentration solutions and films are very similar, as the aggregation is minimized. When the BBT concentration increases, there is a more pronounced bathochromic shift in solid-state films than in solution. This is essentially due to the increase of the π–π intermolecular interactions in polymeric films, while the molecular rotations and vibrations, which are constrained in the solid-state, slow down the relaxations and broaden the energy band.

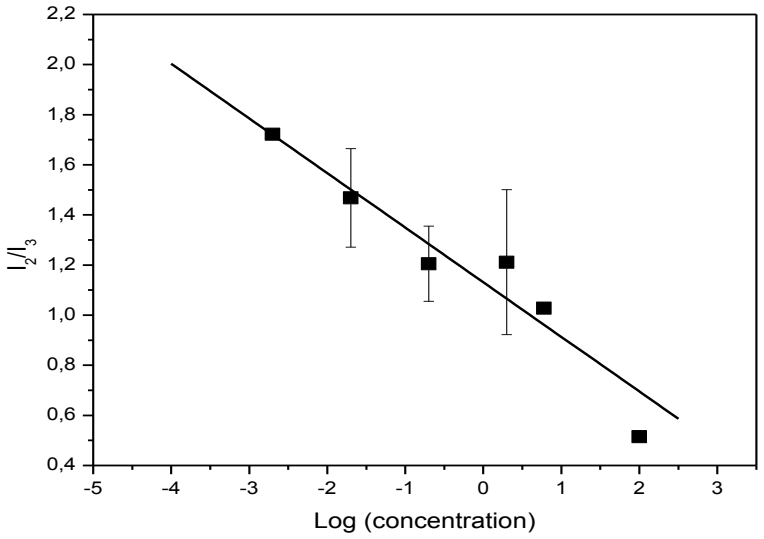

Figure II.4. I_2/I_3 ratio as a function of BBT concentration in both PBS film and THF.

Figure II.4 shows the I_2/I_3 ratio as a function of BBT concentration based on the average of three measurements. I_2/I_3 is the ratio of the intensity of the first and second fluorescence peaks, corresponding to the second and third vibronic transitions in the

emission spectrum. Since the I_2/I_3 ratio decreases logarithmically with increasing BBT concentration, it can qualitatively be used for determining the local BBT concentration and its solubility, especially in polymeric films. The photophysical data demonstrate that spectral changes induced by concentration or intermolecular interactions can be detected even at low BBT concentrations, proving its high sensitivity as a potential local concentration probe.

Laser Flash Photolysis

Although high fluorescence quantum yields of BBT were measured in various solvents, the less than unity values imply additional excited state deactivation modes other than fluorescence. Laser flash photolysis was subsequently used to probe BBT's excited state and to identify long-lived transients. This is of particular interest given that its photophysical properties such as its time-resolved and steady-state behaviors have not been previously investigated. Figure II.5 shows that direct excitation of BBT at 355 nm by laser flash photolysis produces a visible transient. To assign the strongly absorbing transient observed at 500 nm, it was quenched with successive additions of 1,3-cyclohexadiene (CHD). The transient intensity is then decreased while the lifetime is shortened with the addition of CHD, as shown in Figure II.2 and its inset, respectively. It can be concluded that the observed transient is a triplet given that it is quenched with the known triplet quencher (CHD), taken together with its first-order kinetics (τ_o = 14.4 μs). The triplet nature is further confirmed by the phosphorescence emission measured at 77 K (inset of Figure II.1).

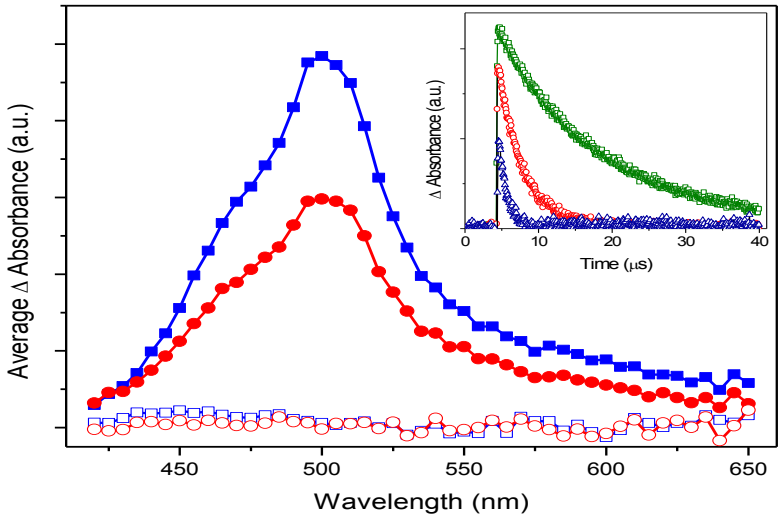

Figure II.5. Transient absorption spectra of BBT recorded in acetonitrile at 5.9 and 9.8 μs before (blue solid square and red solid circle, respectively) and after (blue open box and red open circle, respectively) adding 60 μL of 1,3-cyclohexadiene (CHD) after a laser pulse at 355 nm. Inset: Decay kinetics of BBT monitored at 500 nm before (green) and after adding 20 (red) and 60 (blue) μL of 1,3-cyclohexadiene as a triplet state quencher.

According to the energy conservation principle, that is, $\Phi_{fl} + \Phi_{IC} + \Phi_{ISC} \approx 1$, the singlet deactivation by intersystem crossing (ISC) to the triplet state can be approximated as contributing ~ 16% from the combined temperature-dependent fluorescence measurements. The observed triplet signal implies that BBT undergoes singlet deactivation by ISC. The collective steady-state and time-resolved measurements confirm that both nonradiative means, IC and ISC, are minor deactivation processes of the excited singlet manifold, relative to fluorescence. The simplified BBT Jablonski diagram for the deactivation processes and their estimated contributions are schematically depicted in Figure II.6.

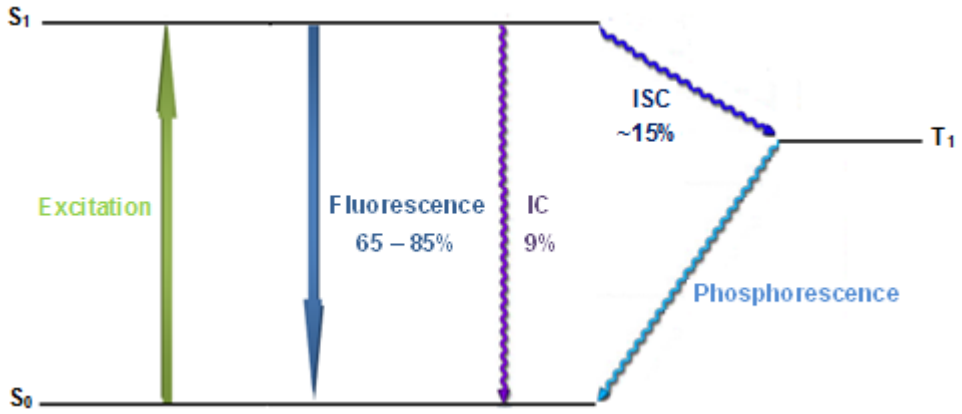

Figure II.6. Schematic representation of the BBT energy dissipating processes.

Cyclic Voltammetry

In addition to the photophysical properties of BBT, cyclic voltammetry was undertaken to probe the redox properties of BBT and to obtain important information relating to its stability at higher temperatures.

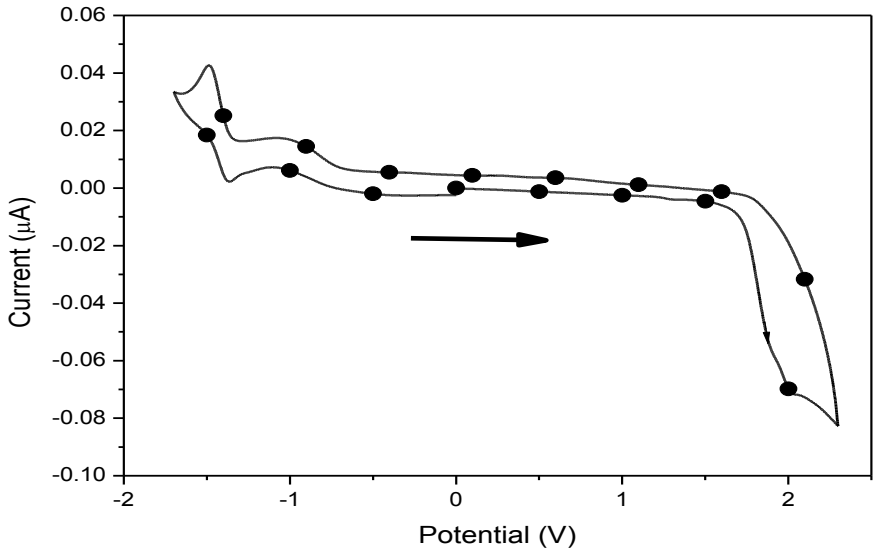

Figure II.7. Cyclic voltammogram of BBT recorded in acetonitrile at 100 mV/s against Ag/AgCl with Bu_4NPF_6 as the supporting electrolyte.

According to Figure II.7, BBT undergoes a one-electron oxidation process, demonstrating its p-doping-type behavior. The high oxidation potential implies that BBT is stable under ambient conditions and that it is unexpected to be oxidized at high temperatures. The electrochemical oxidation results in a highly reactive radical cation, confirmed by the irreversible behavior of cyclic voltammetry, regardless of the scan rate. Conversely, BBT is reversibly reduced at low potential, confirming its reversible n-doping character.

Table II.2. BBT electrochemical properties.

E_{ox}[a] /V	E_{red}[b] /V	HOMO/eV	LUMO/eV	E_g[c]/eV
1.99	-1.40	6.28	3.23	3.1

[a]Oxidation potential. [b] Reduction potential. [c] Electrochemical energy gap.

From the cyclic voltammetry data, the HOMO energy value can be calculated from the ionization potential (IP), according to IP = E_{onset}^{ox} + 4.4, where E_{onset}^{ox} is the oxidation potential onset in volts versus the SCE electrode. Similarly, the LUMO energy level is derived from the electron affinity (EA), calculated from the reduction onset potential (E_{onset}^{red}) according to EA = E_{onset}^{red} + 4.4. The HOMO and LUMO levels are reported in Table II.2, which shows that the measured electrochemical E_g thus calculated is equal to the spectroscopic E_g. The electrochemical and spectroscopic data confirm that BBT is highly conjugated. This is further supported by the theoretically calculated molecular orbitals, using DFT, depicted in Figure II.8. It is evident that the HOMO is delocalized across the entire molecule, responsible for BBT's high degree of conjugation. Conversely, the LUMO is located exclusively on the central thiophene.

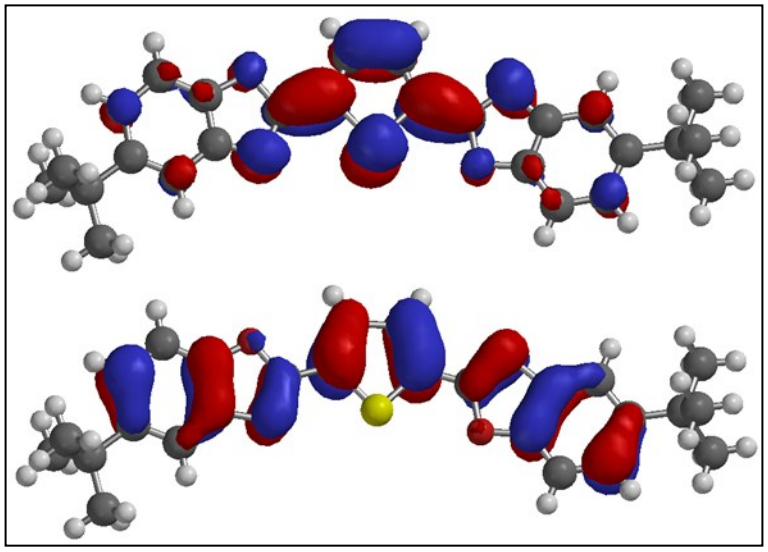

Figure II.8. BBT LUMO (top) and HOMO (bottom) features calculated by DFT, using the 6-31g* basis set and the X-ray crystallographic data.

Crystal Structure

The crystallographic properties of BBT, not determined to date, can complement the behavior found by fluorescence. BBT crystallizes in the monoclinic space group $P2_1/n$, with four molecules in the unit cell. The BBT molecular structure is characterized by a 2-fold rotation axis passing through the S atom and the midpoint of the C─C single bond in the thiophene ring, but this symmetry is not retained in the crystal phase. According to Figure II.9, the two benzoxazolyl rings exhibit a mutual antiorientation and the whole molecular symmetry is C1.

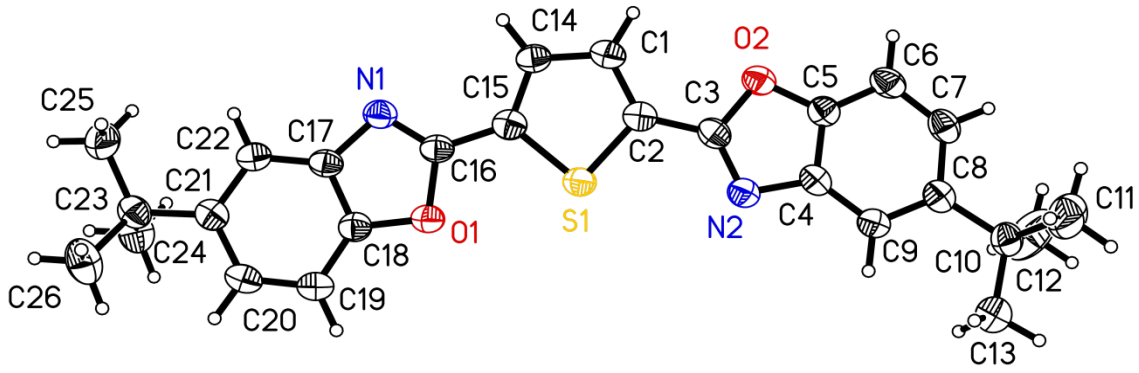

Figure II.9. BBT molecular structure, with atomic displacement parameter ellipsoids at the 50% probability level.

The S1···C2 and S1···C15 bond lengths [1.720 (2) and 1.723 (3) Å] are in good agreement with those found for other structures containing a substituted thiophene ring: 1.709 (2) and 1.709 (2) Å,[33] 1.722 (3) and 1.734 (3) Å,[34] 1.705 (3) and 1.712 (2) Å,[35] 1.726 (17) and 1.727 (18) Å,[36] and 1.707 (6) and 1.729 (6) Å.[37] Moreover, the C2···C3 and C15···C16 bond lengths [1.443 (4) and 1.436 (3) Å] are also comparable to those found in similar molecules [1.460 (2) and 1.455 (2) Å] for the 2,5-bis(1-butyl-benzimidazol-2-yl)thiophene[36] and [1.465 (8) and 1.426 (8) Å] for the 2,5-bis(4-biphenylyl)thiophene.[37]

The dihedral angles between the thiophene plane and benzene rings are 4.95 (12)° and 10.43 (12)°, and the dihedral angle between these two benzene rings is 11.35 (12)°. The benzoxazolyl ring systems are twisted by 4.99 (10)° and 10.26 (10)° out of the mean plane that passes through the thiophene ring. The whole molecule shows an important deviation from planarity, with the largest deviation from the mean plane of all non-H atoms of -1.7686 (26)° for atom C24. The unsymmetrical bow-shaped form of the molecule can be seen in Figure II.10. This shape is consistent with the results of a quantum mechanical calculation performed on a simplified model of BBT,[38] leading to a model in which the molecule adopts a complex banana-shaped structure due to the thiophene 2,5-disubstitution that limits the whole molecule planarity.

The dihedral angles between the oxazole and phenyl rings are small: 0.55 (12)° and 1.22 (13)°. The slight non-coplanarity of the aromatic rings in the solid state[13,39] helps in

minimizing intermolecular interactions, thus maintaining the π-orbital overlapping and the conjugation.[40]

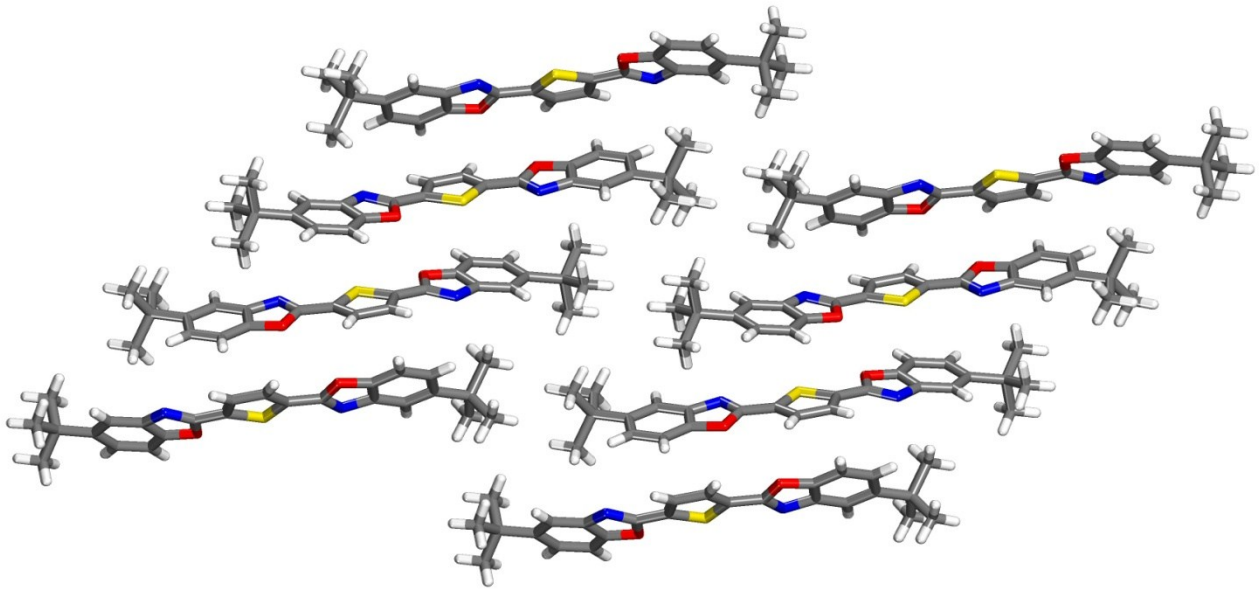

Figure II.10. Projection along the *a*-axis showing the BBT crystal packing.

The general crystallographic profile is characterized by a layered arrangement with the molecules aligned along the *c*-axis and a low degree of parallelism between them. These banana-shaped molecules exhibit particularly interesting features. The BBT structure is made from a network, alternating layers of molecules showing a limited degree of packing (Figure II.10). Within the layers, the molecules pack via moderate π—π stacking interactions. The π—stacked molecules are staggered relative to each other and overlap at a perpendicular distance of 4.21 (1) Å. These interactions involve a distance of 3.79 (1) Å between centroids of the five-membered ring of the benzoxazole group and the central thiophene ring. This stacking is limited by the very cumbersome *t*-butyl groups of two neighboring molecules that come into contact and prevent perfect overlap between the two layers. A similar stacking interaction was observed in 2,5-bis(2-cyano-2-thienylvinyl)thiophene between shifted thiophene rings featuring distances between aryl centroids of 3.78 and 3.91 Å.[41]

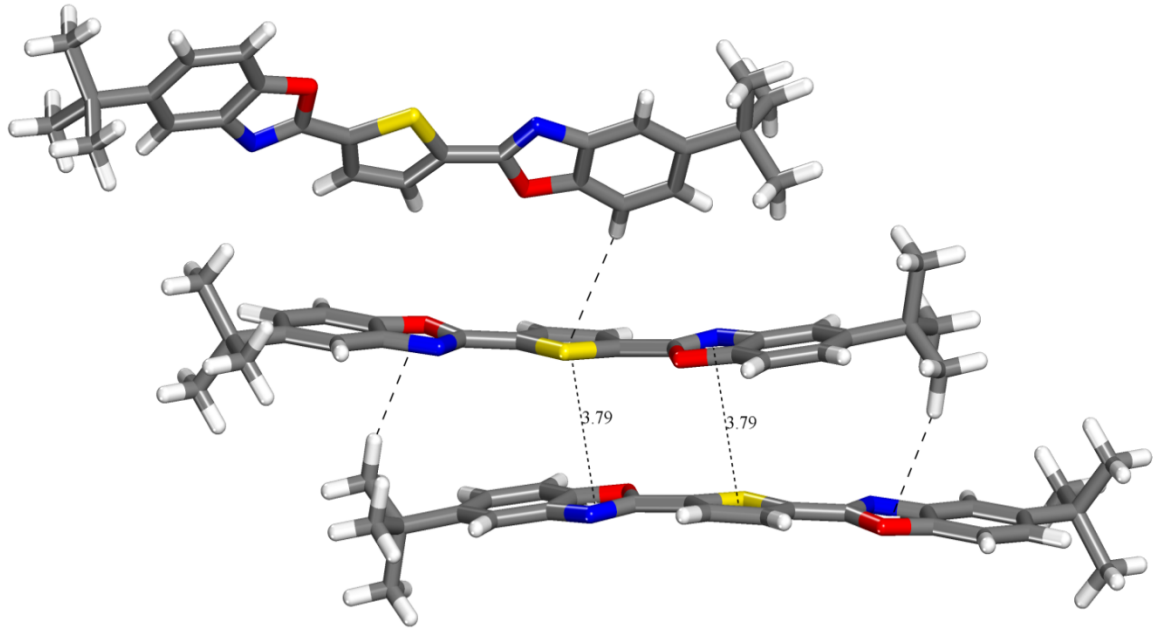

Figure II.11. Part of the BBT crystal structure, showing the π-stacking and the C─H···π interaction between two neighboring molecules. For clarity, H atoms bonded to C atoms that are not involved in the motif shown have been omitted. Featured interactions are shown as dashed lines.

The interaction between layers features a C─H···π contact (Figure II.11) involving both the thiophene ring and the oxazole ring separated by a distance of 2.82 (1) Å between the terminal hydrogen of the *t*-butyl group and the oxazole ring. The distance between the terminal hydrogen of the phenyl ring and the thiophene centroid is 2.81 (1) Å. Atoms C9 and C25 in the BBT molecule act as hydrogen-bond donors to the thiophene and oxazole rings of the molecule, respectively (Figure II.11), independent of the orientation of the aryl acceptors. A similar C─H···π intermolecular interaction was found in 3-(5-chloro-3-methyl-1-phenylpyrazol-4-yl)-1,5-di-2-thienylpentane-1,5-dione.[42] The fluorescence spectrum (Figure II.5) corroborates a similar arrangement involving limited and weak C─H···π and π─π-stacking interactions for the aggregates structure, as found in the extended three-dimensional structure of the crystalline material.

II.4. Conclusions

BBT is highly fluorescent and might be a suitable replacement for conventional fluorophores such as BBS. Its high fluorescence yield in most organic solvents, regardless of their polarity and proticity, as well as in polymeric films, further makes BBT a suitable fluorescence reference for actinometric fluorescence studies. BBT is also advantageous because of its photochemical and thermal inertness, in contrast to BBS, which undergoes deformation, temperature, and photoinduced conformational changes. BBT photophysical properties, such as its time-resolved and steady-state behaviors, have been investigated for the first time and reveal that, although the primary deactivation mode of the singlet excited state is by fluorescence, BBT also deactivates by both IC and ISC, albeit collectively < 35%. In solution and especially when distributed in semi-crystalline PBS, spectral changes and the bathochromic shift shown by BBT as a function of its concentration are due to aggregation of ground state molecules, with the absence of a singlet excited state deactivation by excimer formation confirmed by the monoexponential lifetime of 1.7 ns. The aggregate formation is relatively independent of the BBT concentration, which is in contrast with BBS that shows concentration-dependent excimer formation. The high fluorescence of BBT, which is solvent-independent, taken together with its high solubility in common organic solvents, makes it a viable sensor for polymeric and solution studies, and a potential substitute for the well-known fluorophore BBS, in addition to its probable use as a color indicator. The bent nature of BBT (observed by XRD), which is due to the twisting of the planes of the benzoxazolyl moieties from the plane made by the central thiophene, limits the number of possible intermolecular interactions making it inherently soluble in most organic solvents. This contrasts with its analogue, BBS, which is soluble only in hot highly-boiling chlorinated solvents such as tetrachloroethane.

Acknowledgements

The authors gratefully acknowledge financial support from the Canada Foundation for Innovation, Nanoquebec, Centre for Self-Assembled Chemical Structures, Natural Sciences and Engineering Research Council of Canada, and Fonds québecois de la

recherche sur la nature et les technologies. W.G.S. thanks the Humboldt Foundation and the Royal Society of Chemistry for fellowships allowing the manuscript to be drafted. A.F. thanks the Tunisian Government for a scholarship of excellence.

Supporting Information

Table II.3. BBT X-ray crystal data.

Empirical formula	$C_{26}H_{26}N_2O_2S$
Mr	430.55
Temperature (K)	150
Crystal size (mm)	0.15×0.10×0.05
Crystal system	Monoclinic
Space group	$P2_1/n$
a(Å)	17.9167(7)
b(Å)	6.2563(2)
c(Å)	21.1871(8)
α(°)	90
β(°)	107.512(2)
γ(°)	90
V(Å^3)	2264.87(15)
Z	4
D_c (gcm^{-3})	1.263
Radiation	Cu-K_α
μ(mm^{-1})	1.462
F(000)	912
θ range (°)	3.86 - 67.13
Measured Reflections	27199
Independent reflections (R_{int})	4009 (0.052)
Completeness to θ max	0.988
Observed reflections [I>2 σ(I)]	3173
Number of parameters	286
R_1 I>2 σ(I) (all)	0.0509 (0.0680)
wR_2 I>2 σ(I) (all)	0.1277 (0.1390)
GoF	1.065
Data/parameter ratio	14.01
Largest difference peak, hole (e Å^{-3})	0.403/-0.270

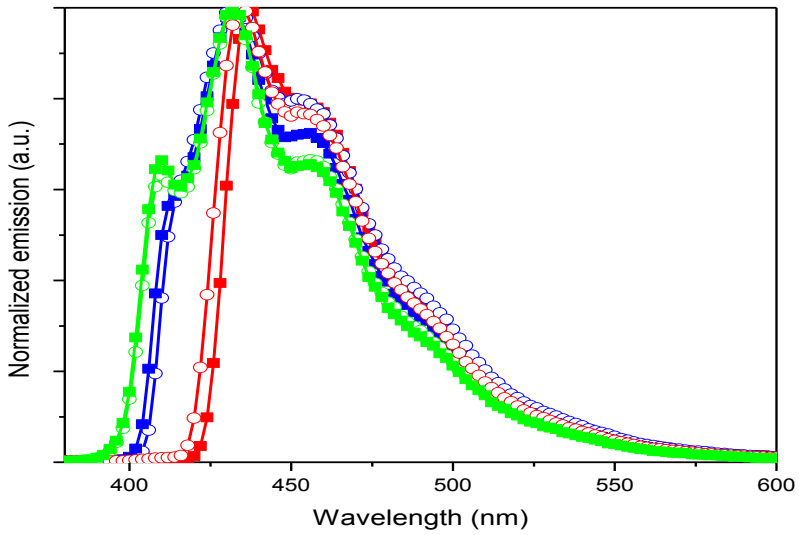

Figure II.12. Normalized BBT fluorescence spectra at λ_{exc} = 378 nm and at various BBT concentrations in THF using the front-face geometry at 30° (○, x µM; ○, 1/40 x µM; ○, 1/320 x µM) and at 90° (■, x µM; ■, 1/40 x µM; ■, 1/320 x µM).

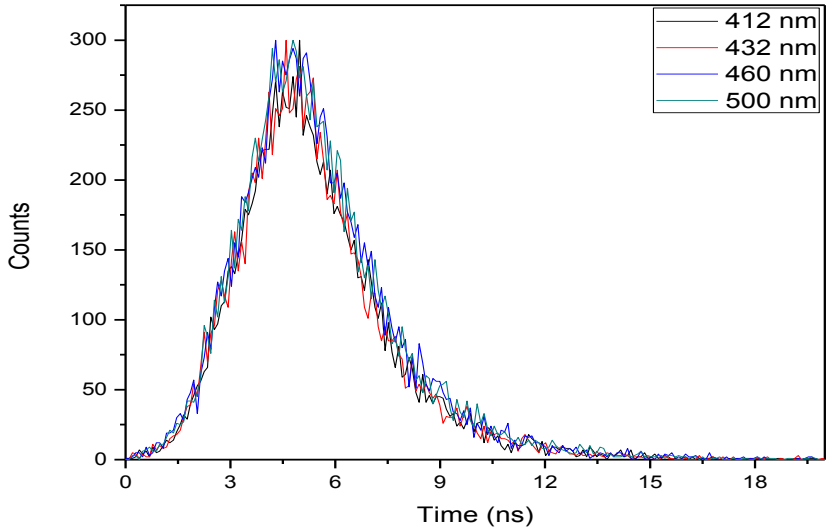

Figure II.13. BBT fluorescence decay as a function of time in THF at ambient temperature at a concentration of 0.15 mM measured at different wavelengths.

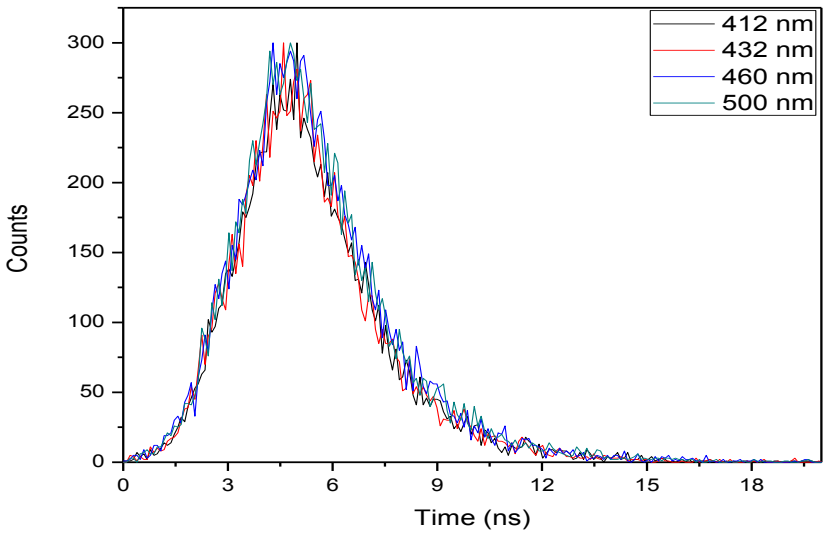

Figure II.14. BBT fluorescence decay as a function of time in THF at ambient temperature at a concentration of 0.25 mM measured at different wavelengths.

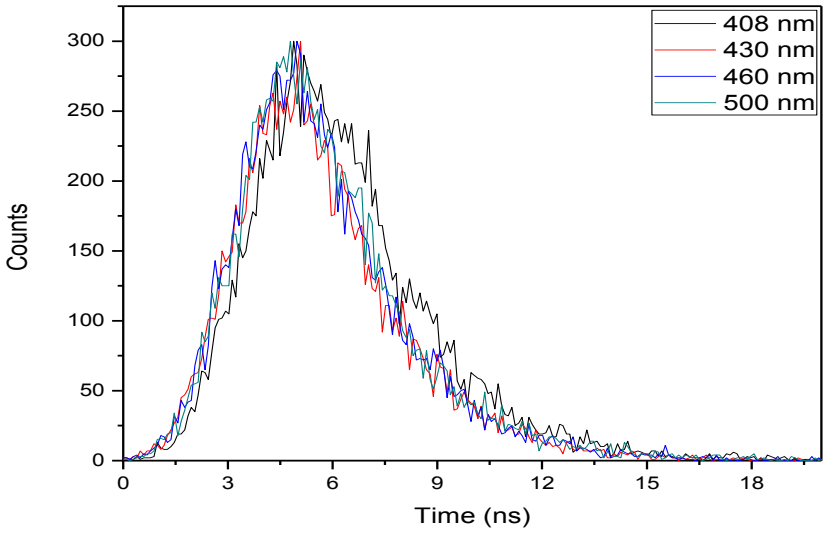

Figure II.15. BBT fluorescence decay as a function of time in THF at ambient temperature at a concentration of 2.5 mM measured at different wavelengths.

References

(1) Irie, M. *Chem. Rev.* **2000**, *100*, 1685.

(2) Momotake, A.; Arai, T. *J. Photochem. Photobiol. C* **2004**, *5*, 1.

(3) Bischoff, P.; Hutter, C.; Puebla, C.; E.P. 1294846, **2001**.

(4) Bur, A. J.; Roth, S. C. *Polym. Eng. Sci.* **2004**, *44*, 898.

(5) Pucci, A.; Bertoldo, M.; Bronco, S. *Macromol. Rapid Commun.* **2005**, *26*, 1043.

(6) Pucci, A.; Ruggeri, G.; Bronco, S.; Bertoldo, M.; Cappelli, C.; Ciardelli, F. *Prog. Org. Coat.* **2007**, *58*, 105.

(7) Sing, C. E.; Kunzelman, J.; Weder, C. *J. Mater. Chem.* **2009**, *19*, 104.

(8) King, N. R.; Whale, E. A.; Davis, F. J.; Gilbert, A.; Mitchell, G. R. *J. Mater. Chem.* **1997**, *7*, 625.

(9) Ward, I. M. *Structure and properties of oriented polymers*; Applied Science Publishers: London, **1975**.

(10) Liu, M. O.; Lin, H. F.; Yang, M. C.; Lai, M. J.; Chang, C. C.; Liu, H. C.; Shiao, P. L.; Chen, I. M.; Chen, J. Y. *Mater. Lett.* **2006**, *60*, 2132.

(11) Adachi, C.; Tsutsui, T.; Saito, S. *Appl. Phys. Lett.* **1990**, *56*, 799.

(12) Kim, J. S.; Seo, B. W.; Han, E. M.; Gu, H. B. *Mol. Cryst. Liq. Cryst.* **2001**, *370*, 35.

(13) Kim, J. S.; Seo, B. W.; Gu, H. B. *Synth. Met.* **2003**, *132*, 285.

(14) Liu, M.; Guo, B.; Zou, Q.; Du, M.; Jia, D. *Nanotechnology* **2008**, *19*, 205709.

(15) Nam, N. P. H.; Cha, S. W.; Kim, B. S.; Choi, D. S.; Jin, J. I. *Synth. Met.* **2002**, *130*, 271.

(16) Wang, J.; He, Z.; Mao, H.; Du, Y.; Wang, Y. *J. Lumin.* **2007**, *122*, 268.

(17) Yamaguchi, R.; Moriyama, K.; Sato, S. *Mol. Cryst. Liq. Cryst.* **2008**, *488*, 210.

(18) Yang, J.; Gordon, K. C. *Chem. Phys. Lett.* **2003**, *375*, 649.

(19) Yang, J.; Gordon, K. C.; Mc Quillan, A. J.; Zidon, Y.; Shapira, Y. *Phys. Rev. B* **2005**, *71*, 155209.

(20) Yang, J. H.; Gordon, K.; Robinson, B. H. *Synth. Met.* **2003**, *137*, 999.

(21) Zhang, R. Z., H.; Shen, J. *Synth. Met.* **1999**, *105*.

(22) McGregor, N.; Pardin, C.; Skene, W. G. *Aust. J. Chem.* **2011**, *64*, 1438.

(23) Kasha, M. *Discuss. Faraday Soc.* **1950**, *9*, 14.

(24) Fourati, M. A.; Maris, T.; Bazuin, C. G.; Prud'homme, R. E. *Acta Crystallogr., Sect. C: Cryst. Struct. Commun.* **2010**, *66*, o11.

(25) Khun, H. J. B., S. E.; Schmidt, R. *Pure Appl. Chem.* **2004**, *76*, 2105.

(26) Karstens, T.; Kobs, K. *J. Phys. Chem.* **1980**, *84*, 1871.

(27) Bolduc, A.; Dufresne, S.; Hanan, G. S.; Skene, W. G. *Can. J. Chem.* **2010**, *88*, 236.

(28) Antoniadis, H.; Inbasekaran, M.; Woo, E. P. *Appl. Phys. Lett.* **1998**, *73*, 3055.

(29) Masetti, F.; Elisei, F.; Mazzucato, U. *J. Lumin.* **1996**, *68*, 15.

(30) Lakowicz, J. R. *Principles of Fluorescence Spectroscopy*; Springer: New York, **2006**.

(31) Grimsdale, A. C.; Leok Chan, K.; Martin, R. E.; Jokisz, P. G.; Holmes, A. B. *Chem. Rev.* **2009**, *109*, 897.

(32) Pope, M.; Swenberg, C. E. *Electronic Processes in Organic Crystals and Polymers*; Oxford University Press: New York, **1999**.

(33) Özbey, S.; Kaynak, F. B.; Ertas, E.; Ozturk, T. *Acta Crystallogr., Sect. C: Cryst. Struct. Commun.* **2005**, *61*, o393.

(34) Rodinovskaya, L. A.; Shestopalov, A. M.; Chunikhin, K. S. *Tetrahedron* **2002**, *58*, 4273.

(35) Kazak, C.; Aygün, M.; Turgut, G. O., M.; Özbey, S.; Büyükgüngör, O. *Acta Crystallogr., Sect. C: Cryst. Struct. Commun.* **2000**, *56*, 1044.

(36) Pan, W. L.; Xu, Y. M.; Sun, Y.; Shao, C.; Lin, D. Y.; Song, H. C. *Analyt. Sci.* **2007**, *23*, x95.

(37) Hotta, S.; Goto, M. *Adv. Mater.* **2002**, *14*, 498.

(38) Pucci, A. C., C.; Bronco, S.; Ruggeri, G. *J. Phys. Chem. B* **2006**, *110*, 3127.

(39) Ciofalo, M., Ph.D. thesis, University of Pisa, **1992**.

(40) Mukamal, S.; Tretiak, S.; Wagersreiter, T.; Chernyak, V. *Science* **1997**, *277*, 781.

(41) Wagner, P.; Officer, D. L.; Kubicki, M. *Acta Crystallogr., Sect. E* **2006**, *62*, o5931.

(42) Trilleras, J.; Quiroga, J.; Cobo, J.; Low, J. N.; C., G. *Acta Crystallogr., Sect. E* **2005**, *61*, o1892.

CHAPITRE III: Photophysical and Electrochemical Investigations of the Fluorescent Probe, 4,4'-Bis(2-Benzoxazolyl)Stilbene*

Abstract

In solution, 4,4'-bis(2-benzoxazolyl)stilbene (BBS) was found to exhibit consistently high absolute fluorescence quantum yields ($\Phi_{fl} \geq 0.88$) and a monoexponential lifetime, both independent of BBS concentration. The BBS steady-state and time-resolved photophysics were investigated by different techniques, in order to understand the various deactivation pathways. Non-radiative deactivation of BBS singlet excited state by intersystem crossing was found to be negligible. Other than fluorescence, the excited state of BBS was found to be deactivated by *trans-cis* photoisomerization. At low concentrations (≈ 5 μg/mL), UV spectroscopy and laser flash photolysis showed concordant results that the photoinduced cis-isomer gradually replaced the original absorption spectrum of the pure trans-isomer. However, at high concentrations (≈ 0.2 mg/mL), ^{1}H NMR and DOSY measurements confirmed that irradiating BBS at 350 nm induced a conversion from the *trans*-BBS into its *cis*-isomer by photoisomerization. It was further found that the stilbene moiety of both isomers was photocleaved. The resulting photoproduct was an aldehyde that was oxidized under ambient conditions to its corresponding carboxylic acid, i.e., 4-(1,3-benzoxazol-2-yl)benzoic acid. The structure of the photoproduct was unequivocally confirmed by X-ray diffraction. Spectroscopic investigation of BBS showed a limited photoisomerization after irradiation at 350 nm of a *trans*-solution. The BBS electrochemistry showed irreversible oxidation, resulting in an unstable and highly reactive radical cation, while the cathodic process was found to be reversible giving rise to a radical anion and showing its n-doping character.

---

*Fourati, M. A., Skene, W. G., Bazuin, C. G. and Prud'homme, R. E. J. Phys. Chem. A **2013**, ASAP, DOI: 10.1021/jp312598c.

III.1. Introduction

An extended π-conjugation gives 4,4'-bis(2-benzoxazolyl)stilbene (BBS) optical properties that can lead to its use as photoactive switches[1,2] and as a fluorescent brightener in textiles,[3] detergents and other materials.[4,5] Furthermore, BBS's capacity to form excimers, leading to a change of its color under UV illumination at high concentrations in polymer films, has opened the door for applications in host–guest systems as a molecular probe of deformation and temperature.[6-8] Its anisotropic flat shape could also be used to produce polarized light in oriented macromolecular matrices.[9] In addition, BBS exhibits resistance to solvent extraction as well as high melting and degradation temperatures, above 300 °C, that satisfy the regulations of the U. S. Food and Drug Administration (FDA), thus enabling its use as an additive for food and consumer packaging materials.[10]

The spectroscopic properties of BBS are in part courtesy of the central stilbene. This provides a conjugated framework across which the electron rich benzoxazoyl termini delocalization can occur, resulting in a high degree of conjugation. The rigid framework is additionally responsible for its intense emission. Similar to other stilbene derivatives, BBS potentially can photoisomerize between its *trans* and *cis* isomers.[11-14] This competing excited state deactivation process could affect BBS' fluorescence properties, and in turn, limits its use in applications that require intense emission.[15-17] For this reason, it would be beneficial to determine whether BBS can be photoisomerized and under what conditions. To the best of our knowledge, the BBS photoisomerization dissipating energy processes have not been previously studied.

Although BBS has been used for different applications because of its optical and thermal properties, no extended opto-electrochemical studies of this fluorophore have been pursued. In particular, it would be interesting to probe the BBS photophysics to get a clear idea about the different energy dissipating processes that may be responsible of the lowering of its fluorescence quantum yield, which remains its greatest asset. Such studies are pivotal for determining the fluorescence BBS limitations and for its use as a universal fluorophore. Our purpose is to report the BBS photophysics and electrochemistry to try to better exploit its advantages.

III.2. Experimental

Materials

4,4'-Bis(2-benzoxazolyl)stilbene (97%, melting point > 300 °C) was purchased from Aldrich Chemicals. The compound was purified by sonicating and heating the material in the given solvent. The undissolved solids were subsequently removed by filtering upon cooling the solution and the filtered solution was then used for the measurements.

Spectroscopic Measurements

Absorption measurements were done on a Varian Cary-500 UV-Visible spectrometer, and the solvent absorption spectra were subtracted from the spectra of the analyzed samples, having a concentration of 5 μg/mL. Fluorescence emission spectra were recorded at ambient temperature in 10 mm cuvettes, excited at the corresponding absorption maximum, using an Edinburgh Instruments FLS-920 combined steady-state and time resolved fluorimeter. The fluorescence lifetimes were measured according to standard time-correlated single photon counting methods, with the FLS-920 apparatus, by fitting the data with a monoexponential decay function. The calculated values have an experimental error of approximately 10%. Absolute fluorescence quantum yields were measured by using an integrating sphere, and used to quantify the efficiency of the emission process by taking the ratio of photons absorbed to photons emitted through fluorescence at a particular wavelength in the same period of time.[18,19]

The HOMO and LUMO frontier molecular orbitals were calculated semi-empirically using DFT methods available in Spartan 06 with 6-31g* basis set. The bond angles, distances, torsions, and other parameters used for the theoretical calculations were experimentally derived from the X-ray data for BBS.[20]

Laser Flash Photolysis (LFP)

The triplet–triplet absorption spectra were measured in anhydrous 1,1,2,2-tetrachloroethane (TCE) (from Aldrich Chemicals) at a BBS concentration of 5 μg/mL using a Luzchem mini-LFP system, excited at 355 nm from the third harmonic of a

Continuum YAG:Nd Sure-lite laser, using a 175 W Xenon lamp. An average of 15 shots per wavelength was used for generating the transient absorption spectrum. The samples were dissolved in anhydrous TCE in static quartz cuvettes, and had an absorbance of less than 0.4. All samples were purged with nitrogen for more than 20 min before LFP analyses.

Photoirradiation

The sample for UV-measurement was degassed in a 20 mL vial by bubbling nitrogen directly into the solution for about 30 min before sealing the container to avoid contamination from air. The sample was then irradiated with 350 nm lamps in a Luzchem photoreactor. A small volume of the irradiated solution was removed from the reactor and transferred into a quartz 10 x 10 mm cell at prescribed times, and the absorbance spectrum was measured. For the NMR studies, the sample was introduced into a J-Young 7 mm tube at high concentration (≈ 0.2 mg/mL). The tube was heated and placed in an ultrasound bath flowed by three successive freeze-pump-thaw cycles before it was sealed and irradiated at 350 nm in the same photoreactor. The NMR tube was then taken out at different times for measuring NMR spectra. For the crystallographic studies, a degassed 0.2 mg/mL BBS solution in TCE was irradiated for 10 hours by using 350 nm lamps in the Luzchem photoreactor.

^{1}H NMR

A typical sample was prepared by dissolving a 0.2 mg/mL solution of BBS in $CDCl_3$ or in deuterated TCE (both from Aldrich Chemicals) in a J-Young 7 mm tube by alternating between heating and placing the sample in an ultrasound bath in order to avoid precipitation and to accelerate solubility. The tube was sealed and it was subjected to three successive freeze-pump-thaw cycles. Spectra were run on a Bruker AV-400 MHz spectrometer for all compounds dissolved in $CDCl_3$. MestRe-C and TopSpin softwares were used for NMR data processing. Chemical shifts were found relative to TMS and they were derived from spectra simulations using both Chem Draw Ultra 8.0 and DFT calculations. Diffusion experiments were performed at 298 K on a Bruker AVII-400 MHz spectrometer, which was equipped with a diff60 probe. A standard stimulated-echo pulse

sequence was used with a gradient duration (δ) of 1 ms, a diffusion time (Δ) of 40 ms, a repetition time of 5 s and 16 gradients values. An average of around 128 scans was accumulated.

Crystallographic Study

A needle yellow crystal (0.20 × 0.03 × 0.03 mm^3), suitable for X-ray diffraction analysis, was obtained by partial slow evaporation from a TCE solution after UV irradiation at 350 nm, triggering an increase of the concentration of 0.2 mg/mL to about 0.8 mg/mL. The single crystal study was carried out at 100 K using a Bruker APEX II diffractometer equipped with an Incoatec microsource generator producing Cu Kα radiation, a three-circle platform goniometer and an APEX2 CCD detector.

The structure was solved by direct methods using SHELXS 97.[21] All atoms from the main molecule were refined with anisotropic thermal displacement parameters. Hydrogen atoms were positioned geometrically and refined with a riding model, with C—H distances of 0.95 Å and Uiso (H) values constrained to be 1.2 times Ueq of the carrier atom. The structure contains an included solvent molecule that was found highly disordered. Several electron density peaks were located that did not assemble to a recognisable fragment of TCE molecule. So the solvent contribution was taken on using the SQUEEZE option[22] implemented in the PLATON software.[23]

III.3. Results and Discussion

The photophysical properties of BBS were measured in TCE at a concentration of 5 μg/mL, where it exhibits an absorption maximum at 374 nm, an emission maximum at 434 nm and a molar absorption coefficient of 65 000 M^{-1} cm^{-1}. Chlorinated solvents (TCE, $CHCl_3$ and $CDCl_3$) were chosen for evaluating the physical properties of BBS owing to the high solubility of BBS in these solvents.[24] This is in contrast to other common organic solvents in which BBS is insufficiently soluble, precluding their use for property evaluation. While chlorinated solvents are assumed not to be ideal solvents for photophysical studies because of their propensity to produce radicals upon direct

photoirradiation, these undesired by-products can be avoided by irradiating at wavelengths > 350 nm. Photophysical studies of BBS were therefore done by irradiating at wavelengths outside the absorbance windows of the solvents, being at wavelengths > 254 nm. Irradiations were done in pyrex instead of quartz glassware because of its optical transmission cut-off of < 350 nm. Using pyrex glassware therefore ensures the removal of UV wavelengths from the broad emitting lamps that could potentially induce radical formation upon direct excitation of the chlorinated solvents.

The BBS solution emission has a unique lifetime on the order of 1 ns. The monoexponential emission confirms the absence of bimolecular species. The consistent unimolecular lifetime was observed even when increasing the BBS concentration. Given that previously reported BBS emission yields were done by relative actinometry, which is an imprecise method,[25] we measured its absolute fluorescence quantum yields (Φ_{fl}) more accurately with an integrating sphere.[26] BBS was found to fluoresce strongly in solution with $\Phi_{fl} = 0.88$ in TCE. The measured value is higher than that of *trans*-stilbene (0.80 at 25 °C).[27]

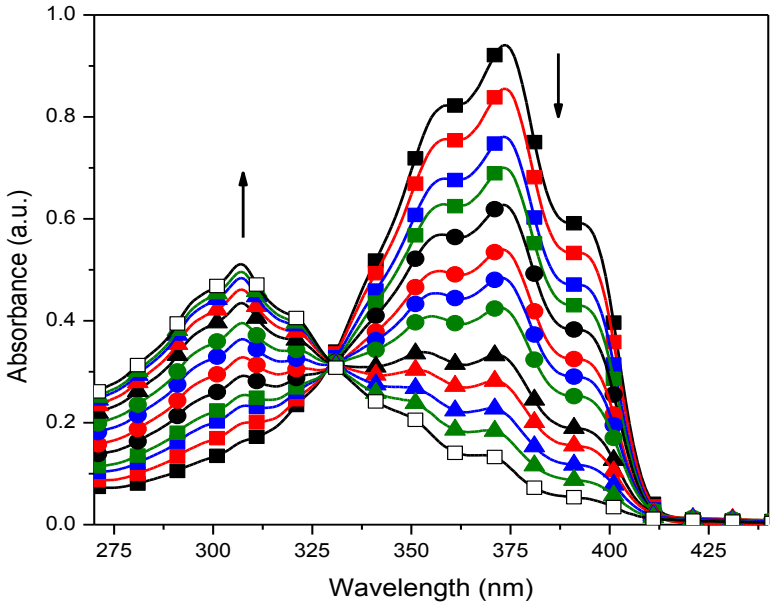

Figure III.1. BBS *trans-cis* photoisomerization in TCE measured by UV spectroscopy at room temperature at 0 (■),10 (■), 30 (■), 40 (■), 60 (●), 80 (●), 100 (●), 120 (●), 160 (▲), 190 (▲), 220 (▲), 250 (▲), and , 320 min (□) after irradiation at 350 nm with a 16 W light source.

The measured absolute Φ_{fl} confirms that BBS is highly fluorescent. However, the lower than unity Φ_{fl} indicates that deactivation processes other than fluorescence occur. The non-radiative deactivation processes were subsequently investigated, notably its photoisomerization. The BBS *trans-cis* photoisomerization was investigated by both steady-state and time-resolved according to UV spectroscopy and laser flash photolysis (LFP), respectively. Figure III.1 shows that the absorption spectrum of *trans*-BBS exhibits three peaks at 358, 374 and 395 nm. Upon irradiating at 350 nm, at room temperature, these three peaks decrease considerably in intensity over a period of 5 hours, without disappearing completely. This is accompanied by a concomitant increase in absorbance at 308 nm, which is assigned to the *cis*-BBS. Figure III.1 also shows the existence of an isosbestic point at 330 nm, at which point the *trans* and *cis* isomers have the same extinction coefficient. This isosbestic point indicates that only two species that vary in concentration contribute to the absorbance. It further confirms the interdependence of the

two species, being the interconversion of the *trans* and *cis* isomers. It should be noted that at longer irradiation times at 350 nm, the isosbestic point vanishes (data not shown) and the intensity of both isomers eventually disappears. This implies that both isomers are converted into a new product with extended irradiation (vide infra).

In a second step, BBS was investigated by LFP in order to confirm the *trans*-*cis* photoisomerization. The advantage of the time-resolved method versus steady-state irradiation is that the transients are instantaneously produced within the short laser pulse (ca. 10 ns). The intense laser power further produces sufficient transients within its pulse for them to immediately be detected. This is in contrast to steady-irradiation that requires extended irradiation times in order to detect any light induced species.

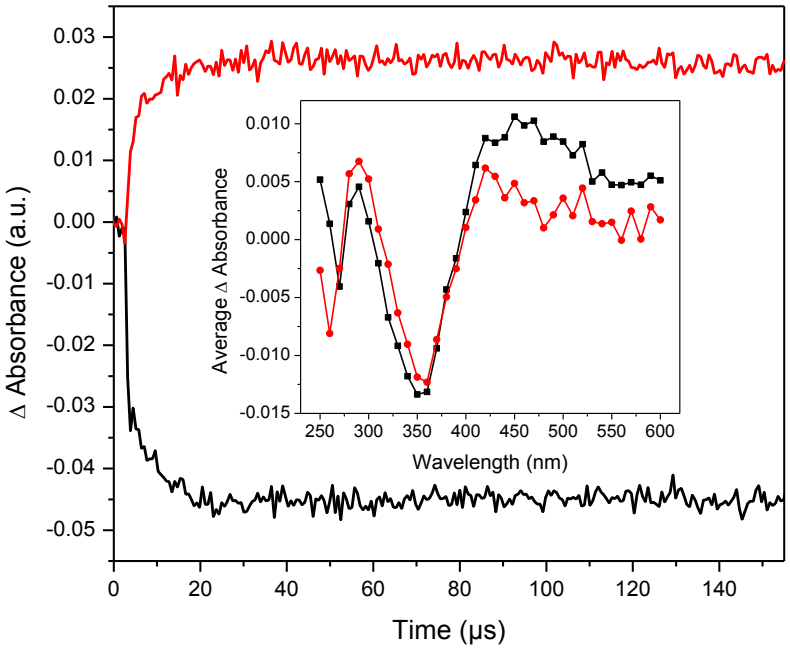

Figure III.2. BBS average transient absorbance response at 308 nm (—), specific to *cis*-BBS, and 374 nm (—), characteristic of *trans*-BBS, in TCE measured 0.3 μs after the laser pulse at 355 nm. Inset: transient absorbance spectra of BBS recorded in TCE at 9.79 (■) and 27.09 μs (●), after the laser pulse at 355 nm.

The inset of Figure III.2 shows the transient absorbance spectra of BBS measured in TCE at 9.79 and 27.09 μs after the laser pulse. The negative Δ absorbance at 350 nm corresponds in part to the ground-state bleaching of the *trans*-BBS and the signal at 300 nm is ascribed to the *cis* isomer. Meanwhile the new absorbance at 450 nm is assigned to the BBS triplet. This was based on its monoexponential decay and its lifetime (8 μs) that is consistent with triplets.[28] Unequivocal proof for the triplet was obtained by quenching the transient with 1,3-cyclohexadiene, which is a well-known triplet deactivator.[29]

The transient absorbance kinetics was measured at both 308 and 374 nm to confirm the identity of the photoinduced products. These wavelengths were chosen because they correspond to the absorbance maximum measured by steady-state. As seen in Figure III.2, the absorbance at 308 nm grows according to first order kinetics with a lifetime of 3.5 μs. It is further obvious that the transient signal does not decay within the time resolution of the LFP instrument. The transient kinetic at 374 nm is the mirror image of that observed at 308 nm. The negative signal is a result of the ground state being depleted. Similar to what was observed at 308 nm, the signal at 374 nm does not recover during the course of the measurement. This implies that the absorbance at 374 nm is irreversibly converted into a photoproduct while the absorbance at 308 nm is the formation of a photoproduct that is stable within the time resolution of the instrument. While the exact photoisomerization mechanism and the lifetimes of the discrete processes cannot be determined, the overall *trans*→*cis* photoconversion is 2.5 μs, according to the LFP measurements. The similar μs kinetics and the mirror image of the two absorbances confirm the interdependence of the signals at 308 and 374 nm. The signal of the *trans*-BBS at 374 nm is therefore converted into the *cis* isomer, which is observed at 308 nm. The results are consistent with the steady-state measurements. From the plateau regions of the kinetics, the molar absorptivity coefficient (ε) of the *cis* isomer can be approximated to be 38 500 M^{-1} cm^{-1} at 308 nm.

The efficiency of photoisomerization cannot accurately be quantified either from the time-resolved or steady-state analyses. However, taking into account the absolute ϕ_{fl} and assuming a minor triplet contribution as per the absorbance at 450 nm, the *trans* → *cis* photoisomerization efficiency is approximately 10%.

NMR spectroscopy was used to both investigate the presence of additional photoinduced processes and to confirm the *trans*-*cis* photoisomerization. The advantage of NMR spectroscopy is that the *cis* and *trans* isomers of stilbene derivatives can readily be distinguished by their distinctive $^{3}J_{HH}$ coupling constants.[30,31] However, this was not possible because of BBS' high degree of symmetry that gives rise to a singlet for the vinylene protons instead of a doublet. Therefore, the chemical shift of the *cis* vinylene protons was estimated by theoretical means using commercial software. This is particularly important given the absence of any reported NMR data for *cis*-BBS. To confirm the accuracy of the predicted chemical shifts of *cis*-BBS, the ^{1}H-NMR spectrum of *trans*-BBS was also calculated. The predicted chemical shifts for the vinylene protons were 6.56 and 7.26 ppm, respectively, for the *cis* and *trans* BBS isomers. The calculated chemical shift for the *trans* vinylene proton (located at position f in Chart III.1) is in accordance with experimental value of 7.32 ppm, as per Figure III.3a.

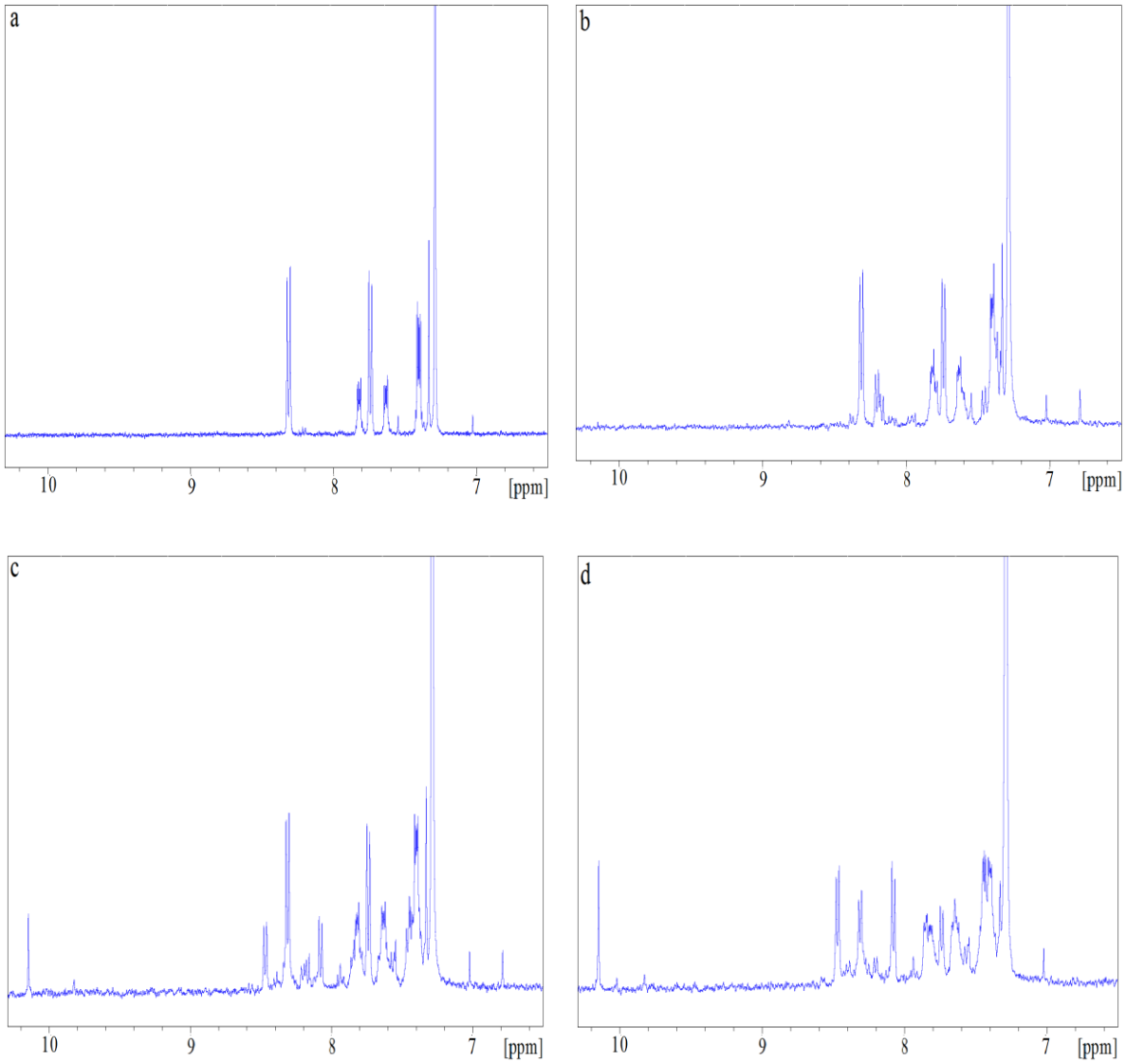

Figure III.3. ^{1}H NMR spectrum, from 6.5 to 10.3 ppm, of *trans*-BBS in $CDCl_3$, after 0 (a), 4 (b), 10 (c) and 20 h (d) of irradiation at 350 nm (light power, P = 16 W).

Figure III.3a shows the NMR spectrum of *trans*-BBS, prior to irradiating at 350 nm. The singlet at 7.32 ppm is assigned to proton-*f* (Chart III.1). It should be noted that there is no signal at around 6.5 ppm that can be ascribed to the *cis*-isomer. Figure III.3b displays the BBS NMR spectrum after 4 h of UV irradiation. It is obvious that a new singlet appears at 6.76 ppm, belonging to *cis*-BBS, in addition to the singlet of *trans*-BBS. The formation of the *cis*-isomer is accompanied by a change of the positions of the closest peaks to the central vinylic bond. Indeed, the intensity of the peaks corresponding to protons at positions

d and *e*, located at 8.33 and 7.74 ppm of *trans*-BBS, decreased progressively, while new peaks corresponding to the same positions appear at 8.22 and 7.59 ppm for *cis*-BBS, respectively. It should be noted that the remaining peaks, belonging to the protons at positions *a*, *b* and *c* remain unchanged. Figure III.3c shows the NMR spectrum after 10 h of UV irradiation. The appearance of a well-defined singlet at 10.15 ppm is consistent with a photoproduct having an aldehyde. The new resonance is accompanied by the emergence of new peaks at 8.48 and 8.08 ppm, corresponding to the protons at positions d and e, respectively. Figure III.3d shows the NMR spectrum after 20 h of UV irradiation, displaying the disappearance of the *cis*-isomer, the increase of the photoproduct singlet at 10.15 ppm and the decrease of the *trans*-BBS singlet at 7.32 ppm. By irradiating the BBS solution for longer times, the singlet at 7.32 ppm, specific to *trans*-BBS, disappears while the peaks specific to the photoproduct become more intense. The emergence of new peaks specific to the protons at positions *d* and *e*, in addition to the appearance of a new well-defined singlet at 10.15 ppm, which has been attributed to an aldehyde, confirm the presence of another conversion process.

By integrating the *cis*-isomer signal at 6.76 ppm relative to the *trans*-peak at 8.33 ppm, it was found that the *cis* integral gradually increases before reaching a plateau of 18% relative to the sum of the *trans*- and *cis*-isomers after 3 h of UV irradiation in $CDCl_3$. After which time, the signal decreases until becoming null after around 14 h of UV irradiation. These results show that another process occurs, leading to a simultaneous conversion of both isomers into a photoproduct, thus suppressing the BBS *trans*-*cis* photoisomerization. Since UV spectroscopy shows a greater conversion from *trans* to *cis*, even when taking into account the difference of the extinction coefficients of the two isomers, a series of absorbance measurements were made with a similar concentration to that used for the NMR study with an initial concentration of ≈ 0.2 mg/mL. After irradiation, an aliquot was removed and it was diluted to 0.005 mg/mL, similar to the concentration used in Figure III.1. This was required in order to not saturate the detector of the UV spectrometer and to get an absorbance below unity for each measurement. This series of measurements led to a *trans*-*cis* conversion similar to that found by NMR in Figure III.3. It appears that a high *trans*-*cis* conversion is obtained upon irradiating at low concentrations (Figure III.1). In

contrast, a low conversion is obtained upon irradiating at high concentrations (Figure III.3). This is probably due to an inner-filter effect and/or self-quenching at high concentrations that favour continuous energy transfer between BBS molecules. On the other hand, the aldehyde signal at 10.15 ppm continuously increases relative to the *trans*-peak at 8.33 ppm. Also, the chemical shifts of the *a*, *b* and *c* protons remain unchanged. These data collectively suggest that the second process does not affect the benzoxazol part of the molecule, but only the stilbene moiety. The higher than normal downfield chemical shift of the aldehyde confirms that it is highly conjugated. This is only possible when it is conjugated with the benzoxazol unit. The photoproduct therefore is most likely from stilbene photooxidation in the presence of trace amounts of residual oxygen. The photocleavage resulting in aldehyde photoproducts is a proven degradation mechanism of stilbenes[32-34] and it makes the *trans-cis* photoisomerization irreversible.

In order to get more information about the presence of a secondary process, diffusion ordered spectroscopy (DOSY) experiments were conducted. DOSY enables to differentiate between blend components since, in a solution of a given viscosity, molecules of various sizes diffuse at different rates.[35-39] The diffusion coefficients (D_{diff}) of the individual species can be determined by the DOSY experiments and related to their molecular hydrodynamic volume. These experiments were conducted at identical concentration and temperature in $CDCl_3$.

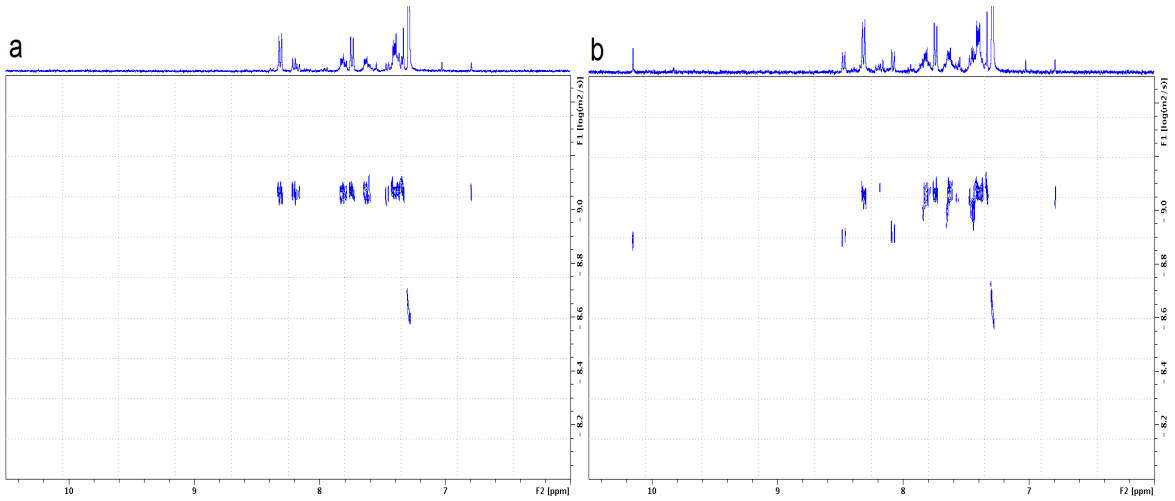

Figure III.4. DOSY NMR results for BBS, after 4 (a) and 10 h (b) of UV irradiation. All spectra were recorded in $CDCl_3$ at room temperature at 400 MHz. The x-axis represents the standard ^1H dimension, from 6 to 10.5 ppm, and the y-axis represents the diffusion dimension.

Figure III.4 shows the diffusion coefficient (D_{diff}) as a function of the chemical shift between 6 and 10.5 ppm after 4 (a) and 10 h (b) of UV irradiation. Figure III.4a shows that the *trans*-BBS original signals at 8.33, 7.74 and 7.32 ppm, as well as the *cis*-isomer signals at 8.22, 7.59 and 6.76 ppm, corresponding to protons *d*, *e* and *f*, have the same diffusion coefficient of 0.8 10^{-9} $m^2 \bullet s^{-1}$. Figure III.4b shows that, after 10 h of UV irradiation, the emerging peaks at 8.48 and 8.08 ppm corresponding to protons *d* and *e*, respectively, have higher diffusion coefficients of the order of 1.2 ─ 1.3 10^{-9} $m^2 \bullet s^{-1}$, as well as the new singlet, located at 10.15 ppm. These results show that these three peaks do not belong to the original BBS, but to a new product. Therefore, the D_{diff} values are so different, before and after a prolonged UV irradiation, that a standard deviation of up to 10% cannot affect the understanding of the conversion. The presence of two singlets at 7.02 and 7.54 ppm are evident in Figure III.4. These are assigned to impurities because they are always present. They additionally diffuse rapidly, which confirms that they are smaller than BBS. According to Figure III.3A, these impurities are minor and they are present in less than 2 mole %. While the commercial source of BBS is only 97% pure, it was purified by alternating between heating and sonication, followed by filtering. This leads to purer BBS than the original commercial source. Moreover, these impurities do not interfere with the

isomerization studies since they do not contain a vinyl group and they do not absorb at the wavelengths used for photoirradiation. On the other hand, the solvent ($CDCl_3$) diffusion coefficient is the same, within uncertainty, for the different solutions, showing a similar viscosity before and after irradiation. The Stokes-Einstein equation, applicable for spherical molecules and describing diffusion phenomena, is:

$$\boldsymbol{D_{diff} = \frac{k_B T}{6 \pi \eta r}} \quad \text{(III.1)}$$

where D_{diff} is the diffusion coefficient, r the hydrodynamic radius of the molecule, k_B the Boltzmann constant, T the temperature and η the viscosity. D_{diff} is inversely proportional to the hydrodynamic radius. By assuming that the molecules are spherical, the higher value of D_{diff} after 10 h of UV irradiation proves that the BBS molecule is converted into a molecule of lower hydrodynamic radius. Meanwhile, the new well-defined singlet at 10.5 ppm confirms it has an aldehyde. In contrast, a broad resonance would be observed for a carboxylic acid, whose chemical shift would be concentration-dependent. According to Equation III.1, the hydrodynamic radius of the photoproduct is estimated to be 1.6 times smaller than BBS.

To gain a deeper understanding of the products formed from UV irradiation and, more specifically, to unequivocally identify both the photoproduct and *cis*-BBS, crystallographic studies were conducted. For this, a 0.2 mg/mL solution of BBS in TCE, similar in concentration to that used for NMR measurements, was irradiated at 350 nm for 10 h. The resulting solution contained both BBS isomers and the photoproduct. This was confirmed by NMR (Figure III.3c). The solvent was then partially evaporated, as described in the experimental section. Unlike what was expected, the single crystal that formed upon partial solvent evaporation was neither the *cis*- nor the *trans*-isomer. In fact, the X-ray diffraction of the single crystal confirmed that the photoproduct was a carboxylic acid, 4-(1,3-benzoxazol-2-yl)benzoic acid (BBA) (Figure III.5). The latter is a result of photocleavage of the stilbene moiety, leading to two half-molecules with an acid terminal function for each. While an aldehyde photoproduct was observed in NMR studies, this

intermediate is readily oxidized to BBA under the aerobic crystallization conditions, according to known means.[40,41] Irradiation of BBS at 350 nm therefore leads to *trans-cis* photoisomerization and the two isomers are photooxidized with residual oxygen. The resulting aldehyde photoproduct is further oxidized to BBA. The conversion of both photoisomerization and photocleavage is shown in Chart III.1. The photocleavage is concentration-dependent and is slow at concentrations ≤ 5 µg/mol and faster at concentrations ≥ 0.2 mg/ml.

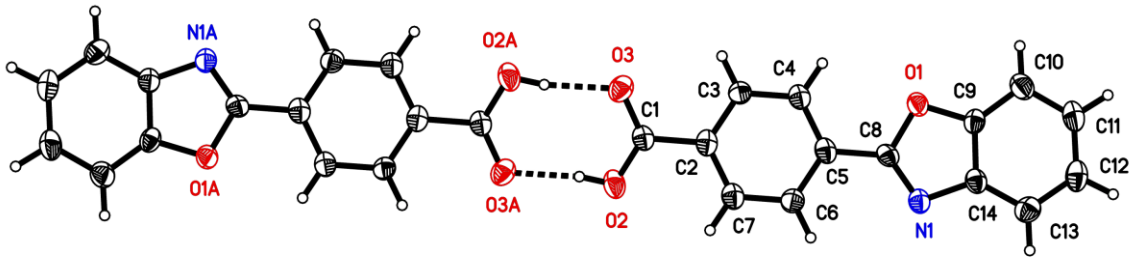

Figure III.5. Atomic displacement ellipsoid plot of BBA. The second molecule (atoms labelled with suffix A) are generated by the symmetry operation –x-1, -y-1, -z. Hydrogen bonds are shown as dotted lines. Ellipsoids are drawn at the 50% probability level and hydrogen atoms are represented by sphere of arbitrary size.

BBA was found to crystallize in the triclinic space group P-1 with one independent molecule in the asymmetric unit. It is almost planar and the angle between the benzene ring and the benzoxazolyl group is only 1.50(14)°, which is smaller than that found in BBS (2.30(16)°).[20] The different BBA molecules were stable due to intermolecular interactions. Indeed, Figure III.5 shows that two BBA molecules form a dimer, linked by two hydrogen bonds involving the carboxylic acid groups according to the classical graph set motif $R_2^2(8)$.[42]

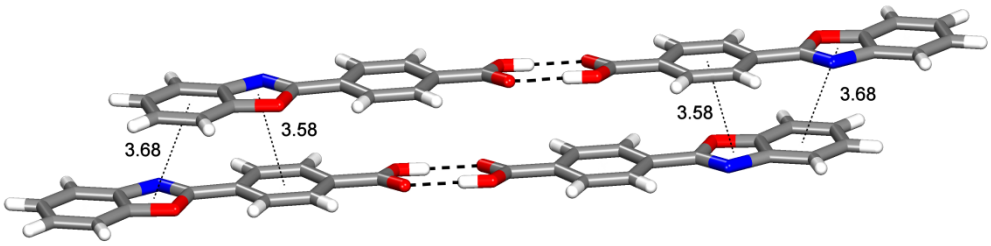

Figure III.6. View of the π-stacking interactions between two hydrogen-bonded dimers. Hydrogen bonds and the shortest distances between ring centroids involved in π-stacking interactions are indicated by dotted lines.

Figure III.6 shows that π-stacking interactions between the benzene and the oxazole rings enable a packing with the shortest centroid to centroid distances of 3.58 and 3.68 Å. The chains of dimers are arranged parallel to the *a*-axis and the molecules from these chains are connected to a neighbouring chain via C─H···O interaction (d(C─O) = 3.26 Å) to form layers in the (*a*, *b*) plane. It should be noted that the disordered solvent molecules occupy the remaining space between the layers (35 % of the unit-cell volume).

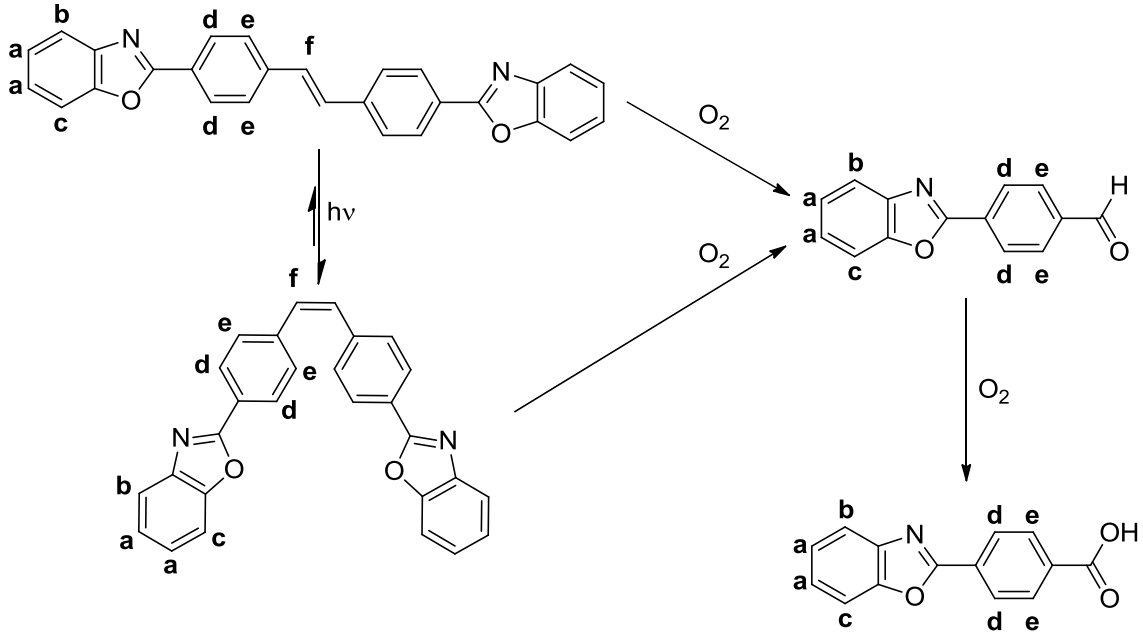

Chart III.1. BBS *trans-cis* photoisomerization, and conversion of both isomers in BBA.

The most interesting property of BBS is its fluorescence. While extended characterization of the *trans* isomer is possible, the *cis* isomer has not previously been characterized. This is primarily owing to the difficulty in isolating the sterically hindered isomer. It would nonetheless be beneficial to characterize the fluorescence of the *cis* isomer for gaining valuable insight into both the photoisomerization process and to determine the limit of usefulness of BBS as a fluorescence probe. For these reasons, we extended our fluorescence studies to include the *cis* isomer. However, given the challenges in isolating the pure *cis* isomer, spectral characterizations were done indirectly on mixed samples having both *cis* and *trans* isomers. According to Figure III.7, three well-defined peaks, located at 412, 434 and 464 nm, are seen in the *trans*-BBS fluorescence spectrum. These are assigned to the 0─0, 0─1 and 0─2 radiative transitions, respectively, and they are characteristic of BBS monomers. In comparison, the absorption spectrum exhibits three ill-defined peaks at 358, 374 and 395 nm. Due to the increased conjugation of BBS relative to unsubstituted stilbene, there is an increase of the absorbance band region. No spectral changes were observed for the *trans*-absorbance spectrum with increasing the BBS concentration.

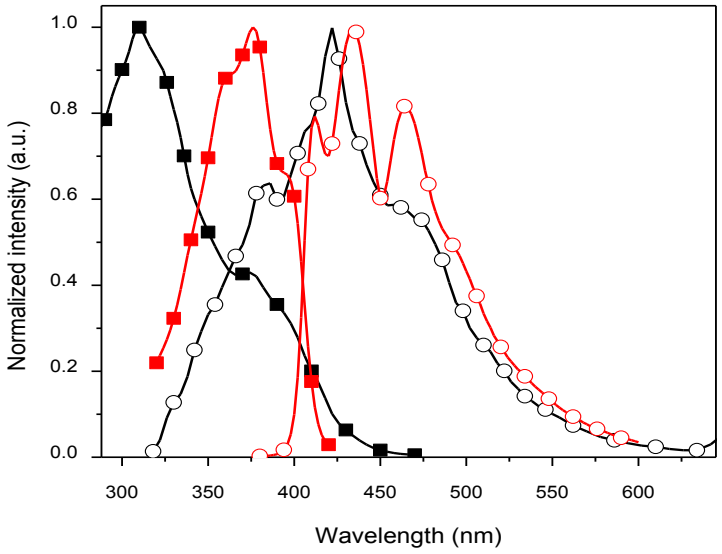

Figure III.7. Normalized absorption and emission spectra in TCE of BBS before UV irradiation: absorbance (■) and fluorescence at λ_{exc} = 374 nm (○); and after 5 h of irradiation at 350 nm: absorbance (■) and emission at λ_{exc} = 308 nm (○).

Figure III.7 also shows the spectroscopic features of a solution of *trans*-BBS irradiated for 5 h at 350 nm. The absorption spectrum exhibits an intense peak at 308 nm and a shoulder at 375 nm. These are assigned to the absorbance maximum of the *cis*- and *trans*-isomers, respectively (vide supra). Similarly, the emission spectrum shows a maximum at 422 nm and two shoulders at 384 and 474 nm. These shoulders are specific to *cis*- and *trans*-BBS, respectively, while the emission maximum at 422 nm results from an overlap between the emissions of the two BBS isomers. The emission of the *cis*-isomer is then hypsochromically shifted relative to the *trans*-spectrum and the presence of both isomers even after prolonged irradiation suggests a photostationary *cis*-*trans* conversion. This hampers accurate determination of the spectroscopic data specific to *cis*-BBS. Since the *cis*-isomer was impossible to isolate, the solution obtained after 5 h of UV irradiation was used to measure the fluorescence quantum yield and the lifetime of the *cis*- and *trans*-BBS mixture relative to the pure *trans* isomer. Only qualitative information is possible given that both isomers have different molar extinction coefficients and they do not absorb the same number of photons. Both the mixed isomer and pure *trans*-isomer solutions had similar fluorescence lifetimes, being ca. 1 ns. In contrast, the fluorescence quantum yield decreased from 0.88 for pure *trans*-BBS to 0.67 for the solution containing a mixture of both isomers.

A rough estimate of the energy-gap (E_g), i.e., the absolute energy difference between the ground (HOMO) and excited (LUMO) states, was calculated from the intercept of the normalized absorption and emission spectra (Figure III.7). The approximated values are 3.1 eV for *trans*-BBS and 3.4 eV for the irradiated solution (for 5 h) containing *trans*- and *cis*-isomers.

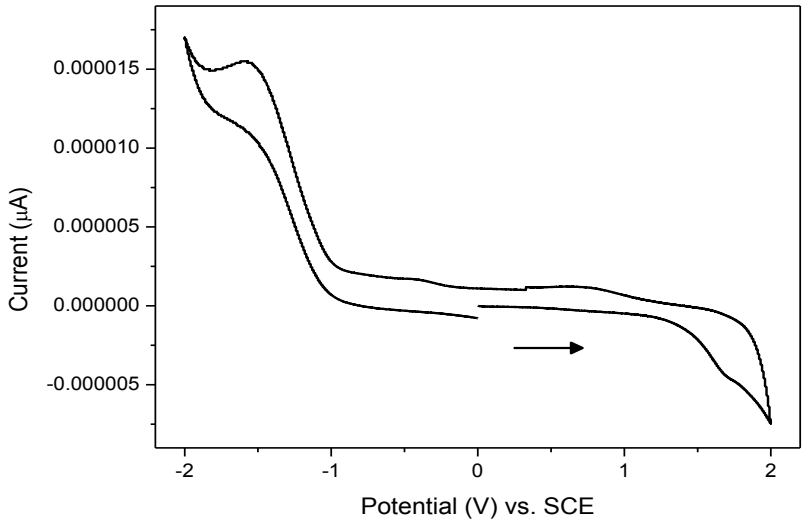

Figure III.8. Cyclic voltammogram of *trans*-BBS recorded in TCE at 100 mV/s against SCE with Bu_4NPF_6 as the supporting electrolyte.

The energy-gaps cannot only be obtained from the fluorescence spectra, as shown in the previous section, but they can also be obtained by cyclic voltammetry. According to Figure III.8, *trans*-BBS undergoes a one-electron oxidation process, demonstrating its p-doping-type behavior. The oxidation results exhibit an irreversible behavior of cyclic voltammetry, regardless of the scan rate, indicating a highly reactive radical cation. Conversely, BBS undergoes a reversible electrochemical reduction at low potential that confirms its n-doping character.

Table III.1. *trans*-BBS electrochemical properties.[a]

E_{ox}[b]/V	E_{red}[c]/V	IP[d]/eV	EA[e]/eV	E_g^{el}[f]/eV
1.66	-1.79	5.72	2.87	2.9

[a] The electrochemical data are reported against SCE. [b] Oxidation potential. [c] Reduction potential. [d] Ionization potential. [e] Electron affinity. [f] Electrochemical energy-gap.

From the cyclic voltammetry data, we can calculate E_{onset}^{ox}, which is the oxidation potential onset versus the SCE electrode, and E_{onset}^{red}, which is the reduction potential onset. Their values, taken from Figure III.8, are given in Table III.1. The HOMO energy value can be calculated from the ionization potential (IP), according to IP = E_{onset}^{ox} + 4.4. Similarly, the LUMO energy level is derived from the electron affinity (EA), according to EA = E_{onset}^{red} + 4.4. The IP and EA values of BBS are also reported in Table III.1. The difference between the HOMO and LUMO energy levels gives the electrochemical energy-gap, E_g^{el} (2.9 eV in Table III.1) that is similar to the spectroscopic energy-gap, E_g (3.1 eV from Figure III.7). The high degree of conjugation of the BBS molecule is confirmed, first, by both the electrochemical and spectroscopic data and, second, by the theoretically calculated molecular orbitals that are depicted in Figure III.9. The latter show the delocalization of the HOMO along the rigid backbone of BBS, confirming its high degree of conjugation. Conversely, the LUMO is located exclusively on the central stilbene moiety.

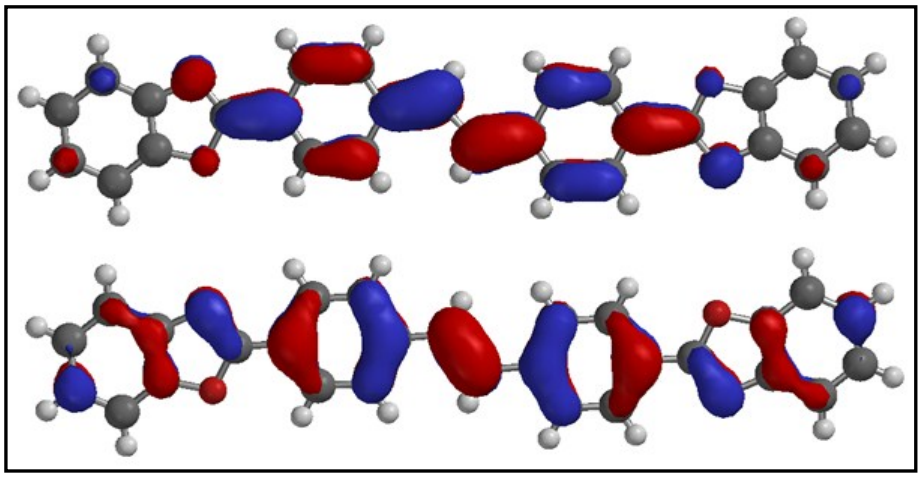

Figure III.9. BBS LUMO (top) and HOMO (bottom) features calculated by DFT, using 6-31g* basis set and the X-ray crystal data.[141]

III.4. Conclusions

In solution, BBS fluoresces with high quantum yields ($\Phi_{fl} \approx 0.88$), regardless of its concentration. The steady-state and time-resolved photophysics of this stilbene-derivative

fluorophore have been investigated for the first time in this study by absorbance, laser flash photolysis and NMR spectroscopy, in order to unravel its quenching mechanism, while its fluorescent and electrochemical features were studied by fluorescence spectroscopy and cyclic voltammetry, respectively.

Although the primary deactivation mode of the BBS singlet excited state is by fluorescence, it also deactivates by *trans*-*cis* photoisomerization. Intersystem crossing to the triplet state was found to be negligible and excimer formation was non-existent, proved by a concentration-independent monoexponential lifetime, of the order of 1 ns.

At low concentrations (≈ 5 μg/ml), irradiating BBS at 350 nm induces a *trans*-*cis* photoisomerization. However, at higher concentrations (≥ 0.2 mg/ml), this process is accompanied by formation of an oxidized photoproduct, occurring by photocleavage at the stilbene moiety. The resulting aldehyde is oxidized to its corresponding carboxylic acid under ambient conditions. X-ray crystallography confirmed that the oxidized photoproduct was 4-(1,3-benzoxazol-2-yl)benzoic acid and that it arranged as dimers. The secondary process kinetics was found to be concentration-dependent and seems to be too slow to be detected at low concentrations. The limited photoisomerization at high concentrations was proved by a combined absorption and emission spectra of both *trans*- and *cis*-species. Electrochemistry of *trans*-BBS exhibits an irreversible oxidation. In contrast, BBS was reversibly reduced at low potentials, resulting in a stable radical anion, thus confirming its n-doping character, and corroborating its characteristics as an electron-acceptor molecule.

Acknowledgements

The authors gratefully acknowledge financial support from the Natural Sciences and Engineering Research Council of Canada, the Fonds Québécois de la Recherche sur la Nature et les Technologies, the Canada Foundation for Innovation, NanoQuébec and the Centre for Self-Assembled Chemical Structures. They also thank Thierry Maris and Cédric Malveau, from Université de Montréal, for their help in X-ray diffraction and diffusion ordered spectroscopy experiments, respectively. W.G.S. thanks both the Humboldt

Foundation and the Royal Society of Chemistry for fellowships allowing the manuscript to be drafted. A.F. thanks the Tunisian Government for a scholarship of excellence.

Supporting Information

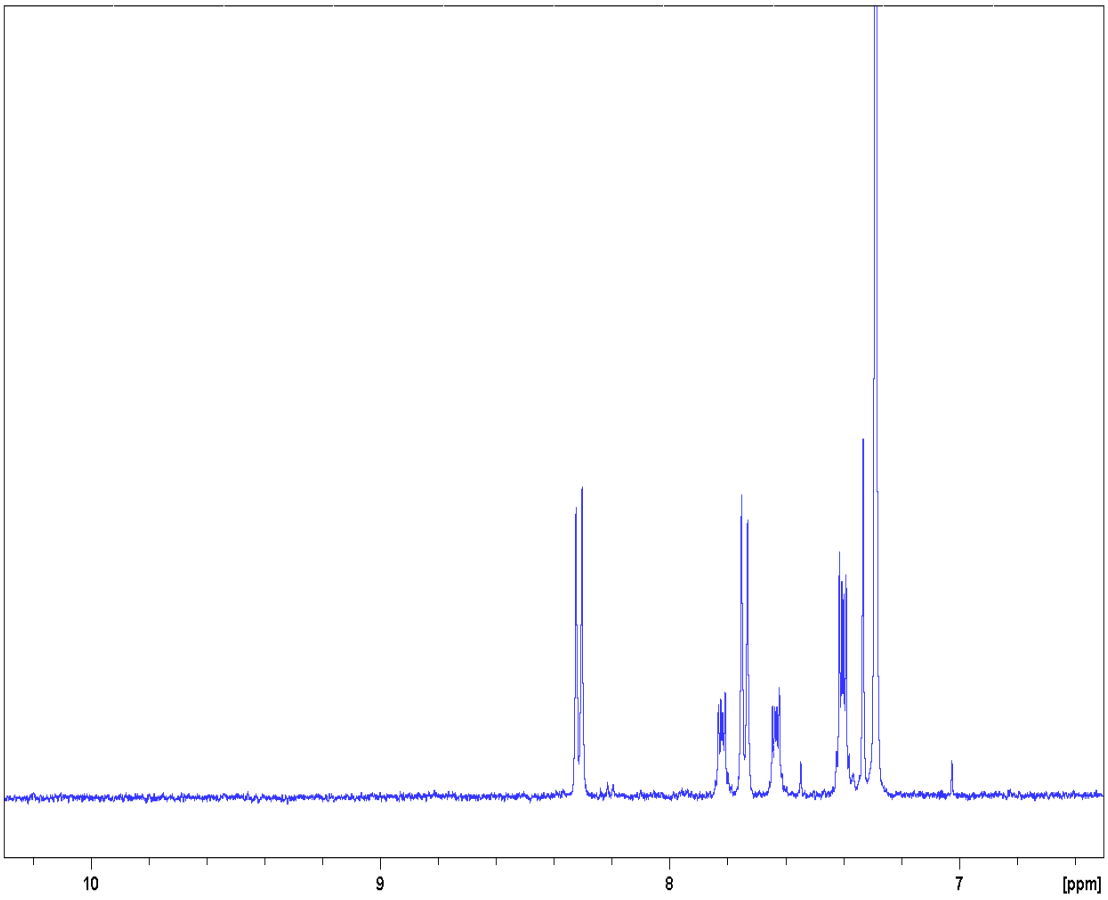

Figure III.10. Magnification of the ^{1}H NMR spectrum, from 6.5 to 10.3 ppm, of *trans*-BBS in $CDCl_3$, after 0 h of irradiation at 350 nm (light power, P = 16 W).

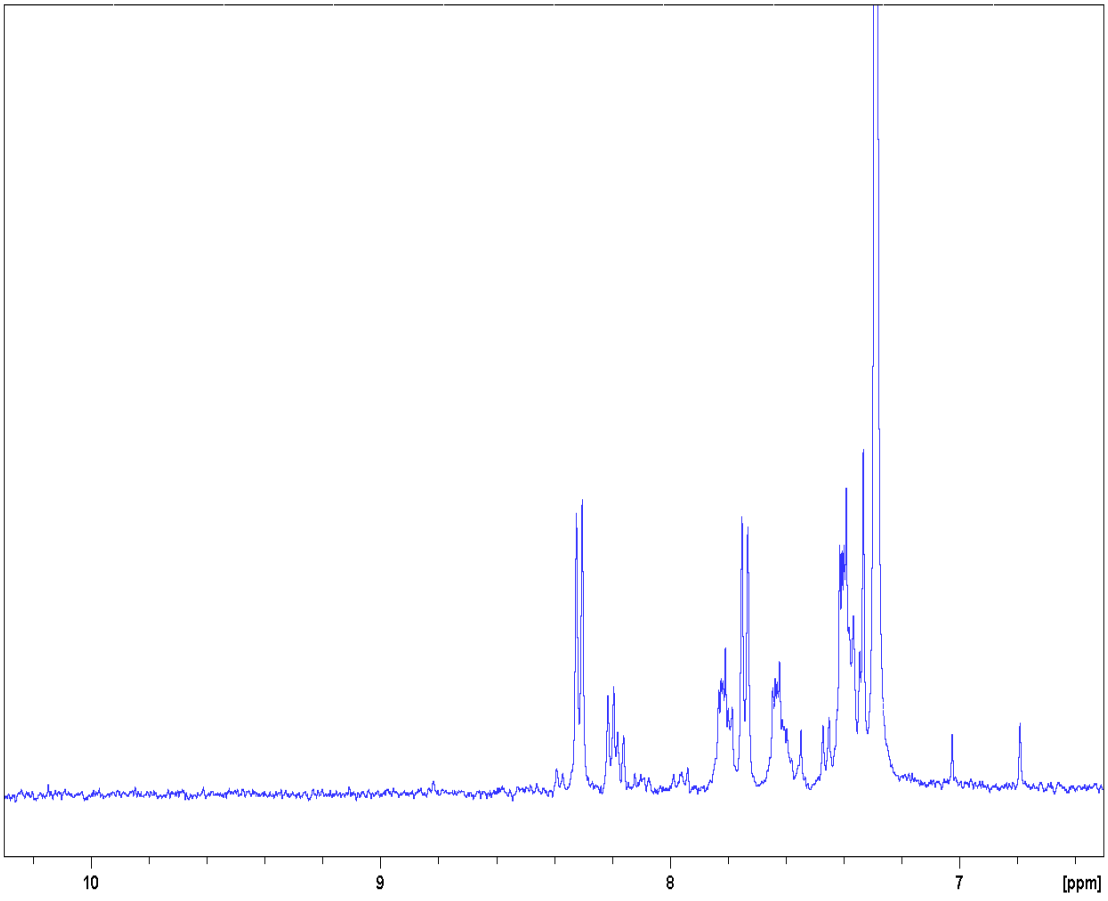

Figure III.11. Magnification of the ^{1}H NMR spectrum, from 6.5 to 10.3 ppm, of *trans*-BBS in $CDCl_3$, after 4 h of irradiation at 350 nm (light power, P = 16 W).

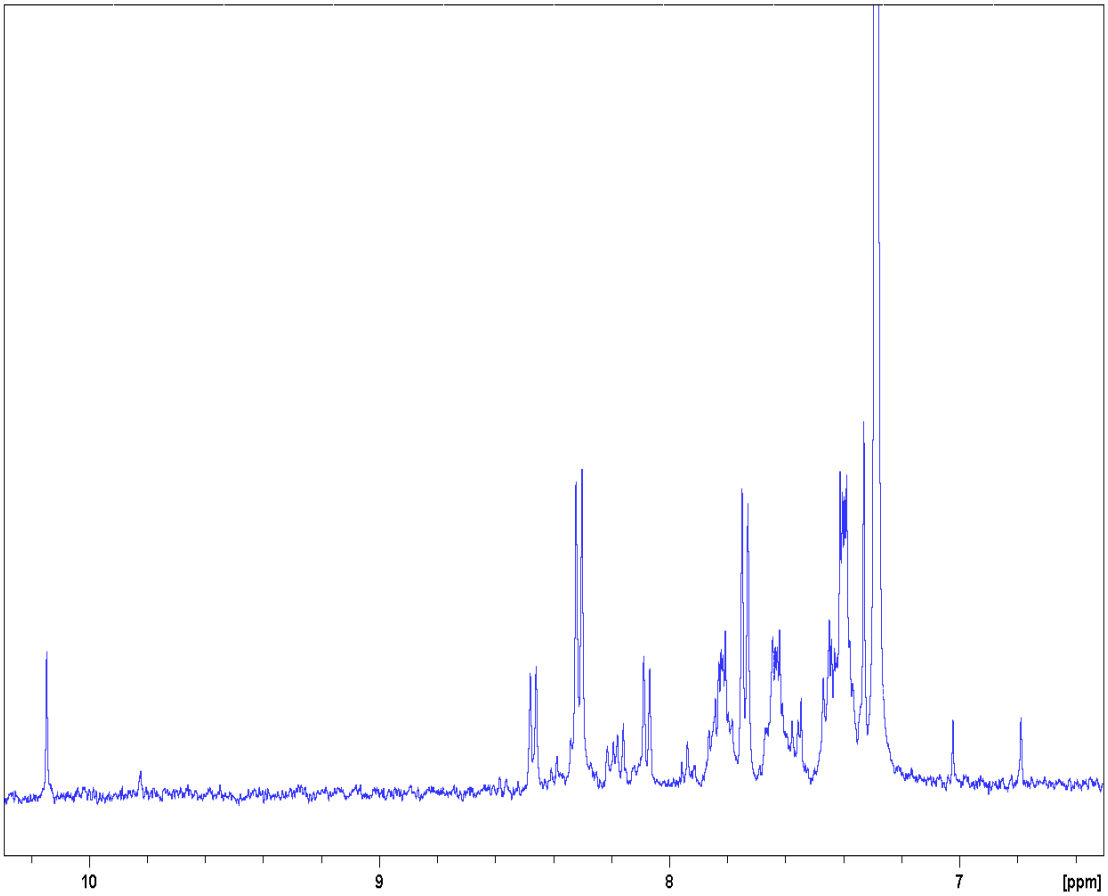

Figure III.12. Magnification of the ^{1}H NMR spectrum, from 6.5 to 10.3 ppm, of *trans*-BBS in $CDCl_3$, after 10 h of irradiation at 350 nm (light power, P = 16 W).

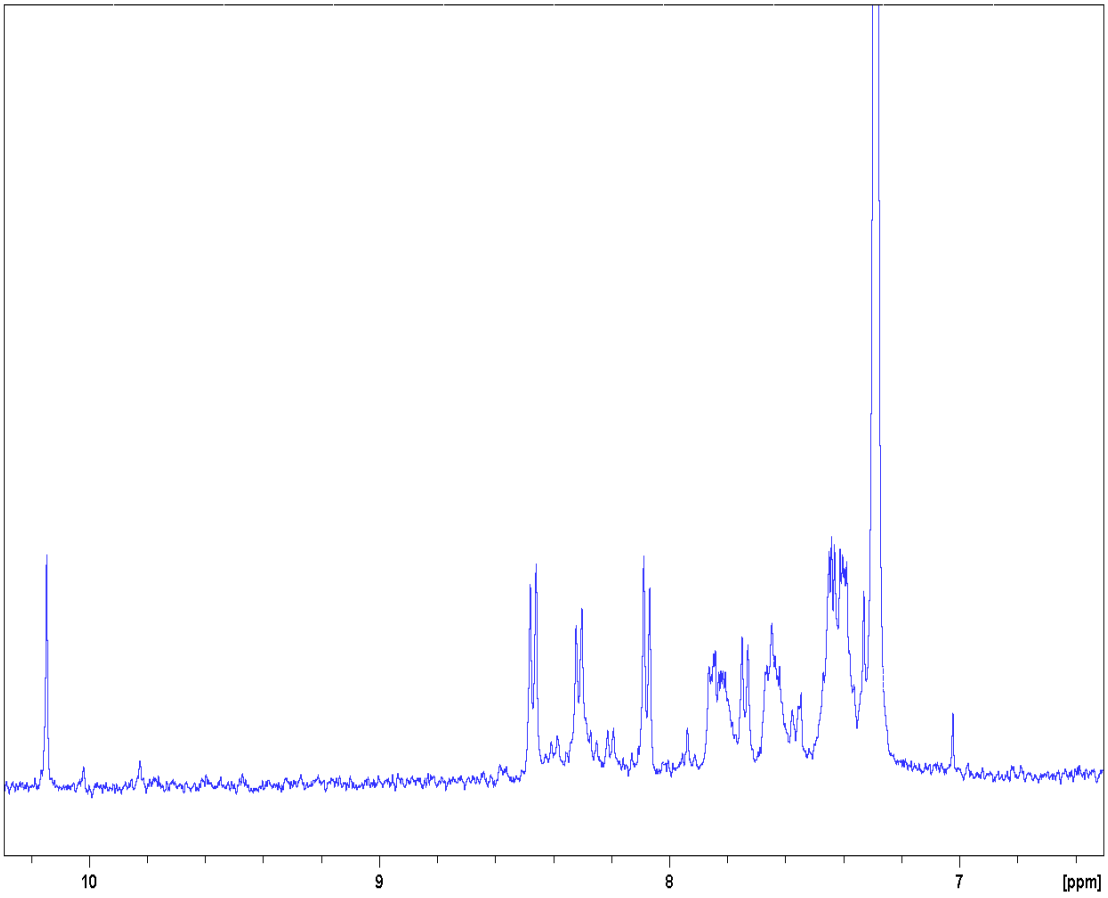

Figure III.13. Magnification of the ^{1}H NMR spectrum, from 6.5 to 10.3 ppm, of trans-BBS in $CDCl_3$, after 20 h of irradiation at 350 nm (light power, P = 16 W).

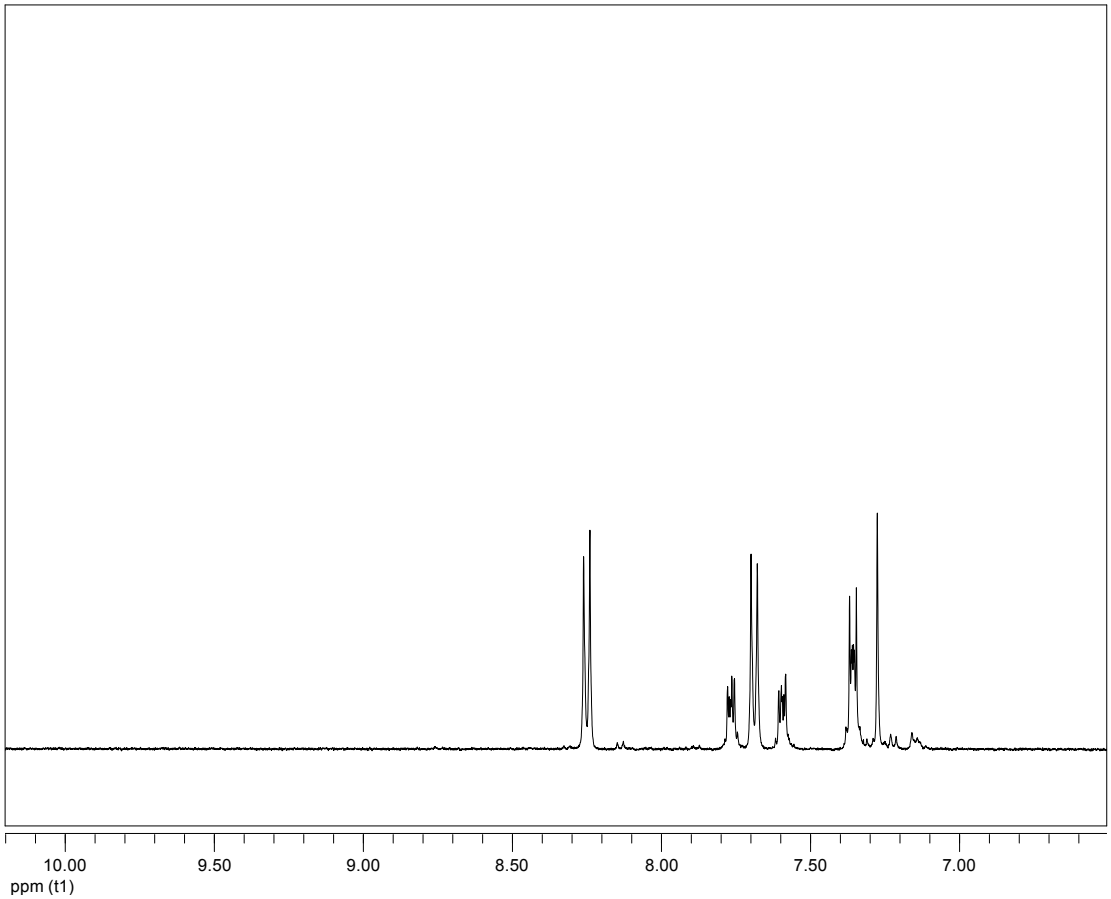

Figure III.14. ^{1}H NMR spectrum, from 6.5 to 10.2 ppm, of trans-BBS in *d*-TCE, before irradiation at 350 nm (light power, P = 32 W).

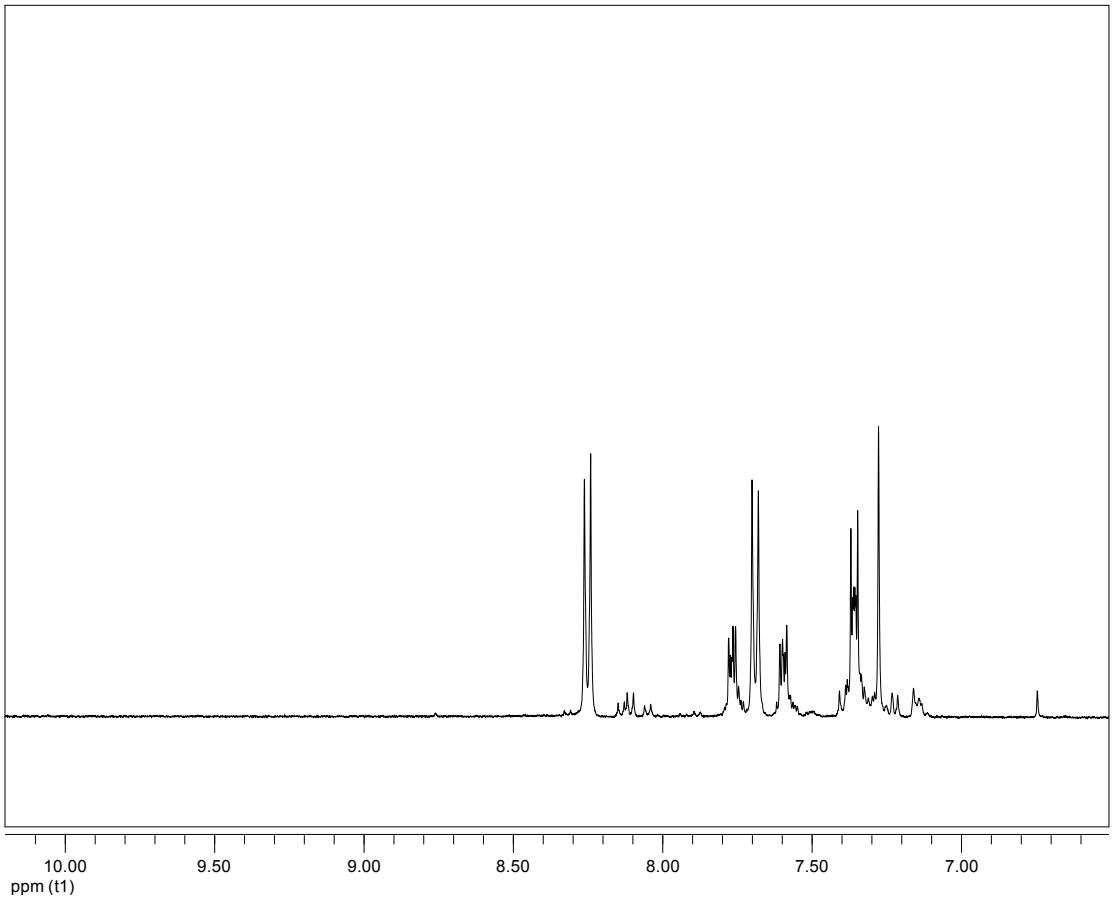

Figure III.15. ^{1}H NMR spectrum, from 6.5 to 10.2 ppm, of trans-BBS in *d*-TCE, after 2 h of irradiation at 350 nm (light power, P = 32 W).

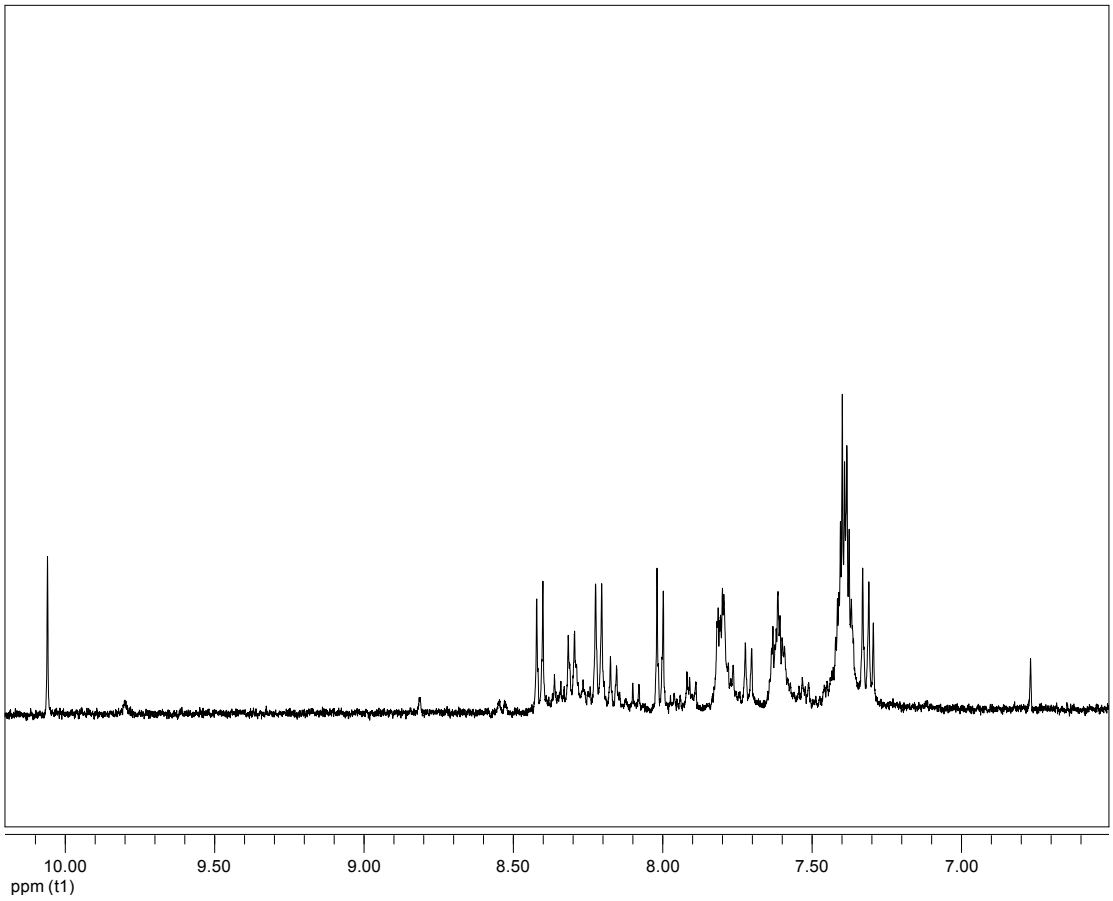

Figure III.16. ^{1}H NMR spectrum, from 6.5 to 10.2 ppm, of trans-BBS in *d*-TCE, after 5 h of irradiation at 350 nm (light power, P = 32 W).

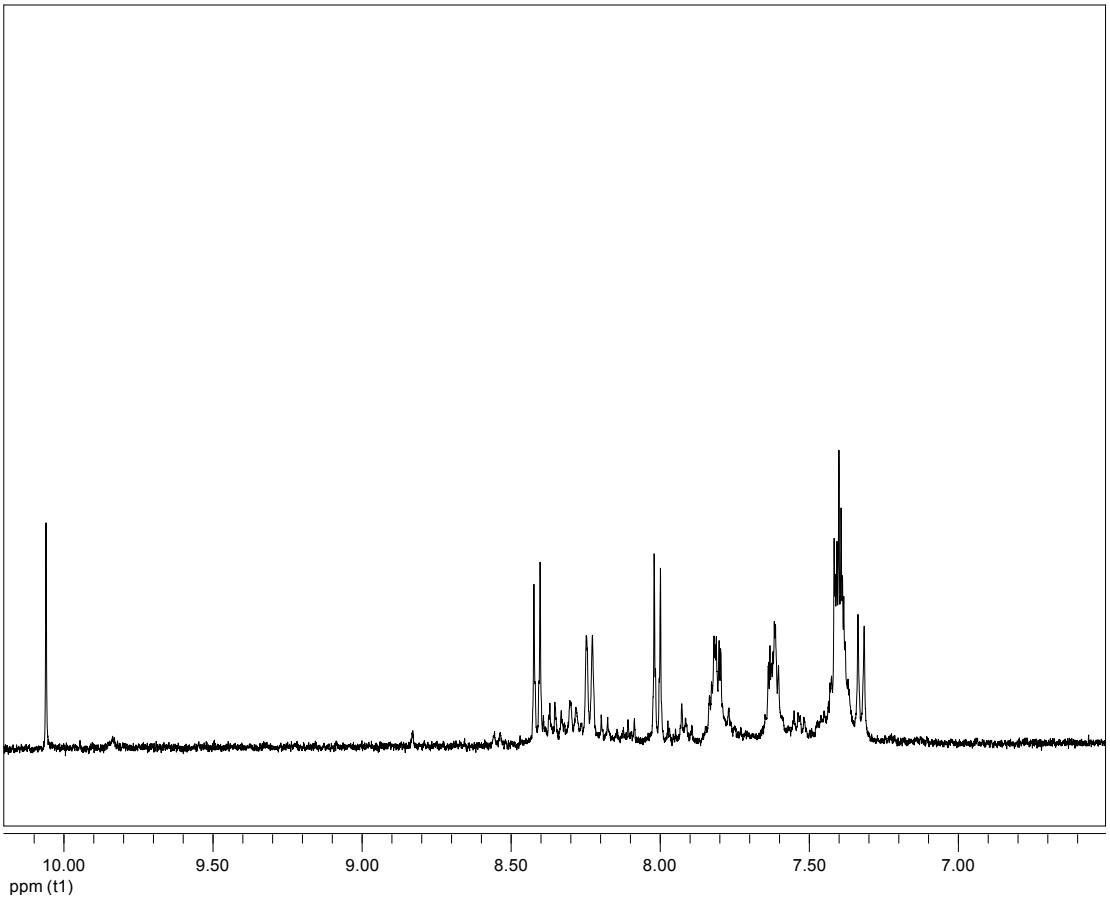

Figure III.17. ^{1}H NMR spectrum, from 6.5 to 10.2 ppm, of trans-BBS in *d*-TCE, after 9 h of irradiation at 350 nm (light power, P = 32 W).

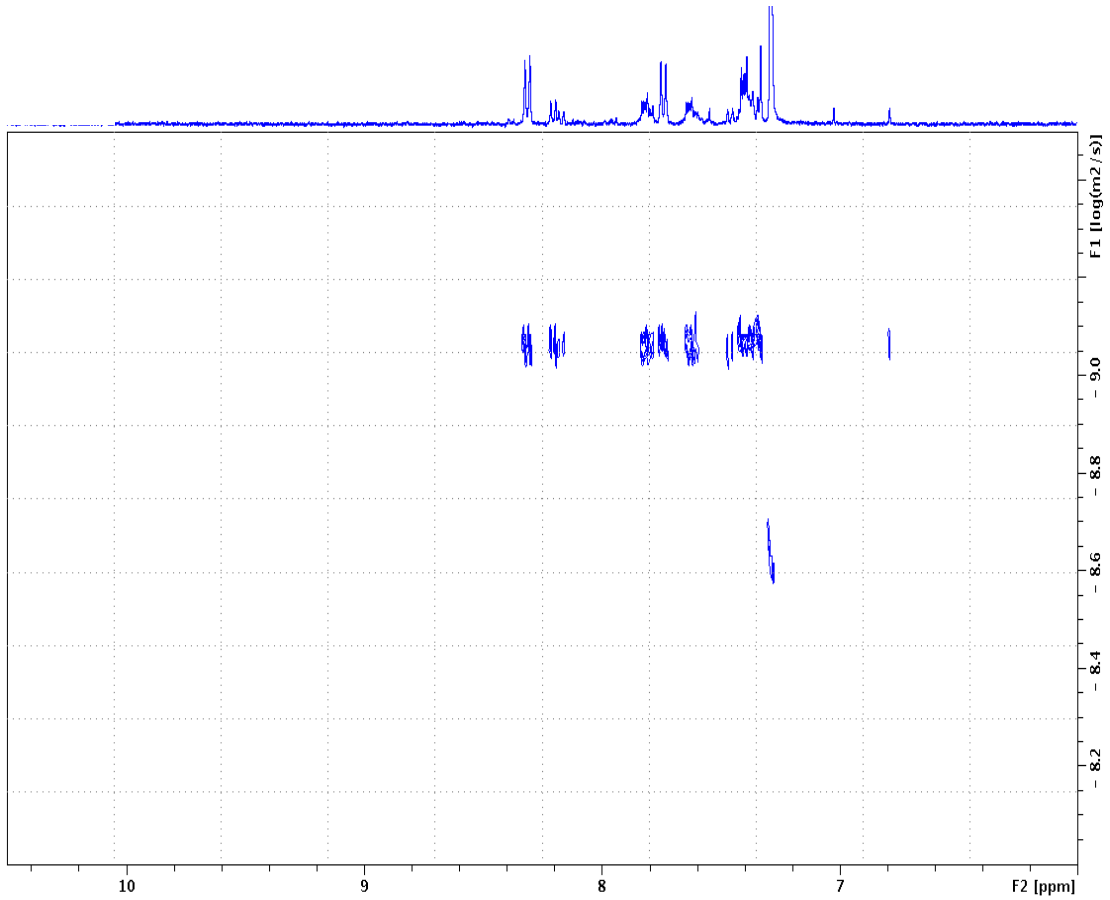

Figure III.18. DOSY NMR results for BBS after 4 h of UV irradiation, recorded in $CDCl_3$ at room temperature at 400 MHz. The x-axis represents the standard ^1H dimension, from 6 to 10.5 ppm, and the y-axis represents the diffusion dimension.

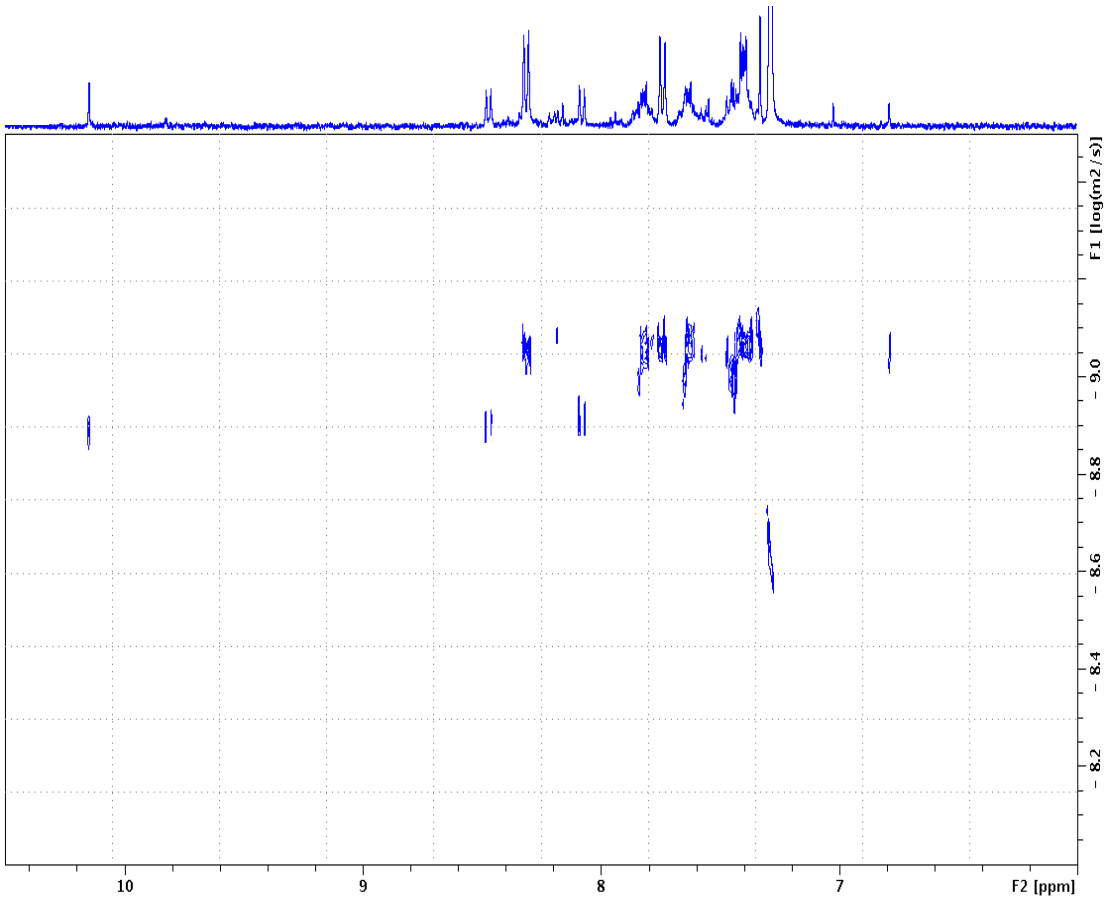

Figure III.19. DOSY NMR results for BBS after 10 h of UV irradiation, recorded in $CDCl_3$ at room temperature at 400 MHz. The x-axis represents the standard ^1H dimension, from 6 to 10.5 ppm, and the y-axis represents the diffusion dimension.

References

(1) Irie, M. *Chem. Rev.* **2000**, *100*, 1685.

(2) Momotake, A.; Arai, T. *J. Photochem. Photobiol. C* **2004**, *5*, 1.

(3) Bischoff, P.; Hutter, C.; Puebla, C.; E.P. 1294846, **2001**.

(5) Bur, A. J.; Roth, S. C. *Polym. Eng. Sci.* **2004**, *44*, 898.

(6) Pucci, A.; Bertoldo, M.; Bronco, S. *Macromol. Rapid Commun.* **2005**, *26*, 1043.

(7) Pucci, A.; Ruggeri, G.; Bronco, S.; Bertoldo, M.; Cappelli, C.; Ciardelli, F. *Prog. Org. Coat.* **2007**, *58*, 105.

(8) Sing, C. E.; Kunzelman, J.; Weder, C. *J. Mater. Chem.* **2009**, *19*, 104.

(9) Pucci, A.; Cappelli, C.; Bronco, S.; Ruggeri, G. *J. Phys. Chem. B* **2006**, *110*, 3127.

(10) Jervis, D. A. *Plast. Addit. Compd.* **2003**, *5*, 42.

(11) Seydack, M.; Bendig, J. *J. Fluoresc.* **2000**, *10*, 291.

(12) Saltiel, J.; Megarity, E. D. *J. Am. Chem. Soc.* **1972**, *94*, 2742.

(13) Saltiel, J.; Marinari, A.; Chang, D. W. L.; Mitchener, J. C.; Megarity, E. D. *J. Am. Chem. Soc.* **1979**, *101*, 2982.

(14) Saltiel, J.; Sun, Y. P. *J. Phys. Chem.* **1989**, *93*, 6246.

(15) Arai, T.; Tokumaru, K. *Chem. Rev.* **1993**, *93*, 23.

(16) Meier, H. *Angew. Chem.* **1992**, *31*, 1399.

(17) Whitten, D. G. *Acc. Chem. Res.* **1993**, *26*, 502.

(18) Johnson, A. R.; Lee, S.-J.; Klein, J.; Kanicki, J. *Rev. Sci. Instr.* **2007**, *78*, 96101.

(19) Porrès, L.; Holland, A.; Pålsson, L.-O.; Monkman, A. P.; Kemp, C.; Beeby, A. *J. Fluoresc.* **2006**, *16*, 267.

(20) Fourati, M. A.; Maris, T.; Bazuin, C. G.; Prud'homme, R. E. *Acta Crystallogr., Sect. C: Cryst. Struct. Commun.* **2010**, *66*, o11.

(21) Sheldrick, G. M. *Acta Cryst. A* **2008**, *64*, 112.

(22) van der Sluis, P.; Spek, A. L. *Acta Crystallogr. A* **1990**, *46*, 194.

(23) Spek, A. L.; Platon, *A Multipurpose Crystallographic Tool*; Utrecht University: Utrecht, The Netherlands, **2010**.

(24) Karstens, T.; Kobs, K. *J. Phys. Chem.* **1980**, *84*, 1871.

(25) Bolduc, A.; Dufresne, S.; Hanan, G. S.; Skene, W. G. *Can. J. Chem.* **2010**, *88*, 236.

(26) Birch, D. J. S.; Birks, J. B. *Chem. Phys. Lett.* **1976**, *38*, 432.

(27) Carmichael, I.; Hug, G. L. *J. Phys. Chem. Ref. Data* **1986**, *15*, 1.

(28) Scaiano, J. C. *CRC Handbook of Organic Photochemistry*; CRC Press: Boca Raton, **1989**.

(29) Abraham, R. J.; Fisher, J.; Loftus, P. *Introduction to NMR Spectroscopy*; Wiley: Chichester, **1988**.

(30) Lambert, J. B.; Shurvell, H. F.; Lightner, D. A.; Cooks, R. G. *Organic Structural Spectroscopy*. Upper Saddle River, NJ, **1998**.

(31) Seiber, R. P.; Needles, H. L. *Textile Res. J.* **1972**, *42*, 261.

(32) Murthy, R. S.; Bio, M.; You, Y. *Tetrahedron Lett.* **2009**, *50*, 1041.

(33) Baucherel, X.; Uziel, J.; Jugé, S. *J. Org. Chem.* **2001**, *66*, 4504.

(34) Yin, P.; Wu, P.; Xiao, Z.; Li, D.; Bitterlich, E.; Zhang, J.; Cheng, P.; Vezenov, D. V.; Liu, T.; Wei, Y. *Angew. Chem. Int. Ed.* **2011**, *50*, 2521.

(35) Floquet, S.; Lemonnier, J. F.; Kachmar, A.; Rohmer, M. M.; Benard, M.; Marrot, J.; Terazzi, E.; Piguet, C.; Cadot, E. *Dalton Trans.* **2007**, 3043.

(36) Parac-Vogt, T. N.; Van Lokeren, L.; Cartuyvels, E.; Absillis, G.; Willem, R. *Chem. Commun.* **2008**, 2774.

(37) Haupt, E. T. K.; Schaffer, C.; Bogge, H.; Merca, A.; Weinstock, I. A.; Rehder, D.; Muller, A. *Angew. Chem., Int. Ed.* **2009**, *48*, 8051.

(38) Groves, P.; Rasmussen, M. O.; Molero, M. D.; Samain, E.; Canada, F. J.; Driguez, H.; Jimenez-Barbero, J. *Glycobiology* **2004**, *14*, 451.

(39) Bhalerao, U. T.; Sridhar, M. *Tetrahedron Lett.* **1993**, *34*, 4341.

(40) Hirashima, S.-i.; Kudo, Y.; Nobuta, T.; Tada, N.; Itoh, A. *Tetrahedron lett.* **2009**, *50*, 4328.

(41) Bernstein, J.; Davis, R. E.; Shimoni, L.; Chang, N. L. *Angew. Chem. Int. Ed. Inter. Ed.* **1995**, *34*, 1555.

CHAPITRE IV: (E)-4,4'-Bis(1,3-benzoxazol-2-yl)-stilbene at 150 and 375 K*

Abstract

The title compound, a chromophore of formula $C_{28}H_{18}N_2O_2$, crystallizes with the molecule lying on an inversion center to give one-half of a crystallographically independent molecule in the asymmetric unit. The molecule is almost planar, with slight deviation of the benzene rings from the mean molecular plane. The structure is characterized by a herringbone packing arising from several C─H···π and π─π intermolecular interactions. The benzoxazole group is disordered between two orientations, with occupancy factors of 0.669 (10) and 0.331 (10) at 150 K [0.712 (7) and 0.288 (7) at 375 K].

Comment

The title compound, hereinafter denoted BBS, belongs to the well-known class of stilbenes where conjugation between the two phenyl groups allows UV excitation to induce conversion between the *E* and *Z* isomers, making these compounds useful as photoactive switches (Irie, 2000; Momotake & Arai, 2004). This compound is generally employed as a fluorescent brightener in textiles (Bischoff *et al.*, 2001), detergents and other materials (Bur & Roth, 2004). It is also used as an additive for food and consumer packaging materials, due to its compliance with the US Food and Drug Administration regulations (Jervis, 2003). In addition, BBS has applications in host–guest systems as a molecular probe of deformation and temperature in polymer films (Pucci *et al.*, 2005, 2007; Sing *et al.*, 2009). The anisotropic flat shape of the molecule can be exploited to produce polarized light by adding the chromophore to oriented macromolecular matrices (Pucci *et al.*, 2006).

---

*Fourati, M. A., Maris, T., Bazuin, C. G. and Prud'homme, R. E. *Acta Cryst.* **2010**, C66, o11-o14. 10.1107/S0108270109050379.

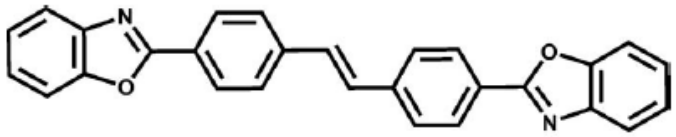

BBS

Figure IV.1 shows the fluorescence spectrum of BBS diluted in poly(1,4-butylene succinate) (PBS) at various concentrations, similar to data reported by Pucci *et al.* (2007). At low concentrations, the fluorescence spectra resemble the spectrum of BBS in tetrachloroethane solution (Pucci *et al.*, 2005, 2007), with emission bands centred at 410, 434 and 464 nm. These spectra are associated with isolated BBS monomers molecularly dispersed in the amorphous phase of PBS. Increasing the BBS concentration from 0.02 to 0.2 wt % induces the emergence of a broad emission band centred at about 500 nm, and is accompanied by a colour change from blue to green. The broad band is attributed to the formation of BBS aggregates, favoured by π—π interactions of BBS molecules in planar conformation, thus allowing excimer emission (Pucci *et al.*, 2005, 2007).

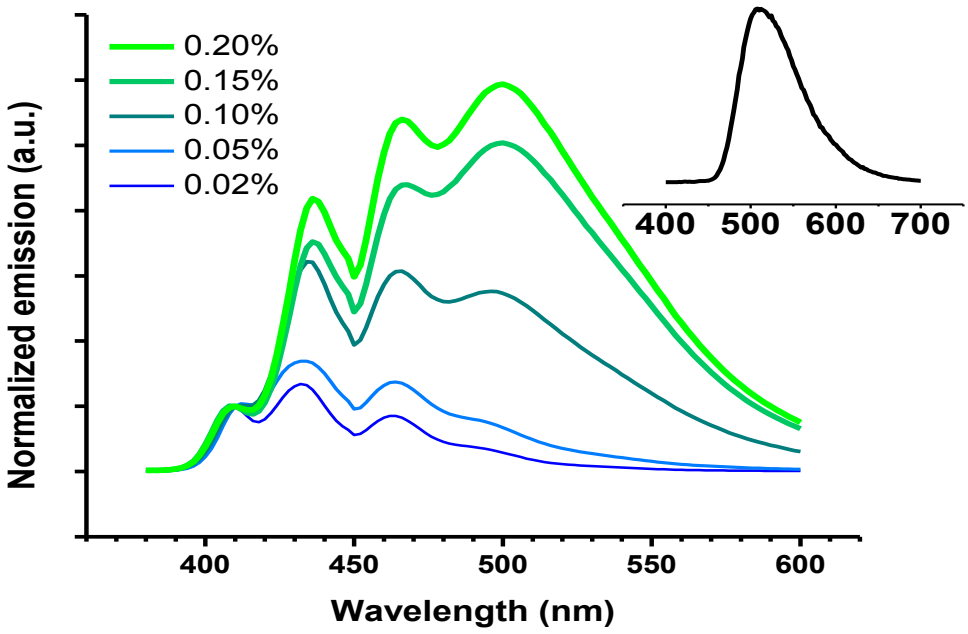

Figure IV.1. Fluorescence spectra of BBS molecules dispersed at various concentrations (wt %) in poly(1,4-butylene succinate) films at λ_{exc} = 374 nm, normalized relative to the peak at 410 nm. Inset: fluorescence spectrum of BBS pellets (compacted powder) containing only BBS aggregates.

For more precise information on BBS stacking characteristics, we report here the single-crystal structure of BBS crystallized from a solution of 1,2-dichlorobenzene. The inset in Figure IV.1 shows that the fluorescence spectrum of the yellow bulk powder displays only the broad band centred at about 500 nm and none of the three bands characteristic of isolated BBS molecules. This indicates that the powder is composed only of excimer-forming aggregates. The latter can be assumed to have the same structure as in the PBS films, as supported by the observation that the X-ray powder diffraction pattern of the bulk sample is consistent with the calculated pattern obtained from the experimental single-crystal data. This allows a correlation to be made between the single-crystal structure of BBS and excimer emission in BBS-containing films.

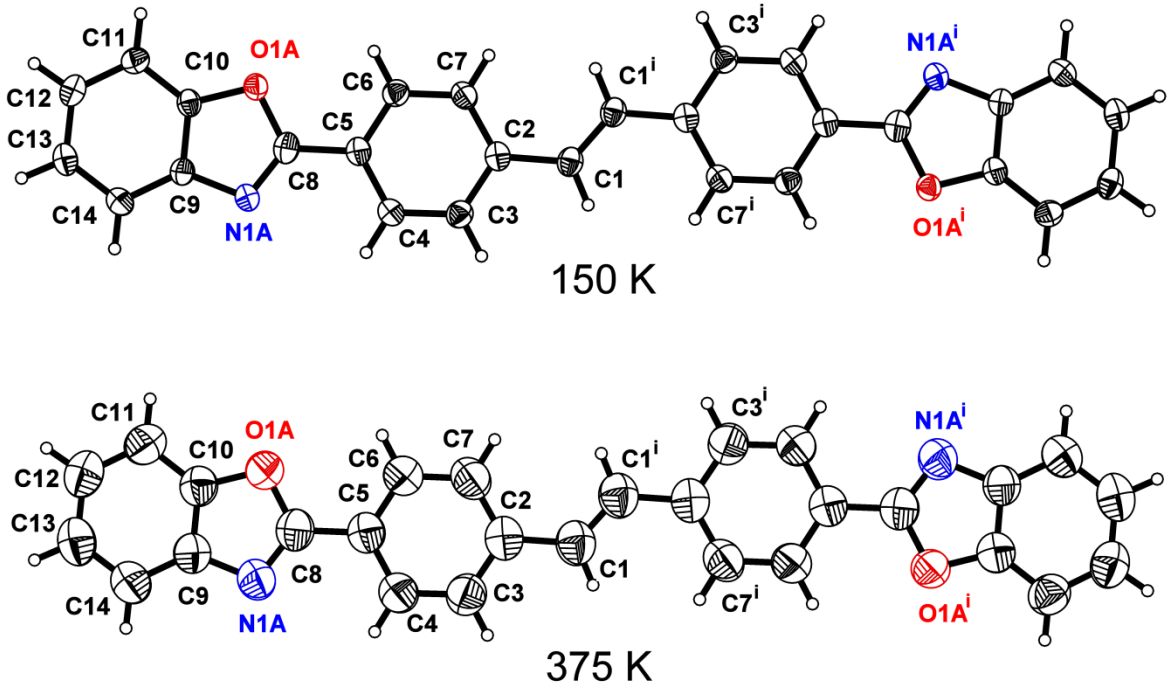

Figure IV.2. The molecular structure of BBS at 150 and 375 K, showing the atom-numbering scheme. Displacement ellipsoids are drawn at the 50% probability level and H atoms are shown as small spheres of arbitrary radii. Only one component of the disordered benzoxazolyl ring is shown. [symmetry code: (i) $\frac{3}{2}-x$, $-y-\frac{1}{2}, -z$].

From the single-crystal structure analysis at 150 K, it is found that the molecule of BBS is almost planar and lies on an inversion centre located at the mid-point of the C=C bond (Figure IV.2). The mean planes of the central benzene rings and the central alkene group are twisted relative to one another by 6.66 (13)°, but the angle between the benzene rings and the benzoxazolyl groups is only 2.30 (16)°. Moreover, the structure of BBS features a network composed of layers in the *bc* plane, with molecules packed in a well-defined herringbone pattern (Figure IV.3), similar to that of stilbene (Harada & Ogawa, 2001, 2004) but unlike other stilbene derivatives (Foitzik *et al.*, 1991; Ohba *et al.*, 2002; Soto Bustamante *et al.*, 1995).

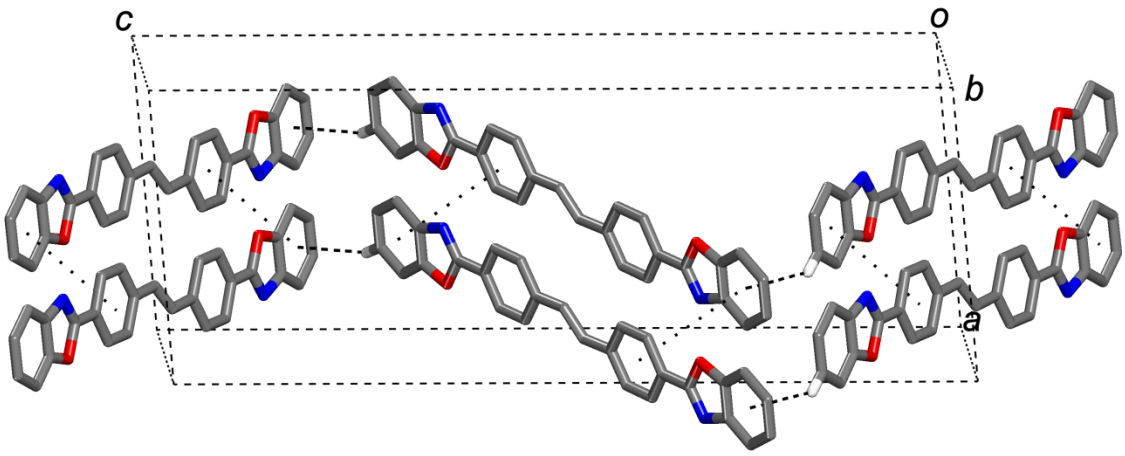

Figure IV.3. A view of the C─H···π and π─π stacking interactions (dotted lines) in one layer of π-stacked molecules of BBS at 150 K.

Within the layers, the flat molecules are packed via π–π stacking interactions and C–H···π contacts. The π–π stacking interactions feature a short centroid–centroid distance of 3.6565 (7) Å between the central benzene ring (C*g*3) and the terminal benzene ring (C*g*4^{ii}), with a dihedral angle of 2.28 (6)° between ring planes [symmetry code: (ii) *x, y – 1, z*]. The π–stacked molecules are staggered relative to one another and the benzene rings overlap at a perpendicular distance of 3.3914 (5) Å. Moreover, a C–H···π contact (Figure IV.3) involves atom H12, with a distance to the terminal benzene ring centroid C*g*4^{iii} of 2.77 (1) Å [symmetry code: (iii) $\frac{3}{2}-x, \frac{1}{2}+y, \frac{1}{2}-z$].

trans-Stilbenes and diazobenzenes are known to be subject to orientational disorder, described as a pedal-like motion wherein the pair of benzene rings rotates around the central double bond like a bicycle pedal (Harada & Ogawa, 2001; Bouwstra *et al.*, 1984). This disorder is dynamic with inter-conversion between the major and minor conformers, the relative populations of which vary with temperature. At lower temperatures, the low occupancy factor of the minor conformer can make the disorder almost invisible (Harada & Ogawa, 2004). Usually, this disorder is detected by a shortening of the central double bond (Masciocchi *et al.*, 2005) and by the appearance in the final Fourier difference map of two residual peaks in the vicinity of the central double bond that arise from the minor

conformer (Harada & Ogawa, 2001, 2004). This was examined for BBS by measuring two different single crystals grown from the same solution, one at 150 K and the other at 375 K. The distance of the central C1=C1^{i} double bond is 1.331 (2) Å at 150 K and 1.306 (2) Å at 375 K [symmetry code: (i) $\frac{3}{2} - x, -y - \frac{1}{2}, -z$]. At 150 K, the value compares well with the normal expected value for a double bond, and the difference Fourier map calculated after the final refinement of BBS (Spek, 2009) did not reveal any significant residual peaks in the region of the C=C bond. At 375 K, the central double bond is significantly shorter than expected but no residual peaks were detected in the final difference Fourier map. This may indicate that at 375 K the crystal is near the onset of dynamic disorder.

On the other hand, disorder related to the benzoxazolyl moiety was detected by the *checkCIF* (Spek, 2009) procedure performed at the end of the refinement. Two bonds, N1–C8 and O1–C10, failed the Hirshfeld difference test (Hirshfeld, 1976), with a very large s.u. of 15 for N1–C8. Examination of the final atomic displacement ellipsoid plot showed that the ellipsoids for atoms N1 and O1 are smaller and larger, respectively, than those for the other atoms of the molecule. These features were attributed to a substitutional disorder between O and N atoms sharing the same position. Such a statistical disorder in benzoxazolyl derivatives has been described previously (Norman *et al.*, 2002; Zhuang *et al.*, 2002). The occupancy factors of the N and O atoms were refined, giving a ratio of 0.66:0.34 between the two possible conformations for the crystal measured at 150 K.

The single-crystal structure of BBS confirms that the BBS molecules have an essentially planar conformation with extensive π–π stacking interactions that allow for excimer formation, giving rise to the emission band centred at 500 nm. More specifically, the molecules are packed into a two dimensional herringbone network, held together by intermolecular π–π and C–H···π interactions. The perpendicular distance of 3.46 Å and the centroid–centroid distances of 3.6–3.7 Å between π–stacked molecules are very close to the pyrene interplanar stacking distance of 3.53 Å (Gilbert & Baggott, 1991). This distance is within the range of 3–4 Å that is considered necessary for excimer formation to take place (Gilbert & Baggott, 1991).

Table IV.1. Comparison of bond lengths (Å) in BBS at 150 and 375 K.

Bond	150 K	375 K
C1—C1^{i}	1.331 (2)	1.306 (2)
C1—C2	1.4656 (17)	1.4659 (14)
C2—C3	1.3981 (17)	1.3854 (15)
C2—C7	1.3990 (17)	1.3940 (16)
C3—C4	1.3853 (17)	1.3837 (14)
C4—C5	1.3917 (17)	1.3906 (15)
C5—C6	1.3957 (17)	1.3796 (14)
C5—C8	1.4520 (17)	1.4474 (14)
C6—C7	1.3760 (17)	1.3796 (14)
C8—N1*A*	1.270 (5)	1.270 (3)
C8—O1*A*	1.382 (4)	1.382 (3)
C9-N1*A*	1.405 (4)	1.398 (3)
C10-O1*A*	1.377 (3)	1.383 (2)

Symmetry code: (i) $\frac{3}{2}-x,-y-\frac{1}{2},-z$.

Experimental

4,4'-Bis(2-benzoxazolyl)-stilbene (BBS) was obtained from Aldrich (97%, m.p. > 573 K) and used without further purification. Yellow needle-like crystals of BBS suitable for X-ray diffraction analysis were obtained by slow evaporation from a solution in 1,2-dichlorobenzene. Poly(1,4-butylene succinate) (Bionolle 1001) was obtained from Showa Highpolymer (Japan). PBS-BBS blends were prepared by melt-processing in a Plasti-Corder Brabender mixer, type DDRV501/DIGI-SYS, using 20 g of the polymer and 0.02 to 0.2 wt % of the chromophore. Films with a thickness of about 80-120 μm were obtained by compression-moulding between two aluminium foils in a press at 473 K, followed by slow cooling to room temperature. Fluorescence emission spectra were recorded at ambient

temperature using an Edinburgh Instruments FLS-920 fluorimeter, operating at an excitation wavelength of 374 nm.

Compound (I) at 150 K

Crystal data

$C_{28}H_{18}N_2O_2$ $V = 1950.72\ (12)$ Å^3

$Mr = 414.44$ $Z = 4$

Monoclinic, $C2/c$ Cu $K\alpha$ radiation

$a = 11.2449\ (4)$ Å $\mu = 0.71$ mm^{-1}

$b = 6.0053\ (2)$ Å $T = 150$ K

$c = 29.0699\ (11)$ Å 0.28 × 0.04 × 0.03 mm

$\beta = 96.4280\ (17)^o$

Data collection

Bruker Microstar diffractometer 17375 measured reflections

Absorption correction: multi-scan 1778 independent reflections

(Sadabs; Bruker, 2009) 1606 reflections with $I > 2\sigma(I)$

$T_{min} = 0.874$, $T_{max} = 0.979$ $R_{int} = 0.045$

Refinement

$R[F^2 > 2\sigma(F^2)] = 0.032$ 4 restraints

$wR(F^2) = 0.091$ H-atom parameters constrained

$S = 1.05$ $\Delta\rho_{max} = 0.21$ e Å^{-3}

1778 reflections $\Delta\rho_{min} = -0.15$ e Å^{-3}

152 parameters

Compound (I) at 375 K

Crystal data

$C_{28}H_{18}N_2O_2$ $V = 2028.08\ (12)\ Å^3$

$Mr = 414.44$ $Z = 4$

Monoclinic, $C2/c$ Cu $K\alpha$ radiation

$a = 11.3459\ (5)$ Å $\mu = 0.69\ mm^{-1}$

$b = 6.0578\ (3)$ Å $T = 375$ K

$c = 29.6234\ (15)$ Å 0.60 × 0.18 × 0.05 mm

$\beta = 95.073\ (3)^o$

Data collection

Bruker SMART 6000 diffractometer 13180 measured reflections

Absorption correction: multi-scan 12519 independent reflections

(Sadabs; Bruker, 2009) 9599 reflections with $I > 2\sigma(I)$

$T_{min} = 0.825$, $T_{max} = 0.966$

Refinement

$R[F^2 > 2\sigma(F^2)] = 0.058$ 4 restraints

$wR(F^2) = 0.176$ H-atom parameters constrained

$S = 1.09$ $\Delta\rho_{max} = 0.19\ e\ Å^{-3}$

12519 reflections $\Delta\rho_{min} = -0.16\ e\ Å^{-3}$

153 parameters

The initial unit-cell parameters were determined by a least-squares fit of the angular setting of strong reflections, collected by a 10.0° scan in 33 frames over three different parts of the reciprocal space. The final unit cell was obtained from the *xyz* centroids of 7849 selected reflections at 150 K (4605 reflections at 375 K) after integration using the *SAINT-Plus* software package (Bruker, 2009).

H atoms were positioned geometrically and refined with a riding model, with C–H = 0.95 Å and *U*iso(H) = 1.2 *U*eq(C). The benzoxazolyl group shows orientational disorder.

It was assumed that atoms N1A and O1B, and atoms O1A and N1B share close positions and the same atomic displacement parameters. During refinement, similarity restraints were applied to the C=N and to the C–O distances. Atoms O1A and O1B were constrained to have the same atomic displacement parameters, as were N1A and N1B. With these restraints, the occupancy factors converged to 0.669 (10) and 0.331 (10) for N1A/O1A and N1B/O1B, respectively, for the crystal measured at 150 K [0.712 (7) and 0.288 (7) at 375 K].

For the crystal measured at 375 K, analysis of the refined solution using *PLATON/TwinRotMat* (Spek, 2009) indicated nonmerohedral twinning about a twofold rotation axis [001]. The *TwinRotMat* routine was used to prepare a modified *hkl* file for use with the HKLF5 option in *SHELXL97* (Sheldrick, 2008). The resulting twin fractions were 0.1102 (16) and 0.8898 (16).

For both data sets, data collection: *APEX2* (Bruker, 2009); cell refinement: *SAINT* (Bruker, 2009); data reduction: *SAINT*; program(s) used to solve structure: *SHELXS97* (Sheldrick, 2008); program(s) used to refine structure: *SHELXL97* (Sheldrick, 2008); molecular graphics: *SHELXTL* (Sheldrick, 2008) and *Material Studio* (Accelrys, 2005); software used to prepare material for publication: *UdMX* (Maris, 2004) and *publCIF* (Westrip, 2009).

Acknowledgements

The authors acknowledge financial support from NSERC (Canada), FQRNT (Quebec), NanoQuébec and the Canadian Foundation for Innovation. We also thank Professor W. Skene, Département de Chimie, Université de Montréal, for useful discussions on the fluorescence experiments. MAF thanks the Tunisian Government for a Scholarship of Excellence.

References

Accelrys (2005). *Material Studio*. Accelrys Inc., Princeton, New Jersey, USA.

Bischoff, P., Hutter, C. & Puebla, C. (2001). Eur. Patent No. EP 1294846.

Bouwstra, J. A., Schouten, A. & Kroon, J. (1984). *Acta Cryst.* C**40**, 428–431.

Bruker (2009). *APEX2*, *SAINT-Plus* and *SADABS*. Bruker AXS Inc., Madison, Wisconsin, USA.

Bur, A. J. & Roth, S. C. (2004). *Polym. Eng. Sci.* **44**, 898–908.

Foitzik, J. K., Paulus, H., Haase, W. & Loub, J. (1991). *Acta Cryst.* C**47**, 1640–1642.

Gilbert, A. & Baggott, J. (1991). *Essentials of Molecular Photochemistry*, pp. 154–155. Oxford: Blackwell Scientific Publications.

Harada, J. & Ogawa, K. (2001). *J. Am. Chem. Soc.* **123**, 10884–10888.

Harada, J. & Ogawa, K. (2004). *J. Am. Chem. Soc.* **126**, 3539–3544.

Hirshfeld, F. L. (1976). *Acta Cryst.* A**32**, 239–244.

Irie, M. (2000). *Chem. Rev.* **100**, 1685–1716.

Jervis, D. A. (2003). *Plast. Addit. Compd.* **5**, 42–46.

Maris, T. (2004). *UdMX*. University of Montréal, Canada.

Masciocchi, N., Scuderi, P. & Maspero, A. (2005). *Acta Cryst.* E**61**, o227–o229.

Momotake, A. & Arai, T. (2004). *J. Photochem. Photobiol. Photochem. Rev.* **5**, 1–25.

Norman, D. W., Edwards, J. P., Vogels, C. M., Decken, A. & Westcott, S. A. (2002). *Can. J. Chem.* **80**, 31–40.

Ohba, S., Hiratsuka, T. & Tanaka, K. (2002). *Acta Cryst.* E**58**, o1013–o1015.

Pucci, A., Bertoldo, M. & Bronco, S. (2005). *Macromol. Rapid Commun.* **26**, 1043–1048.

Pucci, A., Cappelli, C., Bronco, S. & Ruggeri, G. (2006). *J. Phys. Chem. B*, **110**, 3127–3134.

Pucci, A., Di Cuia, F., Signori, F. & Ruggeri, G. (2007). *J. Mater. Chem.* **17**, 783–790.

Sheldrick, G. M. (2008). *Acta Cryst.* A**64**, 112–122.

Sing, C. E., Kunzelman, J. & Weder, C. (2009). *J. Mater. Chem.* **19**, 104–110.

Soto Bustamante, E. A., Hanemann, T., Haase, W., Svoboda, I. & Fuess, H. (1995). *Acta Cryst.* C**51**, 2192–2196.

Spek, A. L. (2009). *Acta Cryst.* D**65**, 148–155.

Westrip, S. P. (2009). *publCIF*. In preparation.

Zhuang, J.-P., Zheng, Y. & Zhang, W.-Q. (2002). *Acta Cryst.* **E58**, o720–o722.

CHAPITRE V: Infrared and Fluorescence Spectroscopy Investigation of the Orientation of Two Fluorophores in Stretched Polymer Films*

Abstract

The simultaneous orientation of poly(1,4-butylene)succinate (PBS) and 4,4'-bis(2-benzoxazolyl)stilbene (BBS) or 2,5-bis(5-*tert*-butyl-benzoxazol-2-yl)thiophene (BBT) in PBS-BBS and PBS-BBT films was investigated during stretching at 80 °C, about 33 °C below the PBS melting temperature. The PBS orientation was first investigated using the 3430 cm^{-1} infrared band and its order parameter $<P_2>$ goes from 0.36 at a local strain of 359 % for pure PBS to 0.66 in blends containing 6 wt % of BBT at a local draw ratio of ≈ 350% (or 0.56 with 5 wt % of BBS). At the same time, BBT shows in the same films an orientation parameter $<P_2>$ reaching a maximum of 0.31 at a local strain of ≈ 350%, using the 1580 cm^{-1} band. Since polarized FT-IR was unable to provide the orientation of BBS due to overlapping bands with PBS, polarized fluorescence spectroscopy was then used and reveals an apparent order parameter of 0.32 for BBS monomers (or 0.34 for BBT monomers), but to no orientation of BBT aggregates and BBS excimers. In other words, the two small molecules behave similarly in terms of orientation independently of their molecular shape and packing. BBS and PBS both exhibit a sharp increase of S and $<P_2>$ when reaching a BBS concentration of ≈ 0.08 wt %, whereas BBT and PBS show a smooth increase of S and $<P_2>$, respectively, in films containing BBT. The sharp increase, or transition in orientation, is accompanied by a conversion of BBS from monomers to excimers, whereas BBT-containing films show a regular increase of the number/size of BBT aggregates. These results indicate that the dye (BBS or BBT) has a profound influence on the orientation of the semi-crystalline polymer (PBS) since its $<P_2>$ almost doubles at dye concentrations above 0.08 wt %. The results also suggest that the use of a fluorescent probe to follow the polymer chain orientation is not applicable for such systems.

---

*Fourati, M. A., Pellerin, C., Bazuin, C. G. and Prud'homme, R. E. Polymer **2013**, *54*, 730-736. 10.1016/j.polymer.2012.11.063.

V.1. Introduction

It has been demonstrated by several groups that luminogenic materials, i.e., polymers in which a small quantity of a fluorescent dye is dispersed, can be used as chemical sensors.[1-4] At very low dye concentrations, the system exhibits monomer emission, indicating a molecular dispersion of the dye inside the polymer. Above a certain critical concentration, which depends upon the solubility of the dye into the polymer matrix, the system exhibits excimer emission indicating dye aggregation.[4-8]

Among many other parameters, it has been shown that the mechanical deformation of the system induces a transition from excimer emission to monomer emission due to the breakup of the aggregates during the deformation.[3,9,10] For example, Crenshaw et al. have dispersed cyano-substituted oligo(phenylenevinylene) derivatives into polyethylene and observed a color change upon deformation, greatly influenced by the degree of crystallinity of the polymer.[9] A second example is that of Pucci et al. who have studied a different system: a stilbene derivative in poly(1,4-butylene succinate) (PBS), a semi-crystalline polymer.[10] Both studies emphasize the presence of aggregates of the order of microns before stretching and the importance of the crystallinity of the polymer.

However, even if the color change upon deformation is well documented in these studies as well as the corresponding fluorescence emission spectra, the analysis remains qualitative. In this work, our goal is to determine quantitatively the orientation of both the dye and the polymer as a function of deformation and dye concentration. For that purpose, we have selected a system that we[11,12] and others[10] have already studied. We used polarized Fourier Transform Infrared (FT-IR) spectroscopy,[13-17] which is a powerful technique for studying the orientation of multi-component systems since the different components may be differentiated via specific infrared bands, e.g., in semi-crystalline polymers,[13,15,18] polymer blends[19-23] or block copolymers.[24] However, it requires a relatively high concentration of small molecule. On the other hand, polarized fluorescence spectroscopy can detect much smaller concentrations, making both techniques complementary. The results show that the orientation of the polymer is much larger than the orientation of the dye and that both are significantly affected by the dye concentration.

V.2. Experimental

Materials

4,4'-bis(2-benzoxazolyl)stilbene (97%, melting point > 300 °C) and 2,5-bis(5-*tert*-butyl-benzoxazol-2-yl)thiophene (99%, melting point ~ 200 °C) (Chart V.1) were purchased from Aldrich Chemicals and used without further purification.

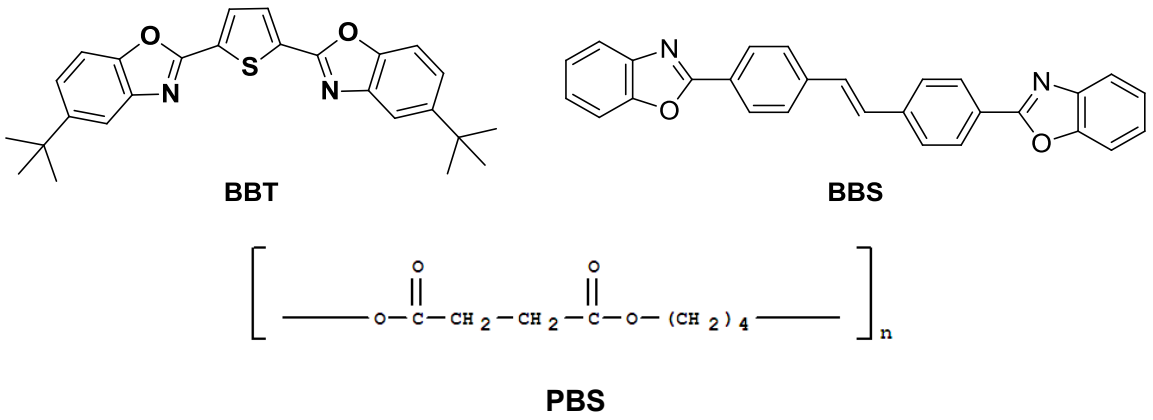

Chart V.1. Structures of 2,5-Bis(5-*tert*-butyl-benzoxazol-2-yl)thiophene *(BBT),* 4,4'-Bis(2-benzoxazolyl)stilbene *(BBS) and* poly(1,4-butylene succinate) (*PBS*).

Poly(1,4-butylene succinate) (PBS) ("Bionolle 1001") (Chart V.1) was graciously supplied by the Showa Highpolymer Company (Japan). PBS is a semi-crystalline polymer, characterized by a glass transition temperature of -34 °C and a melting temperature of 113 °C.

Sample Preparation

The dye-polymer films, PBS-BBS and PBS-BBT, were prepared by melt-processing in a DDRV501/DIGI-SYS Plasti-Corder Brabender mixer by mixing about 20 g of PBS and 0.01 to 5 wt % of BBS, or 0.01 to 6 wt % of BBT, at 200 °C for BBS and 180 °C for BBT, and at 50 rpm for 10 min. The resulting material was compressed and molded between two aluminum foils in a Carver Laboratory Press, under a pressure of 9 tons/m^2 below the fluorophores melting temperatures. The samples were then put in a cold press and were left

to cool at ~10 °C/min to room temperature before removal from the press, under a pressure of 2 tons/m^2, resulting in films with thicknesses of 40-100 μm.

Films used for mechanical deformation were prepared in a dogbone shape having a width of 4 mm and a length of 12 mm between the slits. Films were stretched at 80 °C, far above the PBS glass transition temperature of -34 °C and below its melting temperature of 113 °C, using an Instron model 5565 tensiometer, equipped with an environmental chamber and a 1 kN load cell. Stretching was performed at an elongation rate of 0.1 mm/s with an initial distance between the clamps of 2.5 cm, resulting in a non-homogeneous deformation. To prevent slippage during stretching, Pyrotape was fixed to the extremities of each strip. The actual local draw ratios (λ) were measured from the displacement of ink-marks drawn 1 mm apart onto the films before stretching as follow: $\lambda = \frac{L_f - L_i}{L_i}$ with L_f and L_i the final and initial length between marks, respectively. Following drawing, the chamber door was immediately opened and the temperature allowed dropping quickly to room temperature in order to freeze the orientation.

Polarized Fourier Transform Infrared (FT-IR) and Polarization Modulation Infrared Structural Absorbance Spectroscopy Measurements (PM-IRSAS).

Static polarized FT-IR spectra were recorded with a minimum of 128 scans per sample at a 4 cm^{-1} spectral resolution using a Bruker Vertex 70 spectrometer equipped with a liquid nitrogen-cooled mercury cadmium telluride detector and a KRS-5 wire-grid polarizer (Optometrics).

Polarization modulation infrared linear dichroism was first used by Buffeteau et al.[25-27] for measuring quantitative dichroic difference spectra and enabled the dynamic study of fast deformation and relaxation processes.[20-22,28-33] PM-IRSAS, a technique based on the same concepts and described in detail by Liang et al,[34] allows recording the individual p- and s-polarized spectra by switching the polarization plane of the infrared radiation at high frequency, permitting a direct measurement of the dichroic difference ($\Delta A = A_p - A_s$) spectrum with high sensitivity and 200 ms time resolution.[22] The orientation function, $\langle P_2 \rangle$, is calculated according to:[35]

$$\langle P_2 \rangle = \left(\frac{2}{3cos^2\alpha - 1}\right)\left(\frac{\Delta A}{A_p + 2A_s}\right) = \left(\frac{2}{3cos^2\alpha - 1}\right) T_2 \qquad \text{(V.1)}$$

where α is the angle between the transition dipole moment of the selected vibration and the main chain axis of the polymer. The limiting values of $<P_2>$ are 0 and 1 for random and perfect orientation along the stretching direction, respectively.

PM-IRSAS spectra with a resolution of 8 cm^{-1} were acquired with the same spectrometer using a side-port optical setup and two-channel electronic processing similar to that described elsewhere.[25-27,33,34] Briefly, a linear polarizer, a photoelastic modulator (PEM-90, type II/ZS50, Hinds Instruments) operating at 100 kHz ($2f_m$), a lock-in amplifier (Stanford Research Systems, SR830) with a 30 μs time constant, and two dual-channel electronic filters (Frequency Devices, 90TP/90IPB) were used to generate the double modulation and to isolate the experimental signals. A liquid nitrogen-cooled photovoltaic InSb detector (EG&G Judson) was used.

Fluorescence Measurements

Fluorescence emission spectra were recorded at ambient temperature in 10 mm cuvettes by excitation of the solutions at its corresponding absorption maximum, by using front-face geometry in an Edinburgh Instruments FLS-920 fluorimeter. Origin Pro 8 software by Microcal Origin® was used in the analysis of the emission data. Polarized fluorescence spectra were recorded under isotropic excitation and polarized emission at 0 and 90° by placing a polarizer after the transmission lens. The polarization dependence of the monochromator was corrected by using a solution of the respective fluorophore, either BBT or BBS, in tetrachloroethane. The fluorescence lifetimes were measured according to standard time-correlated single photon counting methods, with the FLS-920 apparatus, by fitting with a monoexponential decay function.

V.3. Results and Discussion

Orientation Investigation by IR

Orientation measurements can be made by IR spectroscopy provided that appropriate bands are available. Table V.1 gives a list of bands that can be considered for PBS and BBT depending on the films thickness and fluorophore concentration.

Table V.1. Band assignment and orientation for PBS and BBT.

Band (cm^{-1})	Assignment	Origin	Orientation
3430	υ(C=O) overtone	PBS	⊥
2850	υ(CH_2 symmetric stretching)	PBS	⊥
1474	CH_2 bending	PBS	⊥
1250-1150	Asymmetric stretching vibration of the ester group	PBS	⊥
3050	υ(C-H) aromatic	BBT	⊥
1580	υ(C=C) aromatic	BBT	⊥

According to Table V.1, PBS exhibits characteristic bands at 3430, 2850 and 1474 cm^{-1}. The bands at 1474 cm^{-1} and in the 1250-1150 cm^{-1} region[36-39] were excluded, even if they show important anisotropy. The large transition dipole moments of the C=O and C─O bonds lead to large absorbances before stretching that do not satisfy Beer's law. The CH_2 symmetric stretching band (2850 cm^{-1}) can be used in evaluating the PBS average orientation function in the blend films since its α angle, between the transition moment and the chain axis, is reported to be 70°.[40,41] The overtone of the C=O stretching band (3430 cm^{-1}) is another good candidate for the evaluation of the PBS chain orientation. Comparison of the T_2 values from this band with the $<P_2>$ values obtained for the 2850 cm^{-1} band revealed that its α angle is 90°. PBS also exhibits lesser used bands at 808 and 656 cm^{-1} that may be used to confirm the results given by the other bands, if necessary. BBT features strong bands at 3050 and 1580 cm^{-1} that can be used for orientation quantification at high concentration while, unfortunately, the strongest BBS bands at 755,

740 and 730 cm^{-1} overlap with PBS bands, preventing quantification of its orientation by IR spectroscopy.

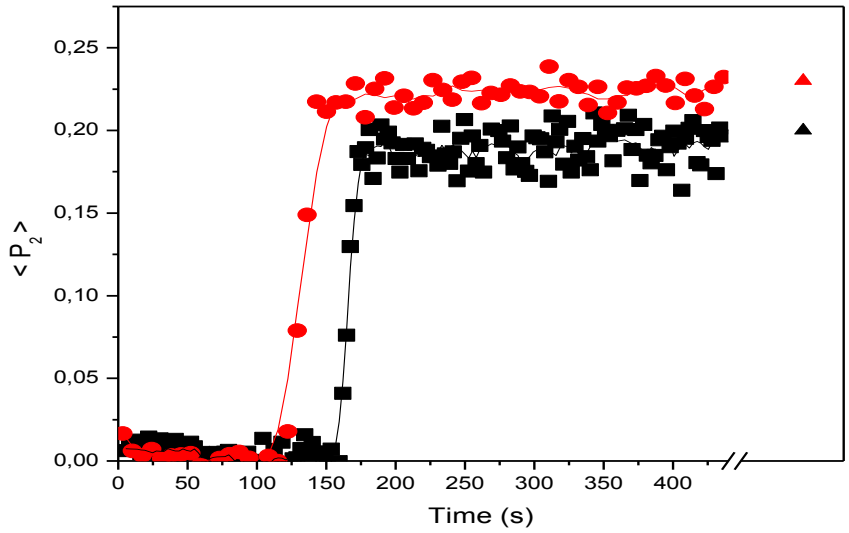

Figure V.1. Pure PBS order parameter $<P_2>$ as a function of time measured by PM-IRSAS for the 3430 cm^{-1} band during and after stretching to a local strain of 195 (■) and 235% (●). The $<P_2>$ values, measured by static polarized FT-IR for the same samples at 195 (▲) and 235% (▲), are shown for comparison.

Figure V.1 shows the variation of the order parameter $<P_2>$ of the 3430 cm^{-1} band as a function of time by PM-IRSAS. Before film stretching, there is no orientation in the PBS film. When the necking front crossed the optical path of the infrared radiation, $<P_2>$ increases to 0.2 or 0.23 at a local draw ratio of 195 or 235%, respectively (N.B: the exact draw ratio was always determined locally from the ink-marks made on the sample; measurements could be made at different local draw ratios because the deformation in the necking area is not homogeneous). It is noteworthy that once $<P_2>$ reaches a plateau, no relaxation of the PBS-based films happens after the stretching is stopped (the sample being kept taut even if it is left at 80 °C for several minutes). Figure V.1 also shows that identical $<P_2>$ values are obtained by static polarized FT-IR for the same stretched samples.

Therefore, a static linear dichroism method can be used in this investigation since orientation relaxation does not occur.

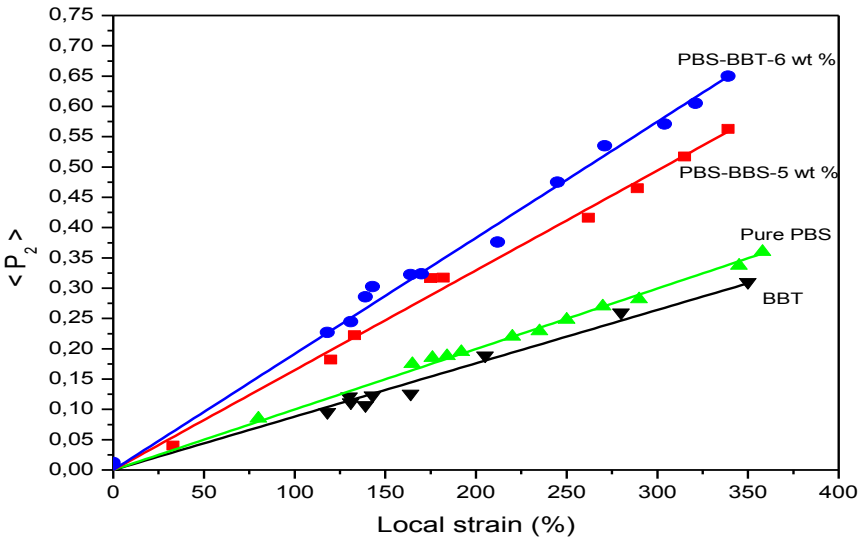

Figure V.2. Orientation function $<P_2>$ as a function of local strain (%) and blend composition for the 3430 cm^{-1} band in pure PBS, in PBS-BBS-5 wt % and in PBS-BBT-6 wt % films, and for the 1580 cm^{-1} band belonging to BBT in PBS-BBT-6 wt % films.

Figure V.2 shows the variation of the PBS order parameter $<P_2>$ as a function of the local draw ratio using the 3430 cm^{-1} band. A linear increase of $<P_2>$ with local strain is observed for the three systems investigated. Interestingly, the presence of a small molecule leads to an orientation enhancement. For example, at a local draw ratio of approximately 350%, $<P_2>$ goes from 0.36 for pure PBS to 0.56 after adding 5 wt % of BBS or to 0.66 after adding 6 wt % of BBT. The effect of a lower fluorophore concentration on $<P_2>$ will be shown later, in Figure V.5.

BBS and BBT are also expected to be oriented when dispersed in a stretched polymer film, like PBS. In this study, different concentrations have been used for the fluorophores up to 6 wt %. It has been previously shown in the literature that BBT forms small amounts of ground-state aggregates whatever its concentration,[12] while BBS is

molecularly dispersed at low concentrations and forms excimers at high concentrations, favored by π—π intermolecular interactions on the order of 3.65 Å.[11] However, it should be noted that the major part of these chromophores remains molecularly dispersed and that stretched films contain almost only molecularly dispersed fluorophores. Due to their low concentrations (≤ 6 wt %) in the blend films, the chromophores' infrared bands are weak relative to those of the PBS matrix. BBT mainly features a useful band at 1580 cm^{-1} (Table V.1), with which $<P_2>$ values were calculated by assuming an angle of 90° between the transition moment and the BBT long axis. Figure V.2 also shows a linear increase of $<P_2>$ for BBT in PBS-BBT-6 wt % films as a function of the local strain. At a local draw ratio of ≈ 350%, the BBT chromophore exhibits a $<P_2>$ of 0.31, similar to the pure PBS orientation but much lower than that of PBS in the same films. The sum of the $<P_2>$ values of PBS and BBT, i.e., 0.67, is equal, within experimental error, to that of PBS in PBS-BBT-6 wt %, i.e., 0.66 at a local draw ratio of ≈ 350%. Indeed, the fluorescent probes may act as "orientation nuclei", inducing locally higher molecular orientation in the neighborhood of the probes.[42]

Many studies have been conducted to quantify the orientation of polymers and to elucidate the variation of their orientation parameter $<P_2>$ with the addition of another molecule, generally a second polymer and, more rarely, a small molecule. Among the most relevant polymer systems, a concentration-dependent orientation parameter with a small increase of the $<P_2>$ of the host polymer was obtained in miscible blends by adding poly(ethylene oxide) or poly(trifluoroethylene) to poly(methyl methacrylate),[43] and by adding poly(phenylene oxide) (PPO) or poly(vinyl methyl ether) (PVME) to polystyrene (PS).[20,44-49] In contrast, a decrease of $<P_2>$ has been reported in immiscible blends by adding, for example, polycarbonate to polyethylene,[50] while no difference in $<P_2>$ was noticed in a compatible blend by adding poly(o-chlorostyrene) to PS.[51]

In the literature, the increase in $<P_2>$ of PS with the addition of PVME or PPO is attributed to the combined effects of friction coefficient and entanglement density. The PS chains form entanglements with PPO or PVME chains, while they form entanglements only among themselves in pure PS samples. Since the molecular weight between entanglements is 7 400, 8 500 and 18 000 g/mol for PPO,[52] PVME20 and PS,[20] respectively, adding

PVME or PPO to PS increases the entanglement density for PS, as compared to pure PS, thus leading to a hindered relaxation. This phenomenon leads to an increase in the PS orientation, up to a PPO concentration of 25%.[48] The friction coefficient between the two species also increases due to the specific intermolecular interactions between them (like between the methoxy group of PVME and the phenyl ring of PS), leading to a hindering of the chain relaxation that occurs during stretching as the second polymer is added into the blend, thereby resulting in a higher measured orientation of the PS host polymer.

If the second species added to the semi-crystalline polymer is a small miscible molecule having a low T_g, the free volume of the system increases and T_g decreases. Indeed, when the small molecules are dispersed between the polymer chains, they space them apart and increase their flexibility. However, DSC measurements on PBS-BBS blends reveal no change of T_g of PBS by adding 5 wt % of BBS or 6 wt % of BBT, showing that the variation of the free volume is minor. Polymer-small molecules interactions gradually replace polymer-polymer interactions and increase the friction coefficient, leading to an increase of $<P_2>$ of the host polymer. At the same time, the "swelling" between polymer chains due to the presence of the small molecules increases the molecular weight between entanglements of the host polymer and has the reverse effect. A major factor, however, is the increase in the degree of crystallinity of the polymer. DSC measurements show that adding 5 wt % of BBS or 6 wt % of BBT leads to an increase of the degree of crystallinity of the polymer matrix by 9 and 10%, respectively, while stretching PBS-BBS-5 wt % and PBS-BBT-6 wt % films at a local draw ratio of ≈ 350% induces an additional increase of the polymer crystallinity by ≈ 4%. As already reported in the literature, such an increase leads to a simultaneous increase in orientation.[3,9,10]

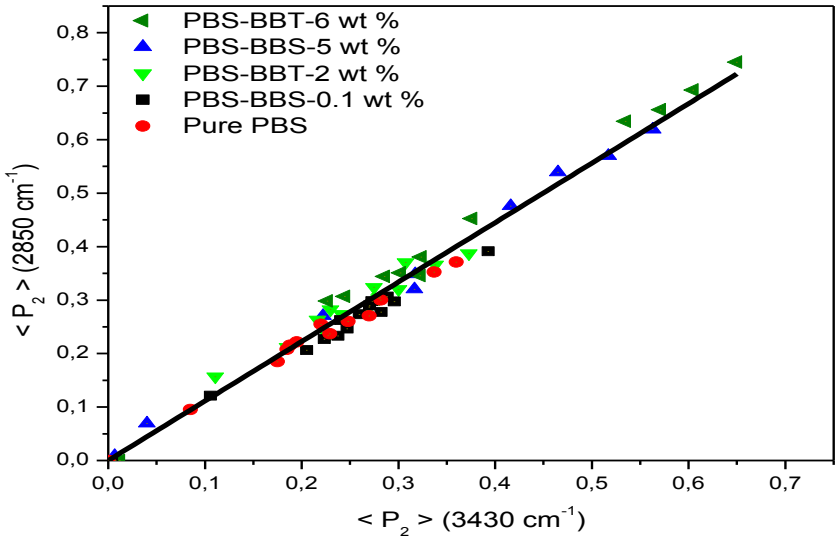

Figure V.3. Orientation function $<P_2>$ of the 2850 cm^{-1} band versus $<P_2>$ of the 3430 cm^{-1} band and the fluorophore concentration (wt %) in different polymeric films (pure PBS: ●; PBS-BBS-0.1 wt %: ■; PBS-BBS-5 wt %: ▲; PBS-BBT-2 wt %: ▼; PBS-BBT-6 wt %: ◀).

In that context, it is useful to recall that the FT-IR analysis is based on bands which are not, as far as we know, specific to the amorphous or crystalline fraction of the polymer. In other words, the FT-IR orientation parameter reported is an average of the orientation of chains in the amorphous and crystalline phases. A limited number of X-ray measurements have been done with a 2D detector in order to confirm the FT-IR results. We have found an orientation parameter of ≈ 0.77 for PBS-BBS-5 wt % and of ≈ 0.84 for PBS-BBT-6 wt % films stretched to a local strain of ≈ 350% that is exclusively specific to the crystalline phase. This means that $<P_2>$ values of 0.66, for example, measured by FT-IR (Figure V.2) correspond to a crystalline phase which has a $<P_2>$ larger than 0.66 whereas the amorphous phase has a lower value. Since BBS and BBT dyes are located in the amorphous phase, one expects smaller values, as noted for BBT in Figure V.2 and which will be confirmed later.

The PBS orientation can also be followed using the 2850 cm^{-1} band. Actually, as shown in Figure V.3, the orientation function $<P_2>$ of the 2850 cm^{-1} agrees very well with that of the 3430 cm^{-1} band for PBS films containing different amounts of BBS and BBT.

The results obtained from the 3430 and 2850 cm^{-1} bands have also been confirmed by both the 808 and 656 cm^{-1} bands.

BBS and BBT Orientation Investigation by Fluorescence Spectroscopy

As BBT and BBS are characterized by different planarities, with a rod-like structure for BBS which shows an extended herringbone packing,[11] and a banana shape for BBT that leads to a limited stacking due to its very cumbersome *tert*-butyl groups and to the 2,5-di-substitution of the thiophene ring,[12] the tendency of these two monomers to be oriented in stretched PBS films was investigated. IR spectroscopy was unfortunately unable to give information about the BBS orientation, as it did for the BBT molecules, for the reasons mentioned above. However, the orientation of both fluorophores can be measured by fluorescence spectroscopy using the ratio $R = {E_{\parallel}}/{E_{\perp}}$, where $E_{\parallel}$ and $E_{\perp}$ are the polarized emission intensities parallel and perpendicular to the stretching direction, respectively. This ratio can be related to an apparent order parameter, S, using the expression: $S = \frac{R-1}{R+2}$.

To enable comparison between BBT- and BBS-based films, dichroic ratios were calculated at the emission maximum of each chromophore. A further measurement was made at a wavelength specific to the fluorophore aggregates in order to investigate a probable difference in orientation depending on the molecular arrangement since both fluorophores feature different spectroscopic characteristics at high concentrations.

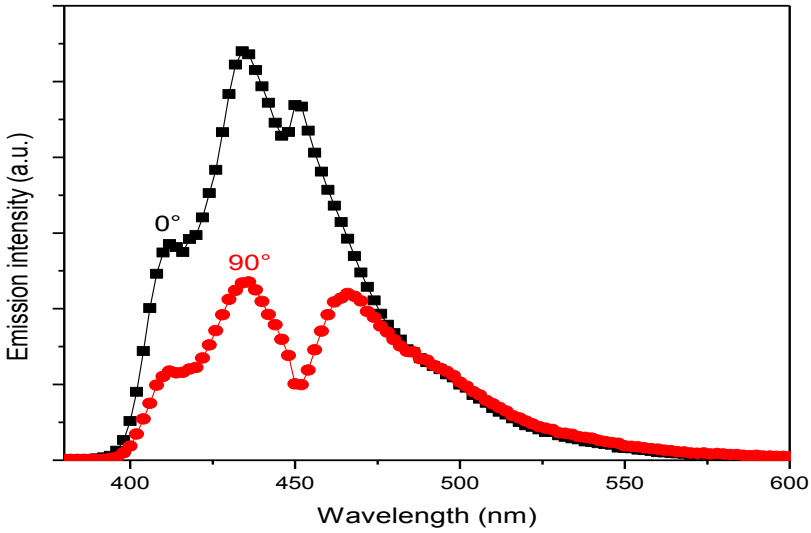

Figure V.4. Polarized emission spectra at 0 and 90° of PBS-BBT-0.01 wt % film stretched to 300% at ambient temperature and at λ_{exc} = 378 nm.

In unstretched PBS-BBT films, molecularly dispersed BBT monomers are characterized by peaks at 408, 430 and 462 nm, while BBT aggregates show a shoulder at around 500 nm. In the same vein, the unstretched PBS-BBS films exhibit three peaks at 412, 434 and 464 nm, specific to BBS isolated molecules, and a band at 500 nm characteristic of BBS excimers, which are present at BBS concentration > 0.05 wt %. The fluorophore monomers and aggregates are randomly oriented prior to stretching the polymer films. Figure V.4 displays the polarized emission spectra at 0 and 90° for uniaxially stretched PBS-BBT-0.01 wt % films after stretching to 300%. The polarized emission spectrum is much more intense at 0° than at 90° for the monomer bands, indicating the development of a significant orientation upon stretching the polymer film. In contrast, the two polarized spectra are identical for the 500 nm band, revealing that the BBT aggregates remain isotropic.

The apparent order parameter (S) of BBT and BBS fluorophores has been calculated at the maximum emission wavelength corresponding to the 0─1 vibronic transition of the chromophores' monomers; this wavelength shifts from 432 to 436 nm for BBS at

concentrations going from 0.01 to 5 wt %, and from 434 to 450 nm for BBT at concentrations going from 0.01 to 6 wt %. In PBS-BBT-6 wt % blends, the BBT analysis by fluorescence spectroscopy results in an apparent order parameter of 0.34, which is similar to that previously obtained by FT-IR, i.e., 0.31.

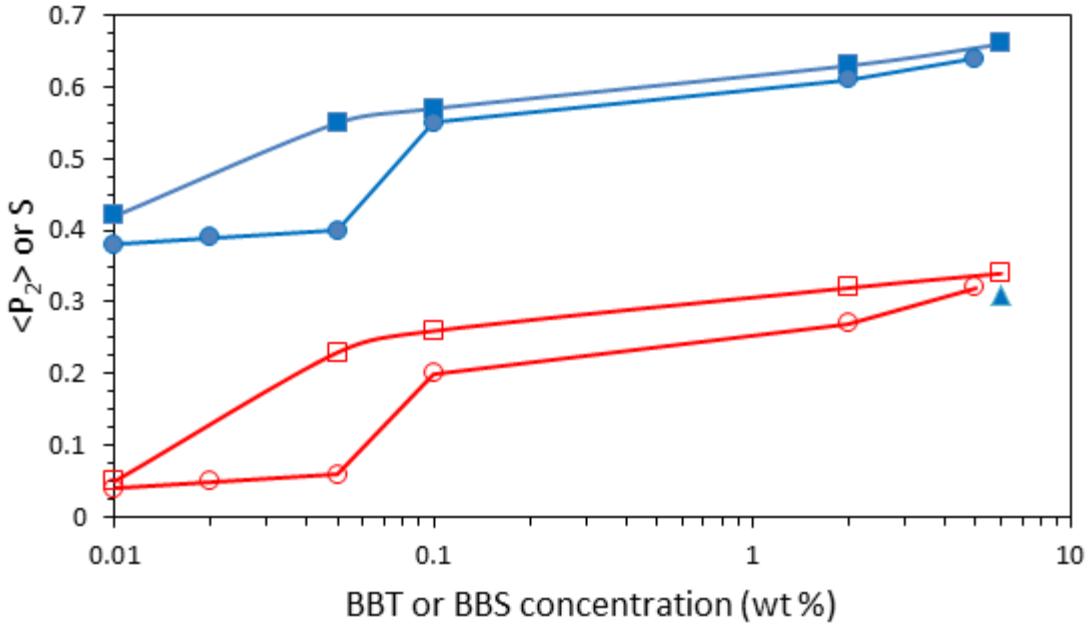

Figure V.5. Orientation function <P_2> of PBS in PBS-BBS (●) and PBS-BBT (■) films, given by IR (blue solid symbols), and apparent order parameter S of BBS (○) and BBT (□), determined by polarized fluorescence spectroscopy (red empty symbols) as a function of BBT or BBS concentration in different polymeric films stretched at local strains of 300 ─ 350%. The <P_2> value corresponding to BBT (▲), determined by IR, is given for comparison.

Figure V.5 shows the variation of the order parameter of PBS, BBT and BBS as a function of the chromophore concentration in stretched films as determined by polarized FT-IR (filled symbols) and polarized fluorescence spectroscopy (empty symbols). According to Figure V.5, the orientation parameters of BBS and PBS in PBS-BBS blends follow a different trend than that of BBT and PBS in PBS-BBT blends as a function of concentration. For PBS-BBS blends, the orientation parameters characterizing the polymer (<P_2>) and the fluorophore (S) remain constant at low concentrations. However, at

concentrations between 0.05 and 0.1 wt %, the two orientation parameters increase abruptly, and more slowly hereafter. In contrast, in the PBS-BBT films, both $<P_2>$ specific to PBS and S of BBT increase regularly for fluorophore concentrations going from 0.01 to 6 wt %.

All BBT-containing blends are characterized by similar fluorescence spectra and a unique lifetime independently of BBT concentration.[142] They contain no excimer but small aggregates whose number/size likely increases with the BBT concentration. However, in the case of BBS, at concentrations ≤ 0.05 wt %, PBS-BBS films exhibit monoexponential decay with a lifetime of 1 ns specific of BBS monomers, while they feature biexponential decay at concentrations ≥ ≈ 0.08 wt % characteristic of BBS monomers and excimers. The latter are destroyed and transformed into monomers by mechanical deformation, and there is a simultaneous increase of the order parameters of both PBS and BBS. It should be noted that both BBS excimers and BBT aggregates are oriented randomly, as indicated by an apparent order parameter of zero.

Figure V.5 also shows that the $<P_2>$ value for PBS almost doubles from 0.36 in the pure polymer up to 0.63 in films containing just 2 wt % of BBT, followed by a plateau for concentrations up to 6 wt % of the additive. Similarly, the apparent order parameter S of BBT is as low as 0.05 at the lowest concentration (0.01 wt %) but it increases drastically and reaches a plateau at 0.32 when 2 wt % of the fluorophore is present. Figure V.5 shows similar values for both fluorophores, suggesting that their specific chemical nature is not the main factor influencing their orientation in stretched films. It is noteworthy that the S values determined by fluorescence spectroscopy are only apparent order parameters. Nevertheless, polarized infrared spectra recorded for the PBS-BBT 6 wt % sample yielded a true $<P_2>$ value for BBT in excellent agreement with the S parameter (Figure V.5) suggesting that the S values are, in first approximation, close to the $<P_2>$ values, making the comparison possible. Interestingly, the sum of $<P_2>$ of the pure PBS, determined by IR, and S of BBT or BBS, given by polarized fluorescence spectroscopy, is similar to the $<P_2>$ of PBS in the corresponding blend film. As a consequence, knowing the orientation parameter of the pure host polymer and of the polymeric blend containing a given concentration of the guest chromophore gives a fair idea of the apparent orientation

parameter (S) of the fluorophore, which remains quite useful especially when the fluorophore infrared bands are overlapped with the host polymer bands.

The ability of the BBS molecules to orient in stretched polymeric films, taken together with their tendency to form excimers and to change the emission color of the films, motivates an investigation of the fluorescent properties of the BBS-based films in order to consider them for various applications.

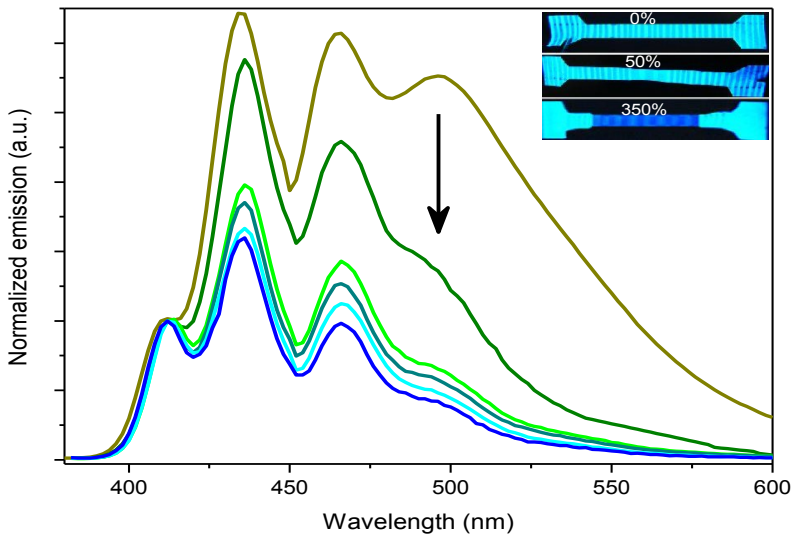

Figure V.6. Fluorescence spectra normalized at 408 nm of PBS-BBS-0.15 wt % films at different strains and at λ_{exc} = 374 nm (0%: dark yellow; 50%: olive; 100%: green; 150%: navy; 280%: cyan; 350%: blue). Inset: Pictures of films stretched to 0, 50 and 350 % draw ratios.

Figure V.6 shows the fluorescence spectra of PBS-BBS-0.15 wt % films stretched at different local draw ratios. The most intense spectrum shows the emission of the undeformed or pristine PBS-BBS film with its BBS monomer characteristics, and BBS excimers with an intense band at around 500 nm that confers to the polymeric film a green emission, under UV illumination at 365 nm. Figure V.6 shows that, after mechanical deformation, the intensity of the excimer band decreases quickly as the local strain increases up to 100% and, then, becomes of low intensity at a local strain of 350%. The

inset of Figure V.6 shows that this intensity decrease is accompanied by a color change, from green to blue at 350% local strain, showing a transition between excimers and monomers that occurs only in the oriented part of the film. These observations are in accord with previous experiments that have shown similar transformations from excimers to monomers accompanied by a color change.[1-3,9,10,53-55]

Similar results have been previously observed for a different concentration of the fluorophore.[10] The BBS molecular arrangement can be monitored by following the I_E/I_{M1} ratio, which is the ratio of the intensity of the excimer band and the first fluorescence peak, with the local strain. At a low BBS concentration of 0.05 wt %, the I_E/I_{M1} ratio decreases from 0.35 in the unstretched sample to 0.17 at a local strain of 100% and remains almost unchanged even at higher strains. Nonetheless, at a higher BBS concentration of 0.15 wt % (Figure V.6), I_E/I_{M1} remains as high as 0.52 at a local strain of 150%, indicating a probable incomplete dissolution of excimers, likely due to their larger initial size. The possibility of easily changing the spectroscopic and luminescence features of PBS-BBS oriented films and their high stability over time may be interesting from a technological point of view, such as for a potential use as a polymer mechanical deformation probe, as suggested earlier by Pucci et al.[10] Nevertheless, unlike BBS, chromophores exhibiting a short-range order,[12] such as BBT, are not capable of changing their spectroscopic features by forming excimers and they keep their monomeric emission color independently of the polymer stretching. Indeed, slight non-coplanarity of the BBT aromatic rings in the solid state confers to BBT a banana-shape, with a torsion angle of 168(8) degrees between two benzoxazole moieties,[12] induced by a 2,5-di-substitution of the thiophene ring, which prevents short π─π intermolecular interactions on the range of 3─4 Å required for an excimer formation. These findings confirm that polymer mechanical deformation directly affects the macroscopic molecular arrangement of BBS and that the formation of excimers depends on the shape of the dispersed small molecules.

V.4. Conclusions

When a film is composed of more than one species, with one or several phases, it is reasonable to expect that the two species will be oriented to different extents, unless there are very strong interactions between them. This is the case, for example, of miscible blends[20,43-49] that show different orientations of their two components.

In the present study, with one component being a semi-crystalline polymer and the second one a small molecule, it is found that the latter is much less oriented than the former. More specifically, at low concentrations, the dye has very little orientation with an S factor smaller than 0.1 whereas, above 0.08 wt %, the ratio $<P_2>$ polymer / S_{dye} is larger than 2. This means that, in such a system, the measurement of the dye orientation cannot be taken as a means of measuring the polymer orientation, as it has been done in the literature (by fluorescence spectroscopy). This method could be considered with caution in the case of an amorphous, one-phase polymer, but not for a semi-crystalline polymer.

This study also exemplifies the need of using more than one experimental method for determining the orientation of a multi-component mixture. In some cases, FT-IR spectroscopy can be used for that purpose.[20,43,45,48,49] However, in the present case, it was not possible because 1) the BBS bands overlapped the PBS bands and 2) the dye (BBS and BBT) concentration was too low. In such cases, a combination of techniques is needed but, fortunately, in this study it was possible to demonstrate that the two techniques provided consistent results.

Acknowledgements

The authors gratefully acknowledge financial support from the Canada Foundation for Innovation, NanoQuébec, Centre for Self-Assembled Chemical Structures, Natural Sciences and Engineering Research Council of Canada, and Fonds Québécois de la recherche sur la nature et les technologies. They also thank Showa Highpolymer Co. for supplying PBS and Damien Mauran for his help with the PM-IRSAS experiments. AF thanks the Tunisian Government for a scholarship of excellence.

References

(1) Donati, F.; Pucci, A.; Cappelli, C.; Mennucci, B.; Ruggeri, G. *J. Phys. Chem. B* **2008**, *112*, 3668.

(2) Kinami, M.; Crenshaw, B. R.; Weder, C. *Chem. Mater.* **2006**, *18*, 946.

(3) Lott, J.; Weder, C. *Macromol. Chem. Phys.* **2010**, *211*, 28.

(4) Pucci, A.; Biver, T.; Ruggeri, G.; Meza, L. I.; Pang, Y. *Polymer* **2005**, *46*, 11198.

(5) Lowe, C.; Weder, C. *Adv. Mater.* **2002**, *14*, 1625.

(6) Kunzelman, J.; Chung, T.; Mather, P. T.; Weder, C. *J. Mater. Chem.* **2008**, *18*, 1082.

(7) Pucci, A.; Bertoldo, M.; Bronco, S. *Macromol. Rapid. Commun.* **2005**, *26*, 1043.

(8) Kunzelman, J.; Crenshaw, B. R.; Kinami, M.; Weder, C. *Macromol. Rapid. Commun.* **2006**, *27*, 1981.

(9) Crenshaw, B. R.; Burnworth, M.; Khariwala, D.; Hiltner, A.; Mather, P. T.; Simha, R.; Weder, C. *Macromolecules* **2007**, *40*, 2400.

(10) Pucci, A.; Di Cuia, F.; Signori, F.; Ruggeri, G. *J. Mater. Chem.* **2007**, *17*, 783.

(11) Fourati, M. A.; Maris, T.; Bazuin, C. G.; Prud'homme, R. E. *Acta Crystallogr., Sect. C: Cryst. Struct. Commun.* **2010**, *66*, o11.

(12) Fourati, M. A.; Maris, T.; Skene, W. G.; Bazuin, C. G.; Prud'homme, R. E. *J. Phys. Chem. B* **2011**, *115*, 12362.

(13) Ajji, A.; Guévremont, J.; Cole, K. C.; Dumoulin, M. M. *Polymer* **1996**, *37*, 3707.

(14) Middleton, A. C.; Duckett, R. A.; Ward, I. M.; Mahendrasingam, A.; Martin, C. *J. Appl. Polym. Sci.* **2001**, *792*, 1825.

(15) Cunningham, A. W., I. M.; Willis, H. A.; Zichy, V. *Polymer* **1974**, *15*, 749.

(16) Cole, K. C.; Ajji, A.; Pellerin, E. *Macromolecules* **2002**, *35*, 770.

(17) Cole, K. C.; Ben Daly, H.; Sanschagrin, B.; Nguyen, K. T.; Ajji, A. *Polymer* **1999**, *40*, 3505.

(18) Lu, X. F.; Hay, J. N. *Polymer* **2001**, *42*, 8055.

(19) Kalkar, A. K.; Siesler, H. W.; Pfeifer, F.; Wadekar, S. A. *Polymer* **2003**, *44*, 251.

(20) Pellerin, C.; Prud'homme, R. E.; Pézolet, M. *Macromolecules* **2000**, *33*, 7009.

(21) Pellerin, C.; Prud'homme, R. E.; Pézolet, M. *Polymer* **2003**, *44*, 3291.

(22) Pellerin, C.; Prud'homme, R. E.; Pézolet, M.; Weinstock, B. A.; Griffiths, P. R. *Macromolecules* **2003**, *36*, 4838.

(23) Messé, L.; Prud'homme, R. E. *J. Polym. Sci. Part B: Polym. Phys.* **2000**, *38*, 1405.

(24) Lee, H. S.; Park, H. D.; Cho, C. K. *J. Appl. Polym. Sci.* **2000**, *77*, 699.

(25) Buffeteau, T.; Desbat, B.; Pézolet, M.; Turlet, J. M. *J. Chem. Phys.* **1993**, *90*, 1467.

(26) Buffeteau, T.; Desbat, B.; Besbes, S.; Nafati, M.; Bokobza, L. *Polymer* **1994**, *35*, 2538.

(27) Buffeteau, T.; Pézolet, M. *Appl. Spectrosc.* **1996**, *50*, 948.

(28) Duchesne, C.; Kong, X. H.; Brisson, J.; Pézolet, M.; Prud'homme, R. E. *Macromolecules* **2002**, *35*, 8768.

(29) Pellerin, C.; Rousseau, M. E.; Prud'homme, R. E.; Pézolet, M. *Appl. Spectrosc.* **2002**, *56*, 17.

(30) Pellerin, C.; Pézolet, M.; Griffiths, P. R. *Macromolecules* **2006**, *39*, 6546.

(31) Nafie, L. A.; Diem, M. *Appl. Spectrosc.* **1979**, *33*, 130.

(32) Marcott, C. *Appl. Spectrosc.* **1984**, *38*, 442.

(33) Buffeteau, T.; Pézolet, M. *Handbook of Vibrational Spectroscopy*; John Wiley & Sons: Chichester, **2002**.

(34) Liang, Y.; Mauran, D.; Prud'homme, R. E.; Pellerin, C. *Appl. Spectrosc.* **2008**, *62*, 941.

(35) Ward, I. M. *Structure and Properties of Oriented Polymers*; Chapman & Hall: London, **1997**.

(36) Nagai, H. J. *Appl. Polym. Sci.* **1963**, *7*, 1697.

(37) Schneider, B.; Stokr, J.; Schmidt, P.; Mihailov, M.; Dirlikov, S.; Peeva, N. *Polymer* **1979**, *20*, 705.

(38) Havrilika, S., Roman, J R., *Polymer* **1966**, *7*, 387.

(39) Dybal, J., Krimm, S. *Macromolecules* **1990**, *23*, 1301.

(40) Neuert, R. S., H.; Hinrichsen, G. *Colloid & Polymer Sol* **1985**, *263*, 392.

(41) Jasse, B. K., J. L. *J. Polym. Sci. Pol. Phys.* **1979**, *17*, 799.

(42) Springer, H.; Neuert, R.; Muller, F. D.; Hinrichsen, G. *Colloid. Polym. Sci.* **1983**, *261*, 800.

(43) Jasse, B.; Tassin, J. E.; Monnerie, L. *Prog. Colloid Polym. Sci.* **1993**, *92*, 8.

(44) Abtal, E.; Prud'homme, R. E. *Macromolecules* **1994**, *27*, 5780.

(45) Faivre, J. P.; Jasse, B.; Monnerie, L. *Polymer* **1985**, *26*, 879.

(46) Lefebvre, D.; Jasse, B.; Monnerie, L. *Polymer* **1981**, *22*, 1616.

(47) Lefebvre, D.; Jasse, B.; Monnerie, L. *Polymer* **1984**, *25*, 318.

(48) Zhao, Y.; Prud'homme, R. E.; Bazuin, C. G. *Macromolecules* **1991**, *24*, 1261.

(49) Pellerin, C.; Pelletier, I.; Pézolet, M.; Prud'homme, R. E. *Macromolecules* **2003**, *36*, 153.

(50) Endo, S.; Min, K.; White, J. L.; Kyu, T. *Polym. Eng. Sci.* **1986**, *26*, 45.

(51) Faivre, J. P.; Xu, Z.; Halary, J. L.; Jasse, B.; Monnerie, L. *Polymer* **1987**, *28*, 1881.

(52) Heymans, N. *J. Mater. Sci.* **1986**, *21*, 1919.

(53) A. Pucci, M. B., S. Bronco *Macromol. Rapid. Commun.* **2005**, *26*, 1043.

(54) Crenshaw, B. R.; Weder, C. *Adv. Mater.* **2005**, *17*, 1471.

(55) Crenshaw, B. R.; Weder, C. *Chem. Mater.* **2003**, *15*, 4717.

CHAPITRE VI: Self-Assembly of Molecular Probes as the Source of Time-Temperature Probes in Polyesters

Abstract

The intrinsic and photophysical properties of the fluorescent molecules 4,4'-bis(2-benzoxazolyl)stilbene (BBS) and 2,5-bis(5-*tert*-butyl-2-benzoxazolyl)thiophene (BBT) have been investigated in solution as well in semi-crystalline poly(butylene succinate) (PBS) and polylactide (PLA). The increase of the BBS concentration in these polymers induces in the fluorescence emission spectra the appearance of a new red-shifted band, specific to excimers, in addition to the three original peaks belonging to isolated molecules. This transformation is accompanied by a significant and easily detectable colour change from blue to green, specific to a transformation from molecular dispersion to phase separation, and by the appearance of a second lifetime specific to excimers. As a consequence, the BBS absolute quantum yield, which was accurately investigated for the first time in the solid-state, decreases while it increases upon mechanical deformation of the polymeric blends due to the excimers breakage. On the other side, the increase of the annealing temperature or time of PLA or PBS films containing excimer-forming BBS chromophores showed a self-assembly of dye molecules into excimers for the first time. This process was found to be helped by an increase of the polymer crystallinity upon annealing, thus providing a broad opportunity for the creation of a wide variety of smart polymers with self-assessing capabilities such as time-temperature indicators. However, unlike the rodlike BBS molecule, BBT was found to be unsuitable for such applications since it does not allow excimer formation due to its bow shape, but it is still of interest since it is characterized by high quantum yields independently of concentration, time, temperature or even host polymer deformation.

VI.1. Introduction

4,4'-bis(2-benzoxazolyl)stilbene (BBS) and 2,5-bis(5-*tert*-butyl-2-benzoxazolyl)thiophene (BBT) are two well-known fluorophores that have been particularly used as optical brighteners in textiles, detergents and other materials,[1-4] as well as additives for thermoplastic materials thanks to their excellent dispersibility in molten polymers and to their high degradation temperatures, allowing them to resist without degradation to the processing temperature, thus satisfying the regulations of the U. S. Food and Drug Administration (FDA), and making them acceptable as additives for the packaging of foodstuffs.[3] It has been recently shown that the incorporation of fluorescent aromatic molecules in polymers by melt-processing can lead to information on the conformation of dye molecules and the orientation of polymer chains.[5] The dispersed fluorescent dyes may also act as molecular probes, thanks to excimer formation, induced by π-π interactions along the aromatic backbones between neighbouring chromophores, that allows them to respond to the molecular environment in which they lie and to report the nature of this environment through their fluorescence spectra. Different excimer-forming dyes have been investigated in various polymer hosts as a function of concentration,[6-12] time[6,7,13-16] and thermal solicitations on plastic films upon dye molecular rearrangement.[6,8,11,14-16]

In this study, two different optical brighteners, BBS and BBT, are incorporated into biodegradable semi-crystalline polyesters, poly(butylene succinate) (PBS) and polylactide (PLA). Here, we report a study of the optical and photophysical properties of both chromophores in the solid-state by measuring for the first time their absolute quantum yields in PBS and PLA films as a function of the fluorophore concentration and the polymer stretching. Such studies are pivotal for determining the limitations of these fluorophores. Our purpose is to compare their features in solution and in the solid-state, and to investigate the factors that influence the most their molecular arrangement. Intrigued by the possibility to extend the sensor applications of the stilbene derivative and maybe of the thiophene derivative to a well-known biodegradable polyester, i.e. polylactide, we aim at exploit their highly interesting fluorescence features for the design of smart polymeric

materials containing sensor molecules capable of reacting to environmental conditions by changing their optical properties and their molecular arrangement.

VI.2. Experimental section

Materials

4,4'-Bis(2-benzoxazolyl)stilbene (97%, melting point > 300 °C) and 2,5-Bis(5-*tert*-butyl-benzoxazol-2-yl)thiophene (99%, melting point ~ 200 °C) were purchased from Aldrich Chemicals and used without further purification.

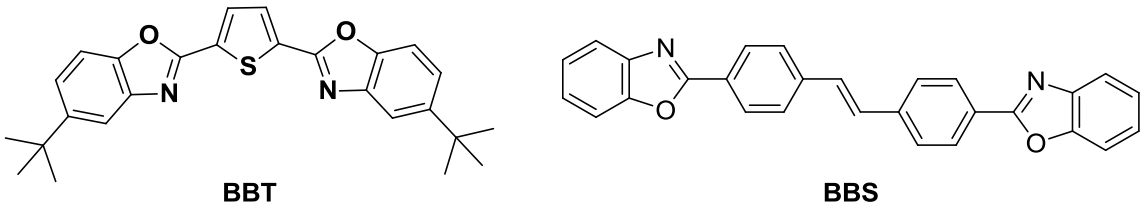

Chart VI.1. Structures of 2,5-bis(5-*tert*-butyl-benzoxazol-2-yl)thiophene (BBT) and 4,4'-bis(2-benzoxazolyl)stilbene (BBS).

Poly(1,4-butylene succinate) (PBS) ("Bionolle 1001") was graciously supplied by Showa Highpolymer Company (Japan) and polylactide (PLA) purchased from Dow Chemical Company. They are semi-crystalline polymers, used primarily for the manufacture of films and packaging, and degradable in compost or activated sludge. They are characterized by melting temperatures of 113 and 170 °C and glass transition temperatures of -34 and 61 °C, respectively.

Film Preparation

A DDRV501/DIGI-SYS Plasti-Corder Brabender mixer was used to prepare the dye-polymer films, i.e. PBS-BBS, PBS-BBT, PLA-BBS and PLA-BBT, by melt-processing. About 20 g of polymer (PBS or PLA) were mixed with different concentrations of fluorophores, i.e. 0.01 to 5 wt % of BBS or 0.01 to 6 wt % of BBT, at 200 °C for BBS-

based films and at 180 °C for BBT-based films, below the fluorophores melting temperatures, and at 50 rpm for 10 min. A Carver Laboratory Press was then used to mold the resulting material between two aluminum foils under a pressure of 9 tons/m^2, resulting in films with thicknesses of 40-100 μm. One part of the obtained material was immediately quenched in an ice-water bath, allowing these films to be used for time-temperature experiments, while the remaining part was cooled at ~10 °C/min to room temperature in a clod press under a pressure of 2 tons/m^2, and the obtained films were prepared in a dogbone shape having a width of 4 mm and a length of 12 mm between the slits, and used for mechanical deformation experiments. The latter were conducted by stretching the PBS-BBS and PBS-BBT films at an elongation rate of 0.1 mm/s at 80 °C, far from the PBS glass transition temperature of -34 °C and below its melting temperature of 113 °C, using an Instron Model 5565 tensiometer, equipped with a 1 kN load cell and an environmental chamber. The latter was immediately opened after drawing to allow the temperature to drop quickly to room temperature in order to freeze the orientation. The actual local strains (λ) were measured by the displacement of ink-marks drawn 1 mm apart onto the films before stretching as follow: $\lambda = \frac{L_f - L_i}{L_i}$ with L_f and L_i the final and initial length between marks, respectively.

Spectroscopic Measurements

Absorption measurements were done on a Varian Cary-500 UV-Visible spectrometer in tetrachloroethane (TCE), and the solvent absorption spectra were subtracted from the spectra of the analyzed samples. Fluorescence emission spectra were recorded at ambient temperature in 10 mm cuvettes, excited at the corresponding absorption maximum, using an Edinburgh Instruments FLS-920 combined steady-state and time resolved fluorimeter. The front-face geometry was used for polymeric films to allow the excitation and emission optical axis to cross in the film plane, while both the front-face and 90° geometries were used for solution fluorescence studies. The fluorescence lifetimes were measured according to standard time-correlated single photon counting methods, with the FLS-920 apparatus, by fitting with a monoexponential decay function. The calculated

values have an experimental error of approximately 10%. Absolute fluorescence quantum yields were measured by using an integrating sphere, and used to quantify the efficiency of the emission process by taking the ratio of photons absorbed to photons emitted through fluorescence at a particular wavelength in the same period of time.[18,19]

VI.3. Results and Discussion

BBS Concentration Effect

The fluorophore absorption features were measured in order to determine exactly the excitation wavelengths that need to be used during the fluorescence measurements, showing values of 374 and 378 nm for BBS and BBT, respectively.

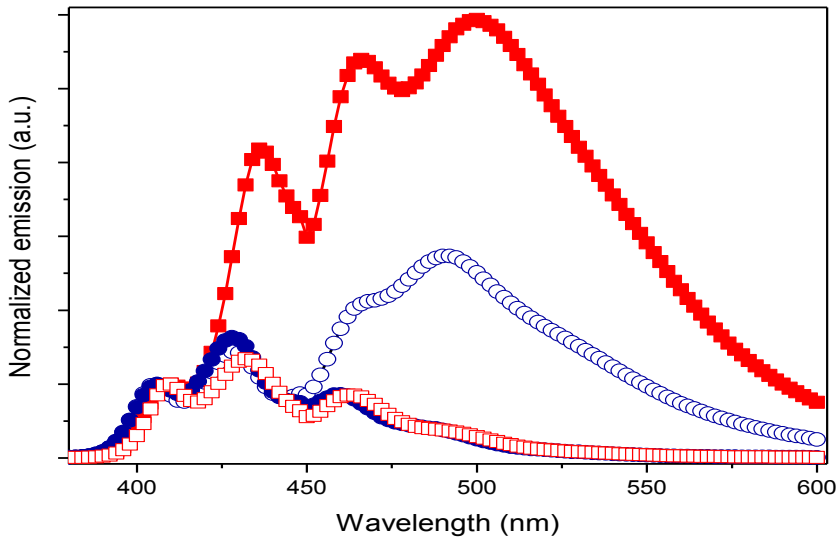

Figure VI.1. Fluorescence spectra of PLA-BBS films at 0.01 (●) and 2 (○) wt %, and of PBS-BBS films at 0.01 (□) and 0.2 (■) wt % (λ_{exc} = 374 nm).

Figure VI.1 shows the fluorescence emission spectra of PBS and PLA films containing different BBS concentrations. For comparison purposes, they were normalized relative to the first peak at 406 and 410 nm, respectively, in PBS and PLA films, taking into

account the change in fluorescence intensity with the film thickness. At low BBS concentrations, the spectra of PBS and PLA films exhibit characteristics that are similar to those of the BBS dye solubilized in TCE with three peaks attributed to the 0─0, 0─1 and 0─2 radiative transitions, i.e. peaks centered at 410, 432 and 462 nm for PBS-BBS-0.01 wt % films and at 406, 428 and 460 nm for PLA-BBS-0.01 wt %. At this concentration, all peaks belong to the molecularly dispersed BBS in the amorphous phase of the semi-crystalline polymer. Figure VI.1 also shows that by increasing the BBS concentration, the emission features change except in the case of the first peak. Indeed, a bathochromic shift of the second and third peaks happens, from 432 to 436 nm and 462 to 466 nm while going from PBS-BBS-0.01 wt % to PBS-BBS-0.2 wt %, and from 428 to 430 nm and 460 to 468 nm from PLA-BBS-0.01 wt % to PLA-BBS-2 wt %. This bathochromic shift is due to the appearance of a new broad emission band that emerges at 490 and 500 nm for PLA-BBS-2 wt % and PBS-BBS-0.2 wt % films, respectively, which is more intense than the BBS single chromophore emission peaks. It seems that, by increasing the BBS concentration, the dye molecules can no longer spread out and are forced to pile up to form aggregates. The appearance of this red-shifted band is favoured by the rod-like shape of the BBS molecules, which were found to exhibit shifted face-to-face π─π stacking interactions[17] with a centroid–centroid distance of 3.6─3.7 Å between π-stacked molecules. The presence of these intermolecular interactions with a stacking distance within the range of 3─4 Å confirms an excimer formation,[18] which is the origin of the emergence of the new band.

Upon excitation with an ultraviolet (UV) light at 350 nm, films containing low BBS concentrations, i.e. PLA-BBS-0.01 wt % and PBS-BBS-0.01 wt %, fluoresce blue, while films enclosing high concentrations of the stilbene derivative, i.e. PLA-BBS-2 wt % and PBS-BBS-0.2 wt %, exhibit green luminescence. This color change from blue to green confirms the conversion between isolated BBS molecules and excimers, respectively, favoured by the high concentration of the rod-like BBS molecules. Similar molecular rearrangement accompanied by a color change upon increase of the chromophore's concentration was found previously.[6-12]

From Figure VI.1, it is clear that the new band intensity is lower in PLA-BBS-2 wt % than in PBS-BBS-0.2 wt %, which shows a different behavior of the BBS molecules in

PLA and PBS. To get a quantitative idea about the excimer formation, Figure VI.2 shows the variation of the I_E/I_{M1} ratio, which is the ratio of the intensity of the excimer (at 490 nm in PLA and 500 nm in PBS) and first vibronic peak for the molecularly dispersed dye (at 406 nm in PLA and 410 nm in PBS), as a function of the BBS concentration. Since there is no shift of the first peak specific to the 0─0 radiative transition after the appearance of the excimer band, it was taken for comparison in order to minimize the contribution of the emerging band on the monomeric peaks.

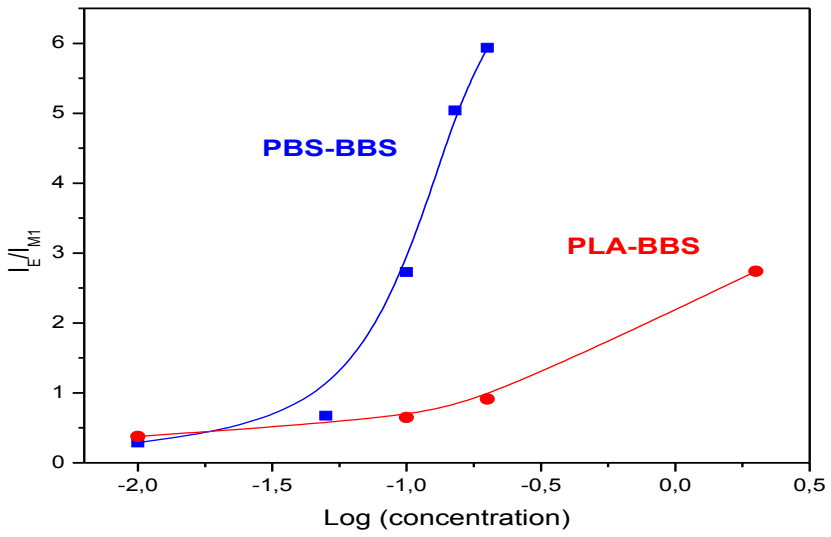

Figure VI.2. I_E/I_{M1} ratio as a function of the BBS concentration in PBS and PLA films.

Figure VI.2 shows a slight increase of the I_E/I_{M1} ratio for PLA-BBS films and a much bigger increase for PBS-BBS films as a function of BBS concentration. The lower tendency of the BBS molecules to form excimers in PLA indicates a better solubility when compared with PBS, probably due to stronger interactions between PLA chains and BBS molecules.

Intrinsic and Photophysical Properties

The BBS and BBT photophysical properties, including their quenching mechanisms, have been recently studied in solution;[19,20] however, it would also be interesting to study and compare their behaviours in the solid-state (in polymeric films). Table VI.1 shows the BBT and BBS intrinsic and photophysical properties measured in solution as well as in PBS and PLA films.

Table VI.1. Spectroscopic data measured in solution and in polymeric films at 378 and 374 nm for BBT and BBS, respectively.

	λ_{fl} [a] (nm)	λ [b] (%)	ϕ_{fl} [c]	τ [d] (ns)
BBS-TCE-0.2 mM	434	—	0.92	1
PBS-BBS-0.01 wt.%	432	0	0.89	1
PBS-BBS-0.15 wt.%	500	0	0.54	1 ; 10
	434	80	0.65	1 ; 10
	434	260	0.72	1 ; 11
PBS-BBS-0.2 wt.%	500	0	0.51	1 ; 9
PLA-BBS-0.01 wt.%	428	0	0.91	1
PLA-BBS-0.2 wt.%	490	0	0.58	1 ; 11
BBT-TCE-0.2 mM	440	-	0.91	1
PBS-BBT-0.01 wt %	435	0	0.74	1
PBS-BBT-2 wt %	442	0	0.68	1
	441	120	0.65	1
	440	270	0.64	1
PBS-BBT-6 wt %	446	0	0.62	1
PLA-BBT-0.01 wt %	429	0	0.76	1
PLA-BBT-2 wt %	434	0	0.71	1

[a] Maximum fluorescence wavelength. [b] Actual local strain measured by ink displacement. [c] Absolute quantum yields calculated with an integrating sphere. [d] Fluorescence lifetime.

In TCE, BBS exhibits an absorption maximum wavelength at 374 nm and an emission maximum wavelength at 434 nm at 0.2 mM. This emission wavelength is similar

to those found in either PBS or PLA films with a low BBS concentration of 0.01 wt %. However, according to Table VI.1, the BBS maximum fluorescence wavelength changes by increasing its concentration due to excimer formation in BBS-containing films. Indeed, increasing the BBS concentration from 0.01 to 0.2 wt % in PBS or to 2 wt % in PLA triggers a bathochromic shift of about 70 nm of the emission maximum wavelength, which shifts from 432 to 500 nm in PBS, and from 428 to 490 nm in PLA. The presence of BBS excimers may be confirmed by following the fluorescence lifetime decay after excitation, which is the average time that a molecule spends in the excited state before emitting a photon, and which is expressed in mathematical terms by Equation VI.1.

$$R(t) = A + B_1 e^{(-t/\tau_1)} + B_2 e^{(-t/\tau_2)} \quad \text{(VI.1)}$$

where *R(t)* is the response of the sample to an infinitely short excitation, B_i the pre-exponential factors, τ_i the characteristic lifetimes, t the time, and A an additional background term. In this paper, the fluorescence decay results are fitted with equations containing one up to four parameters. BBS was found to exhibit a monoexponential lifetime of 1 ns in solution and in polymeric films (PLA and PBS) at a low concentration of 0.01 wt %.

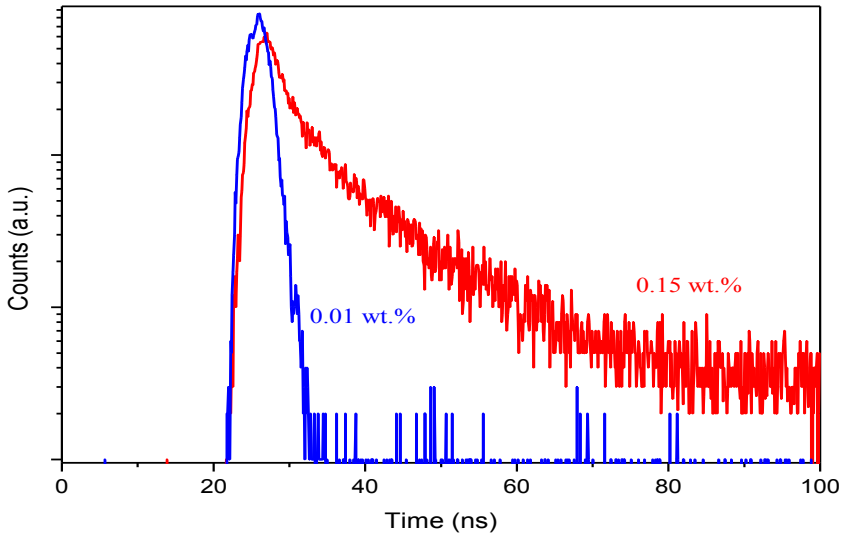

Figure VI.3. Fluorescence decay of PBS-BBS-0.01 wt % (—) and 0.15 wt % (—) films as a function of time at ambient temperature at λ_{exc} = 374 nm and λ_{em} = 500 nm.

Figure VI.3 shows the fluorescence decays of the PBS-BBS films containing 0.01 and 0.15 wt % as a function of time. A single parameter is sufficient to fit the fluorescence decay of the sample with 0.01 wt %, showing the presence of only one fluorescent component, namely the BBS chromophores that are molecularly dispersed in the polymer matrix and that exhibit a lifetime of 1 ns. On the other hand, by increasing the BBS concentration to 0.15 wt % in PBS films, the fluorescence decay fitting requires two parameters, indicating the presence of two species with different lifetimes, corresponding to a mixture of molecularly dispersed BBS chromophores defined by a short lifetime of 1 ns, and excimers characterized by a longer lifetime of around 10 ns. Indeed, excimers show long radiative lifetimes, due to the symmetry forbidden nature of the transition.[21]

Moreover, in this multi-component system, the concentration ratio of monomers can be determined by using Equation VI.2, which uses the B_i pre-exponential factors of Equation VI.1.

$$C_i = \frac{B_i}{B_1 + B_2} \quad \text{(VI.2)}$$

$$\varphi_i = \frac{B_i\,\tau_i}{B_1\,\tau_1 + B_2\,\tau_2} \quad \text{(VI.3)}$$

$$\langle\tau\rangle = \frac{B_1\,\tau_1^2 + B_2\,\tau_2^2}{B_1\,\tau_1 + B_2\,\tau_2} \quad \text{(VI.4)}$$

According to Equation VI.2, the concentration ratio of monomers goes from 100 to 87% for the PBS-BBS films containing 0.01 and 0.15 wt % of BBS, respectively. From Equation VI.3, the excimer relative fluorescence intensity φ_i goes from 0 to 57% for these films with an average lifetime of the entire decay process $\langle\tau\rangle$ that shifts from 1 to 7 ns, according to Equation VI.4. Therefore, the BBS molecular arrangement can easily be followed by measuring the fluorescence lifetime.

Relative actinometry was previously used to measure the fluorescence quantum yields. However, it is an imprecise method that leads to quantum yields that can be known to within 80% accuracy at best[22] and requires similar emission yields and comparable absorption and emission wavelengths for both the sample and the actinometer, which is a reference for which the quantum yield is accurately known.[23] The BBS fluorescence quantum yield was previously determined by this method relative to quinine sulphate, which exhibits a quantum yield of 0.54, leading to quantum yields of 0.2, 0.42 and 0.3 for PBS-BBS films containing, respectively, 0.02, 0.1 and 0.2 wt %.[11] In this paper, absolute and accurate quantum yields were measured with an integrating sphere.[24]

According to Table VI.1, it is evident that BBS exhibits high quantum yields on the order of 0.9 in solution and in PLA or PBS films at 0.01 wt %. However, the quantum yield decreases to 0.54 and 0.51 by increasing the BBS concentration to 0.15 and 0.2 wt % in PBS, respectively, and to 0.58 in PLA at 0.2 wt % due to excimer formation. The fluorescence quantum yield was found to increase by stretching the PBS-BBS-0.15 wt % films from 0.54 to 0.65 and 0.72 for actual local strains of 0, 80 and 260%, respectively. This result confirms the breakage of the BBS excimers and the prevalence of monomers

emission, thus proving the close relationship between the excimer formation and fluorescence lifetime.

On the other hand, BBT exhibits an absorption maximum wavelength at 378 nm and an emission maximum wavelength at 440 nm at 0.2 mM in TCE. The emission features of the PBS-BBT and PLA-BBT blends are quite similar with almost no shift of the emission maximum wavelength even by increasing the BBT concentration from 0.02 to 6 wt % in PBS or to 2 wt % in PLA since the aggregate formation happens even at low concentrations as shown previously.[142] Moreover, unlike BBS, BBT exhibits a monoexponential lifetime of the order of 1 ns specific to isolated BBT molecules, independently of the BBT concentration, state and actual local strain, showing neither excimer formation nor color change. However, a common point with BBS is the strong fluorescence of BBT with a fluorescence quantum yield of 0.91 in TCE, and of the order of 0.6 ─ 0.8 in PLA and PBS films, whatever the BBT concentration (≤ 6 wt %) and the actual local strain. The small decrease of the quantum yield, shown while going from solution to the solid-state, is essentially due to the increase of the π─π intermolecular interactions in polymeric films, and to the hindering of the molecular rotations and vibrations that are present in solution.

The difference in behaviour between the two fluorophores is mainly attributed to their molecular shape. Indeed, the BBS planar conformation in the solid state and the π─π stacking interactions enable the sandwich-type structures, and thus the excimer formation.[17] On the other hand, the BBT unsymmetrical bow-shaped form, due to the thiophene 2,5-disubstitution, as well as the presence of the cumbersome *t*-butyl end groups limit the whole molecule planarity and minimize the intermolecular interactions since the π─stacked molecules overlap at a perpendicular distance of 4.21(1) Å,[19] which does not allow excimer formation.

Time-Temperature Effect

The excimer formation shown by increasing the BBS concentration and proved by a clear color change as well as the BBS high quantum yield in solution and in polymeric films motivate a further study as a function of different parameters such as time and

temperature in order to exploit these coveted features for a probable use as a molecular probe. This study is pivotal since it has been previously shown that BBS may act as a temperature probe in PBS,[11] but not in PLA.[25] The difference of behavior between these two polymers, moreover polyesters, motivates a deeper study of the stilbene derivative comportment in PLA after confirmation of the results obtained in PBS.

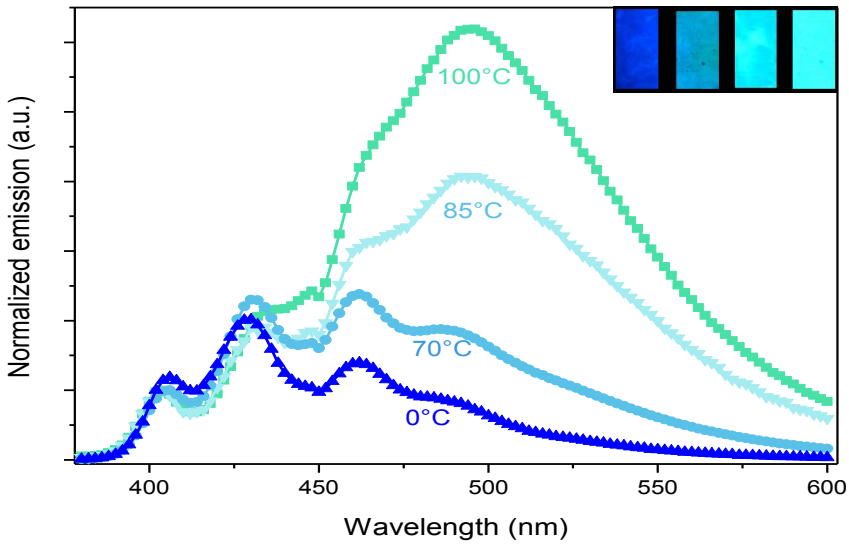

Figure VI.4. Fluorescence spectra of PLA-BBS-0.5 wt % taken at different temperatures (■: 100 °C; ▼: 85 °C; ●: 70 °C; ▲: 0 °C) after quenching at 0 °C (λ_{exc} = 374 nm). Inset: Pictures of films heated to the same temperatures from 0 to 100 °C (left to right).

Figure VI.4 shows the fluorescence spectra of PLA-BBS-0.5 wt % at different temperatures. By quenching the film at 0 °C, the emission spectrum mainly exhibits the three peaks belonging to BBS monomers. However, by increasing the annealing temperature, the excimer band at 490 nm considerably increases until becoming more intense than the peaks specific to the molecularly dispersed chromophores, leading to a huge increase of the I_E/I_{M1} ratio from 0.8 to 6.1. Figure VI.4 inset shows that this ratio variation is accompanied by a clear color change from blue to green, thus mentioning a transfer from monomers to excimers, proving the particular sensitivity of BBS excimers to

thermal stress and, therefore, confirming the opportunity of using the BBS molecule as a molecular probe of temperature in PLA and PBS in particular, and probably in polyesters in general. A similar behaviour has been previously reported for luminescent oligo(p-phenylene vinylene) and other chromophores.[7,8,11,14-16]

It has been previously reported that the PLA-BBS matrix is not sensitive to temperature and exhibits the monomeric features even after annealing at a temperature above the PLA's Tg.[25] This conclusion seems to be hasty since it was drawn for a PLA film containing up to 0.07 wt %, which remains quite low for allowing BBS excimers formation and insufficient to conclude about the BBS behavior as a function of its concentration since no film with higher BBS concentrations have been investigated.[25]

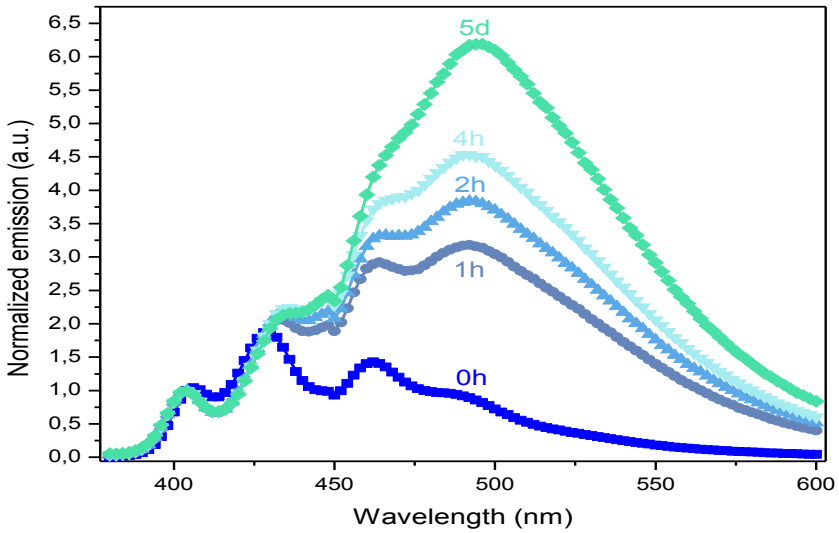

Figure VI.5. Fluorescence spectra of the PLA-BBS-0.5 wt % film at different annealing times at 100 °C and at λ_{exc} = 374 nm.

Figure VI.5 shows the fluorescence spectra of the PLA-BBS-0.5 wt % films after different annealing times at 100 °C. After quenching the sample at 0 °C, the emission spectrum initially (0 h) shows the BBS monomeric features with three well-defined peaks. However, the annealing at 100 °C induces a variation of the peak intensity as a function of

time. Indeed, after only 1 h of annealing, the band at 500 nm increases considerably and becomes even more intense than the original peaks belonging to isolated molecules, leading to an increase of the I_E/I_{M1} ratio from 0.91 to 3.18. This band intensity continues increasing with time until reaching a ratio of 4.5 after 4 h and 6.2 after 24 h, indicating a self-assembly of the BBS molecules, which were initially kinetically trapped upon rapid quenching after melt-processing into excimers, confirmed by a color change from blue to green. The process was found to be very rapid at the beginning since the major part of the molecularly dispersed BBS chromophores is transformed in excimers during the first hour. The value of the I_E/I_{M1} ratio reached 24 h after quenching is similar to that of the freshly prepared and not quenched film. Moreover, a similar value of around 6.1 for the I_E/I_{M1} ratio is obtained after either 24 h at ambient temperature or at 100 °C after quenching. The same phenomenon occurs in PBS-BBS films containing a concentration ≥ 0.1 wt %. However, there is no variation of the I_E/I_{M1} ratio in PLA and PBS films containing 0.01-0.05 wt % neither with temperature nor with time since they do not allow excimer formation due to the very low BBS concentration.

The time effect has been studied at different temperatures above the glass transition temperature of the polymer matrix, i.e. at 70, 85 and 100 °C in PLA films, and at 40, 60 and 80 °C in PBS films. In order to follow the monomer to excimer conversion with the annealing time, the variation of the PLA crystallinity was measured by differential scanning calorimetry (DSC) according to Equation VI.5.

$$\chi = \frac{\Delta H_m}{\Delta H_m^0} \times 100 \qquad \text{(VI.5)}$$

where ΔH_m is the measured melting enthalpy (J/g) and ΔH_m^0 is the melting enthalpy of the perfect PLA crystal (93.1 J/g).[26,27]

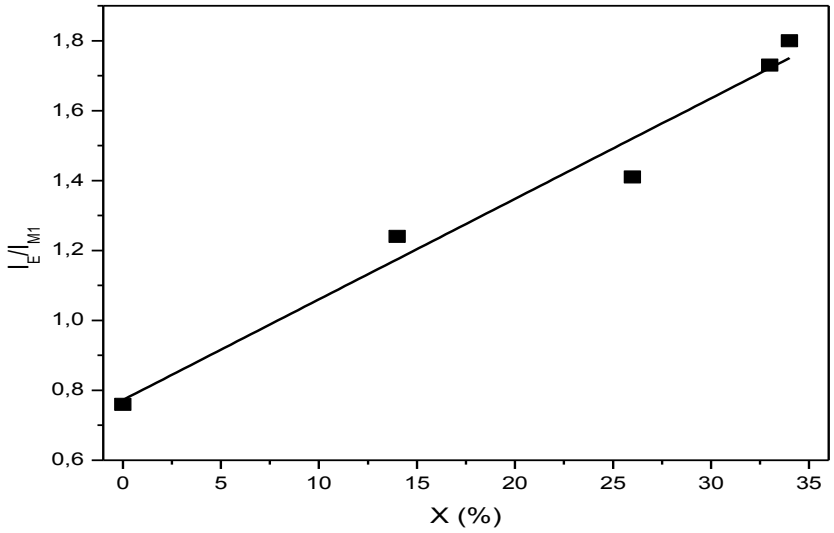

Figure VI.6. Variation of the I_E/I_{M1} ratio of PLA-BBS-0.5 wt % films as a function of DSC crystallinity after annealing at 70 °C.

The BBS molecular dispersion obtained upon quenching at 0 °C whatever the BBS concentration is favoured by the zero DSC crystallinity of the polymer matrix prior to annealing. Figure VI.6 shows the variation of the I_E/I_{M1} ratio of the PLA-BBS-0.05 wt % film as a function of crystallinity for different annealing times at 70 °C, resulting in a good concordance between both parameters. Indeed, a similar behaviour is obtained for the I_E/I_{M1} ratio and crystallinity with time, inducing a gradual increase of both parameters until reaching a plateau. Indeed, the crystallinity goes from 0% at 0 min to 34% after 120 h, while the I_E/I_{M1} ratio goes from 0.76 to 1.8 for the same range of time. The same phenomenon occurs in BBS-containing PBS films where the crystallinity is 30 times higher at the end of the process than before annealing. Moreover, crystallinity reached at high temperatures (close to the PBS crystallization temperature) is much higher than that at lower temperatures. Indeed, for PBS-BBS-0.05 wt % films, the DSC crystallinity reached after 48 h was around 3 times higher at 80 °C than at 40 °C, which is similar to what was observed for PLA-BBS-0.05 wt % while comparing data collected at 100 and 70 °C. This crystallinity increase as a function of temperature, confirmed by DSC, forces the dye

molecules to crowd into the amorphous part whose percentage decreases as a function of the annealing temperature, thus explaining the significant increase of the I_E/I_{M1} ratio as a function of the annealing temperature and as a function of time. These outcomes reveal the importance of the crystallinity of the polymeric blends during excimer formation.

The phase separation kinetics was studied by following the variation of the I_E/I_{M1} ratio as a function of time and temperature. For this study, the results found for PLA-BBS-0.5 wt % and PBS-BBS-0.1 wt % films after annealing during various times at different temperatures between the T_g and the onset of the crystallization peak of the blend determined by DSC experiments are shown in Figure VI.7.

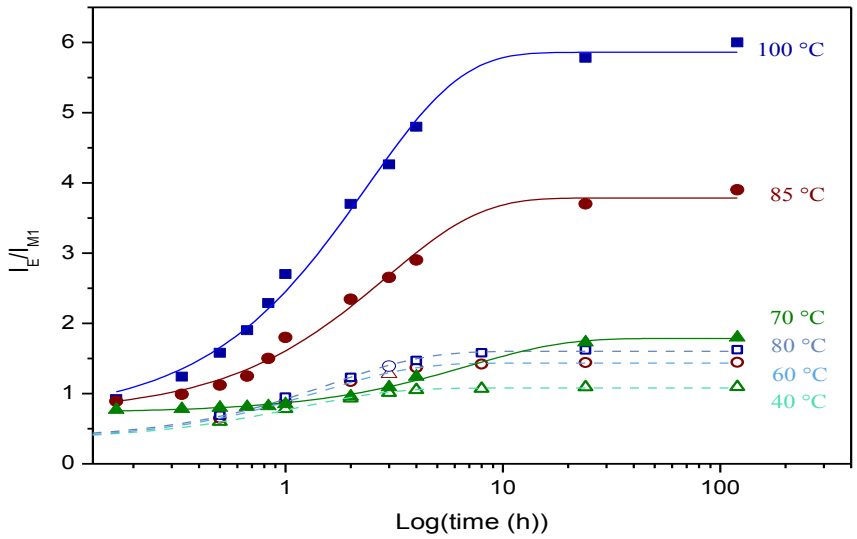

Figure VI.7. Variation of the I_E/I_{M1} ratio of PLA-BBS-0.5 wt % (solid lines) and PBS-BBS-0.05 wt % (dashed lines) films as a function of the annealing time and temperature.

Figure VI.7 shows a similar general behavior for PLA-BBS-0.5 wt % and PBS-BBS-0.05 wt % whatever the annealing temperature. Indeed, by annealing the BBS-containing films at a temperature above the blend T_g, the I_E/I_{M1} ratio increases continuously with the annealing time until reaching a maximum value, which increases by increasing the BBS concentration and/or temperature. Indeed, at 0.5 wt % of BBS, the plateau appears

after around 24 hours whatever the temperature. After annealing at 100 °C of PLA-BBS-0.5 wt %, the I_E/I_{M1} ratio reaches a maximum value of 5.9, which is much higher than that obtained at 85 or 70 °C, i.e. 3.8 and 1.8, respectively, showing that annealing at high temperatures induces a much important tendency to excimer formation. The plateau is also higher by increasing the fluorophore concentration with a maximum value of 1.6 and 5.8 for PBS films containing 0.05 and 0.2 wt %, respectively, after 24 h of annealing at 80 °C. These results show that the BBS chromophore may be used as a time-temperature indicator (TTI) in PLA and PBS films and probably in all polyesters. The plateau is also higher by increasing the fluorophore concentration with a maximum value of 1.6 and 5.8 for PBS films containing 0.05 and 0.2 wt %, respectively, after 24 h of annealing at 80 °C. These results show that the BBS chromophore may be used as a time-temperature indicator (TTI) in PLA and PBS films, and probably in all polyesters. The kinetics of such approach follows an Arrhenius-type behavior, as previously shown for similar blends.[11,14-16,28]

The increase of the I_E/I_{M1} ratio with time and temperature after quenching may be related to several parameters such as an increase of the matrix crystallinity by adding BBS, especially at high concentrations, inducing a decrease of the dyes' translational mobility and leading to an increase of the $I_{E\infty}/I_{M1\infty}$ ratio, as well as of the pre-exponential factor B_2 when compared with B_1, which is consistent with an increase of the extent of excimer formation.

It should be noted that the maximum value of the I_E/I_{M1} ratio is similar to that of an unquenched film and that the plateau is obtained at a same value in PLA-BBS-0.5 wt % and PBS-BBS-0.2 wt % films, confirming the better solubility of BBS in PLA. In contrast to the changes shown above, it was found that PBS or PLA films containing 0.01 up to 6 wt % of BBT show no change even after annealing at high temperatures, thus confirming that the BBT molecule cannot act as a time-temperature molecular probe, unlike the BBS dye.

VI.4. Conclusions

The intrinsic and photophysical properties of BBS and BBT have been investigated in solution and in the solid state by fluorescence spectroscopy. When dispersed in PBS or

in PLA films, BBS is dispersed as isolated molecules at low concentration. However, at high concentrations, the BBS molecules are dispersed as monomers and as excimers with a corresponding lifetime of 1 and 10 ns, respectively. These excimers are induced by strong and short π-π intermolecular interactions and their formation is accompanied by a color change from blue to green.

BBS was found to exhibit strong absolute quantum yields, accurately measured with an integrating sphere for the first time, both in solution and in polymeric films at low concentrations. Nevertheless, the increase of the BBS concentration decreases the fluorescence quantum yield, while the mechanical deformation of the BBS-containing films triggers the opposite phenomenon due to the breakage of the BBS excimers and the prevalence of the isolated molecules. A better solubility of BBS into PLA has been observed when compared with PBS, due probably to stronger interactions.

Actually, it has been demonstrated for the first time that the dispersion of the BBS fluorophore into PLA quenched films induces an excimer formation by increasing the annealing temperature or time. This approach may probably be generalized to the polyesters in general, allowing its use as a time-temperature indicator and providing a broad opportunity for the creation of a wide variety of smart polymers with self-assessing capabilities. This tendency is related to an increase of the polymer crystallinity upon annealing, while the excimers formation strongly depends on the molecular shape since the bow-shaped BBT fluorophore does not form excimers, thus showing a high and an almost unchanged quantum yield independently of concentration, time, temperature and host polymer stretching, making it appropriate for different kinds of applications.

Acknowledgements

The authors gratefully acknowledge financial support from the Natural Sciences and Engineering Research Council of Canada, the Fonds Québécois de la Recherche sur la Nature et les Technologies, the Canadian Foundation for Innovation, NanoQuébec and the Centre for Self-Assembled Chemical Structures. AF thanks the Tunisian Government for a scholarship of excellence.

References

(1) Bischoff, P.; Hutter, C.; Puebla, C.; E.P. 1294846, **2001**.

(2) Bur, A. J.; Roth, S. C. *Polym. Eng. Sci.* **2004**, *44*, 898.

(3) Jervis, D. A. *Plast. Addit. Compd.* **2003**, *5*, 42.

(4) Ward, I. M. *Structure and Properties of Oriented Polymers*; Applied Science Publishers: London, **1975**.

(5) Fourati, M. A.; Pellerin, C.P.; Bazuin, C. G.; Prud'homme, R. E. *Polymer*, **2013**, *54*, 730.

(6) Crenshaw, B. R.; Weder, C. *Chem. Mater.* **2003**, *15*, 4717.

(7) Crenshaw, B. R.; Weder, C. *Adv. Mater.* **2005**, *17*, 1471.

(8) Donati, F.; Pucci, A.; Boggioni, L.; Tritto, I.; Ruggeri, G. *Macromol. Chem. Phys.* **2009**, *210*, 728.

(9) Donati, F.; Pucci, A.; Cappelli, C.; Mennucci, B.; Ruggeri, G. *J. Phys. Chem. B* **2008**, *112*, 3668.

(10) Pucci, A.; Bertoldo, M.; Bronco, S. *Macromol. Rapid Commun.* **2005**, *26*, 1043.

(11) Pucci, A.; Di Cuia, F.; Signori, F.; Ruggeri, G. *J. Mater. Chem.* **2007**, 17, 783.

(12) Pucci, A.; Biver, T.; Ruggeri, G.; Itzel Meza, L.; Pang, Y. *Polymer* **2005**, *46*, 11198.

(13) Crenshaw, B. R.; Burnworth, M.; Khariwala, D.; Hiltner, A.; Mather, P. T.; Simha, R.; Weder, C. *Macromolecules* **2007**, *40*, 2400.

(14) Crenshaw, B. R.; Kunzelman, J.; Sing, C. E.; Ander, C.; Weder, C. *Macromol. Chem. Phys. Chem.* **2007**, *208*, 572.

(15) Kinami, M.; Crenshaw, B. R.; Weder, C. *Chem. Mater.* **2006**, *18*, 946.

(16) Sing, C. E.; Kunzelman, J.; Weder, C. *J. Mater. Chem.* **2009**, *19*, 104.

(17) Fourati, M. A.; Maris, T.; Bazuin, C. G.; Prud'homme, R. E. *Acta Crystallogr., Sect. C: Cryst. Struct. Commun.* **2010**, *66*, o11.

(18) Gilbert, A.; Baggott, J. *Essentials of Molecular Photochemistry*; Blackwell Scientific Publications: Oxford, **1991**.

(19) Fourati, M. A.; Maris, T.; Skene, W. G.; Bazuin, C. G.; Prud'homme, R. E. *J. Phys. Chem. B* **2011**, 115, 12362.

(20) Fourati, M. A.; Skene, W. G.; Bazuin, C. G.; Prud'homme, R. E. Submitted to *J. Phys. Chem. B* **2012**.

(21) van Hutten, P. F.; Krasnikov, V. V.; Brouwer, H. J.; Hadziioannou, G. *Chem. Phys.* **1999**, *241*, 139.

(22) Karstens, T.; Kobs, K. *J. Phys. Chem.* **1980**, *84*, 1871.

(23) Khun, H. J.; Braslavsky, S. E.; Schmidt, R. *Pure Appl. Chem.* **2004**, *76*, 2105.

(24) Bolduc, A.; Dufresne, S.; Hanan, G. S.; Skene, W. G. *Can. J. Chem.* **2010**, *88*, 236.

(25) Pucci, A.; Signori, F.; Bizzarri, R.; Bronco, S.; Ruggeri, G.; Ciardelli, F. *J. Mater. Chem.* **2010**, *20*, 5843.

(26) Shaw, M. T.; MacKnight, W. J. *Introduction to polymer viscoelasticity*; John Wiley & Sons: New Jersey, **2005**.

(27) Tsuji, H.; Ikada, Y. *J. Polym. Sci. Part A: Polym. Chem.* **1998**, *36*, 59.

CHAPITRE VII: Conclusions et perspectives

Les deux fluorophores BBS et BBT ont été souvent employés dans diverses applications sans toutefois aucune investigation approfondie de leurs propriétés intrinsèques que ce soit en solution ou à l'état solide. Dans le même ordre d'idée, la conséquence de l'incorporation de ces chromophores à des matrices polymères, de surcroît biodégradables, est d'autant plus intriguant que très peu d'études se sont intéressées à l'orientation des petites molécules dichroïques et à l'effet engendré sur le comportement et l'aptitude à s'orienter de la macromolécule hôte. La forme moléculaire différente des chromophores motive une investigation approfondie et laisse présager des comportements et des arrangements moléculaires différents dont une probable tendance à former des excimères ou des agrégats dans les films polymères afin de viser des applications technologiques novatrices permettant de combiner les propriétés optiques des fluorophores et les propriétés mécaniques de la macromolécule.

VII.1. Propriétés du BBT et du BBS en solution

Les fluorophores BBS et BBT présentent des propriétés optiques et fluorescentes qui ont conduit à leur utilisation dans divers domaines.[1-20] Cependant, comme toute molécule fluorescente, une désactivation de leur aptitude à fluorescer fortement peut avoir lieu dans certaines circonstances. De ce fait, une investigation approfondie de leurs propriétés intrinsèques, englobant leurs caractéristiques fluorescentes, photophysiques, électrochimiques et cristallographiques est indispensable afin d'optimiser leur utilisation.

Dans un premier temps, nous avons étudié et confirmé les caractéristiques spectroscopiques d'émission et d'absorption de BBS et de BBT en solution et à l'état solide par spectroscopie de fluorescence et spectroscopie UV-visible. Les propriétés photophysiques en général, et fluorescentes en particulier, ont été investiguées dans plusieurs solvants dans le cas du BBT qui présente une solubilité élevée en solution, et seulement dans le tétrachloroéthane (TCE) dans le cas du BBS suite à sa faible solubilité

même après chauffage, exclusivement dans les solvants chlorés à températures d'ébullition élevées. Le TCE a ainsi été utilisé afin de comparer les caractéristiques d'absorbance et d'émission des deux chromophores, qui s'avèrent très semblables.

La caractéristique la plus importante de ces fluorophores est leur aptitude à fluorescer, qui peut être quantifiée à travers des mesures de leurs rendements quantiques de fluorescence. Habituellement, celles-ci sont effectuées par actinométrie relative, entraînant une erreur très élevée sur les valeurs mesurées.[21] Des mesures absolues et plus précises des rendements quantiques de fluorescence des deux fluorophores ont été conduites pour la première fois en solution et à l'état solide à travers l'utilisation d'une sphère d'intégration, diminuant considérablement l'erreur sur la valeur obtenue.[3] Une valeur de 0,9 a été obtenue pour le BBS dans le TCE, alors que des valeurs également élevées de l'ordre de 0,7─0,9 ont été obtenues pour différentes concentrations de BBT dans divers solvants de différentes polarités et proticités. Ces valeurs prouvent la possibilité d'utilisation du BBT comme un substitut approprié pour les fluorophores classiques, tels que le BBS, facilité par leurs similitudes du point de vue spectroscopique et sa meilleure solubilité en contraste avec le BBS. BBT pourrait également être employé comme une référence appropriée pour des études de fluorescence par actinométrie ou comme indicateur coloré grâce à sa couleur verte nettement plus facile à détecter que la couleur jaune du BBS.

En résumé, une investigation des propriétés intrinsèques, en général, des fluorophores BBS et BBT et de leurs propriétés photophysiques, en particulier, a été réalisée pour la première fois.

Malgré les rendements quantiques élevés de fluorescence du BBS et du BBT, les valeurs obtenues demeurent inférieures à l'unité, indiquant la présence de processus de désactivation supplémentaires autres que la fluorescence, tels que par croisement intersystème (CIS) et/ou par conversion interne (CI). L'investigation des propriétés photophysiques des deux fluorophores a été étudiée pour la première fois dans cette thèse, et est d'un intérêt particulier afin de prévenir les moyens de désactivation de leur premier atout, à savoir la fluorescence. Le principe de conservation de l'énergie a permis d'évaluer la désactivation de l'état singulet par CIS vers l'état triplet comme étant négligeable pour le BBS et de l'ordre de 16% pour le BBT, ce qui implique un rendement quantique par CI de

l'ordre de 10% pour le BBS suite à une photoisomérization *trans-cis* et de 9% pour le BBT suite à la dissipation d'énergie probablement via la liaison thiophène-oxazole.

Contrairement à la molécule de BBT, la molécule de BBS présente une double liaison vinylique centrale conjuguée aux groupements phényles avoisinants, lui conférant une tendance à isomériser. À faible concentration (5 µg/mL), l'absorbance à 374 nm, spécifique à l'espèce *trans* du BBS, diminue de façon rapide et irréversible, alors que l'absorbance à 308 nm augmente, prouvant la formation du monomère *cis* pour la première fois. Dans le cas d'une solution de BBS fortement concentrée (0.2 mg/mL), l'irradiation prolongée à l'UV entraîne la photoisomérisation *trans-cis* suivie de la disparition progressive des deux isomères, en plus de la présence d'un processus secondaire aboutissant à une nouvelle molécule de plus petite taille. Cette dernière est un aldéhyde obtenu par photoclivage du BBS, qui s'oxyde à son tour afin de donner le 4-(1,3-benzoxazol-2-yle)acide benzoïque (BBA) dont l'identité a été déterminée par DRX. La cinétique du processus de formation de cette nouvelle molécule a été démontrée comme dépendant de la concentration de BBS en solution avec une vitesse rapide à forte concentration et lente à faible concentration.

Afin d'élargir le champ d'applications des fluorophores BBS et BBT, leurs propriétés électrochimiques ont été étudiées par voltampérométrie cyclique dans le but de sonder leurs propriétés redox et d'obtenir des informations importantes relatives à leurs stabilités à des températures élevées. Cette étude a dévoilé la présence d'un procédé d'oxydation impliquant un électron pour le BBT et le BBS, prouvant un comportement similaire de dopage de type p. Les résultats d'oxydation obtenus par voltampérométrie cyclique montrent un comportement irréversible pour les deux chromophores indépendamment de la vitesse de balayage, indiquant la présence d'un cation radicalaire fortement réactif. Le potentiel élevé d'oxydation de BBT confirme sa stabilité dans les conditions ambiantes. D'autre part, la réversibilité de réduction des deux molécules à faible potentiel confirme leur dopage de type n, dû à la formation d'un anion radicalaire stable, permettant d'améliorer leur utilité comme matériaux fonctionnels grâce à ces propriétés très convoitées.

VII.2. Propriétés du BBT et du BBS dans les films polymères de PLA et de PBS

La molécule de BBS a été proposée dans la littérature comme pouvant servir de sonde moléculaire de température dans le PBS[23] mais pas dans le PLA.[24] La différence de comportement du BBS dans ces deux polymères, de surcroît des polyesters semblables, motive une étude plus approfondie de l'aptitude de la molécule dérivée de stilbène à former des excimères dans le PLA.

Les propriétés d'émission obtenues à faibles concentrations de BBS ou de BBT dans les films polymères PLA ou PBS sont similaires à celles trouvées en solution. Cependant, en augmentant la concentration de ces fluorophores, différents changements spectraux se produisent. En effet, l'augmentation de la concentration de BBT en solution ou dans les films polymères entraîne la diminution de l'intensité du premier pic vibronique et le déplacement bathochromique du second et troisième pic. Ces changements spectraux sont plus prononcés à l'état solide qu'en solution, dû à l'augmentation des interactions intermoléculaires π-π et à l'entrave des rotations moléculaires dans les films polymères. D'autre part, le spectre d'émission de BBS dans les films polymères montre, en plus des trois pics précédemment décrits, une nouvelle bande intense, qui est attribuée à des excimères et qui est accompagnée par un changement de couleur d'émission du bleu au vert, prouvant le passage d'une dispersion moléculaire à une séparation de phases avec des temps de vie de 1 et 10 ns, respectivement, contrairement aux films renfermant le BBT.

Les propriétés cristallographiques des deux fluorophores, non étudiées à ce jour, ont été investiguées par diffraction des rayons X (DRX) afin de comprendre les conditions favorisant les différents changements spectraux. Ces études ont montré une planarité importante des molécules de BBS présentant des interactions d'empilement π–π avec une courte distance centroïde-centroïde de 3,65 (7) Å, facilitant la formation d'excimères sous forme d'escalier et permettant une corrélation entre la structure monocristalline de BBS et la bande émergente aux alentours de 500 nm. D'autre part, les molécules de BBT sont caractérisées par un faible degré de parallélisme, qui s'ajoute à la présence de groupements *t*-butyle encombrants, limitant ainsi l'empilement des molécules de BBT avec une distance de chevauchement de 4,21 (1) Å, empêchant la formation d'excimères dans le cas de BBT mais favorisant la formation d'agrégats induits par l'empilement de molécules voisines, et

ce indépendamment de la concentration, de la longueur d'onde d'excitation et de l'état. Les changements spectraux décelés en fonction de la concentration peuvent être suivis qualitativement via la variation du rapport I_2/I_3, qui est le rapport de l'intensité du second et du troisième pic de fluorescence, permettant ainsi l'utilisation de la molécule de BBT pour sonder sa concentration locale dans un mélange polymère donné et sa solubilité avec une grande sensibilité.

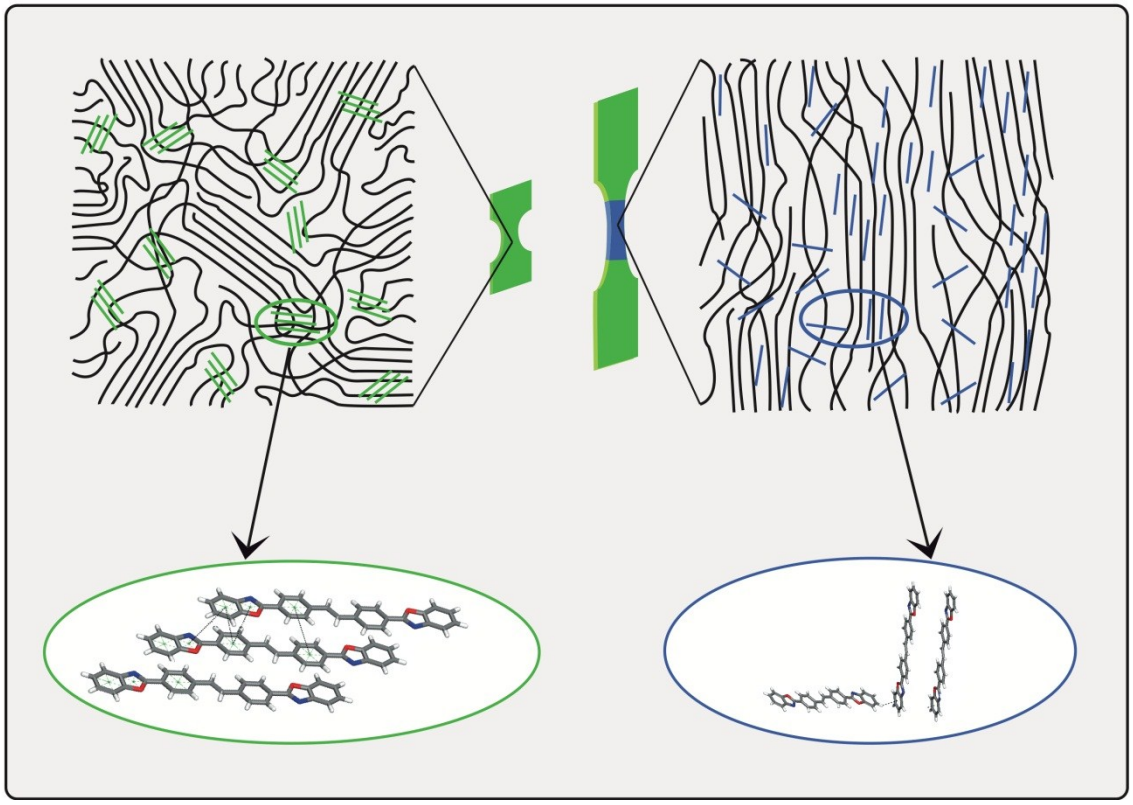

Figure VII.1. Effet de la déformation mécanique sur les chaînes polymères et l'arrangement moléculaire du fluorophore BBS.

Des mesures des rendements quantiques absolus de films polymères renfermant différentes concentrations de BBS ou de BBT ont été réalisées pour la première fois à l'aide d'une sphère d'intégration, résultant en des valeurs élevées de l'ordre de 0,9 dans les films de PLA ou de PBS renfermant 0,01% en poids de BBS, et de l'ordre de 0,6─0,7 indépendamment de l'état et de la concentration de BBT. Par contre, l'augmentation de la

concentration de BBS diminue le rendement quantique de 0,9 à environ 0,6 suite à la formation d'excimères. L'étirement des films PBS-BBS engendre un phénomène inverse après destruction des excimères de BBS. BBS tout comme BBT fluorescent donc fortement en solution ou dans les films polymères et ce indépendamment de leur concentration, motivant ainsi leur utilisation en tant que sondes moléculaires.

La Figure VII.1 montre que la déformation mécanique entraîne l'orientation uniaxe des chaînes polymères, laquelle entraîne à son tour le changement de la luminescence de la partie étirée du film qui passe du vert au bleu, indiquant ainsi la destruction des excimères de BBS et la prédominance de leurs monomères. La possibilité de changer facilement les caractéristiques spectroscopiques et de luminescence des films PBS-BBS orientés et leur grande stabilité au fil du temps peut être intéressante d'un point de vue technologique, comme pour une utilisation potentielle en tant que sonde polymère de déformation mécanique, comme suggéré plus tôt par Pucci et coll.[1,23] L'aptitude de BBS à former des excimères motive également une étude plus approfondie des films polymères renfermant le dérivé du stilbène en fonction de différents paramètres environnementaux.

Après trempe à 0 °C, les films PLA-BBS montrent les caractéristiques des monomères de BBS. Cependant, le recuit de ces films à différentes températures au-dessus de la température de transition vitreuse du polymère ou pour différentes durées de recuit entraîne l'augmentation de l'intensité de la bande des excimères, accompagnée d'un changement de couleur du bleu au vert, jusqu'à l'atteinte d'un maximum qui est de plus en plus élevé quand la température augmente, entraînant un rapport de l'ordre de 6 à 100 °C ou après 24 h. Cet arrangement moléculaire est étroitement lié au taux de cristallinité du film polymère. Ce changement d'émission prouve une sensibilité particulière de la molécule de BBS au stress thermique et au temps ainsi qu'un comportement similaire dans le PBS et le PLA, contrairement aux résultats précédemment rapportés dans la littérature.[24] Le fluorophore BBS peut ainsi être utilisé comme sonde moléculaire de temps et de température dans ces deux polymères en particulier, et probablement dans les polyesters en général.

Les résultats obtenus dans le cas des molécules de BBS et de BBT montrent que les chromophores présentant un ordre à courte distance avec une distance intermoléculaire plus

grande que 4 Å ne sont capables ni de former des excimères ni de changer leurs caractéristiques spectroscopiques. De ce fait, l'investigation par DRX des deux fluorophores ayant des géométries différentes montre que la sélection d'un chromophore destiné à être utilisé comme sonde moléculaire peut s'appuyer sur ses données cristallographiques en général, et sa distance intermoléculaire d'empilement en particulier, qui doit être inférieure à 4 Å afin de permettre l'élaboration d'interactions intermoléculaires π-π suffisamment fortes pour la formation d'excimères.

VII.3. Orientation de PBS et des fluorophores BBT et BBS dispersés dedans

L'orientation des polymères a été largement étudiée que ce soit seuls ou en présence d'un second polymère. Cependant, très peu d'études ont été conduites sur le comportement des polymères en présence d'une petite molécule. Dans cette étude, une augmentation du $<P_2>$ du polymère hôte de 0,36 pour le PBS pur à 0,65 après l'addition de 5% en poids de BBS et à 0,66 après l'ajout de 6% en poids de BBT se produit, résultant essentiellement de l'augmentation du coefficient de friction et de la cristallinité du polymère. En même temps, une augmentation du paramètre d'ordre apparent des chromophores de 0,05 à 0,34 a lieu suite à la destruction des excimères ou agrégats avant l'atteinte d'un plateau. En effet, à de faibles concentrations, le colorant a une orientation réduite avec un paramètre d'ordre apparent inférieur à 0,1 tandis qu'au-dessus de 0,08%, le ratio $<P_2>_{polymère} / S_{colorant}$ est plus grand que 2. Cela signifie que, dans un tel système, la mesure de l'orientation du colorant ne peut pas être considérée comme un moyen pour mesurer l'orientation du polymère, comme cela a été précédemment rapporté dans la littérature. D'autre part, la différence entre le $<P_2>$ du mélange polymère-colorant (PBS-BBS ou PBS-BBT) et le $<P_2>$ du polymère hôte pur permet de déduire le paramètre d'ordre apparent de BBS ou de BBT à une concentration donnée du fluorophore, évitant la nécessité du recours à deux techniques d'analyse différentes.

Finalement, le fait d'allier les propriétés mécaniques et biodégradables de PBS aux propriétés fluorescentes de BBS permet l'augmentation du $<P_2>$ du polymère hôte, mais

également la préparation de sondes de déformation se basant sur la formation d'excimères et le changement de couleur.

VII.4. Perspectives

Malgré la multitude de sujets abordés dans cette thèse, quelques perspectives peuvent être envisagées à ce travail. En effet, il serait intéressant d'élaborer une base de données regroupant les propriétés intrinsèques de divers chromophores afin de faciliter leur sélection selon l'application ciblée, ainsi que d'approfondir la compréhension de la théorie impliquée dans les capteurs en évoquant à la fois la théorie de germination, le modèle de diffusion et la cinétique.

D'autre part, il convient de préciser que très peu d'études se sont penchées sur les mélanges polymère-petite molécule, et il semble judicieux d'investiguer la variation de la taille des agrégats ou des excimères en fonction de la concentration des fluorophores ainsi que le nombre de monomères les constituant afin de comprendre la dépendance et l'augmentation du $<P_2>$ du polymère hôte observées après ajout des petites molécules fluorescentes. Ceci permettra d'élargir l'étude de l'orientation des polymères hôtes après ajout de BBS ou de BBT à d'autres petites molécules en général, et fluorophores en particulier, dans le but de les classer selon leur aptitude à augmenter le $<P_2>$ de la macromolécule de départ et d'élargir leur champ d'application.

Aussi, une voie prometteuse serait d'aborder de nouveaux protocoles de traitement, tel que l'électrofilage de fibres à partir d'une solution de polymère, dotés de propriétés mécaniques pouvant servir comme sonde de déformation, et de colorant, doté de propriétés optiques. Ceci permettrait à la fois de limiter les quantités de matière utilisées et le coût du matériau préparé tout en conférant de nouvelles propriétés à ce dernier et en restant simple dans sa conception.

Afin d'améliorer la solubilité limitée du BBS qui se limite aux solvants chlorés à température d'ébullition élevée, tel que le tétrachloroéthane qui demeure dispendieux et cancérigène, on pourrait apporter des ramifications à la molécule de BBS, sans toutefois entraver les interactions intermoléculaires à l'origine de la formation d'excimères. Cette

modification structurelle peut avoir lieu en incorporant des groupements électro-donneurs ou électro-attracteurs ou encore en agissant sur la conjugaison de la chaîne, ce qui permettrait également d'augmenter la différence entre les longueurs d'onde maximales d'émission des monomères et des excimères, aboutissant ainsi à une détection plus facile du changement de couleur engendré par un stimuli donné.

Dans cette thèse, trois principaux paramètres ont été étudiés : la déformation, le temps et la température. Cependant, il serait intéressant de considérer d'autres stimuli, tels que l'humidité, la pression, la présence de produits chimiques sous forme de liquide ou de vapeur sans oublier les systèmes biologiques. D'autre part, étant donné que les sondes de déformation consistent à exercer une contrainte suffisante afin de détruire les agrégats de colorant, ce phénomène serait facilité par la présence de plus petits agrégats dont la formation pourrait procéder par l'incorporation covalente d'un chromophore aux deux extrémités d'un polymère et l'utilisation d'une assez faible concentration, résultant en de très petits agrégats composés uniquement de deux chromophores. De ce fait, la séparation de phases pourrait aboutir à une destruction optimale des agrégats lors de la déformation, et ce à de très faibles concentrations, diminuant ainsi de manière significative le coût de production de tels matériaux.

D'autres perspectives ressortent de l'ensemble des résultats de cette thèse à propos, notamment, de l'investigation du taux d'agrégation des chromophores BBS et BBT en fonction de la concentration et des paramètres environnementaux. Ces résultats pourraient conduire à élaborer un modèle général permettant de modéliser leur comportement d'agrégation et d'essayer de l'extrapoler et de le généraliser à d'autres molécules fluorescentes dans le but d'élargir encore plus leur exploitation dans divers polymères et conduire à une conception plus rapide des systèmes. Il serait également intéressant de préparer des capteurs basés sur des polymères ayant différentes T_g afin d'offrir une solution à chaque intervalle de température à sonder, d'élaborer des capteurs qui opèrent sur une échelle de temps prolongée de quelques années au lieu de quelques heures, et d'étudier l'effet de vieillissement du polymère sur la cinétique d'agrégation.

Dans cette thèse, les mélanges utilisés étaient composés exclusivement de deux composantes. Il pourrait néanmoins être intriguant d'extrapoler le principe se basant sur la

formation d'excimères à des matériaux comportant une troisième composante qui pourrait influer sur divers paramètres tel que le taux d'agrégation tout dépendamment de sa miscibilité avec le colorant et/ou le polymère, pouvant ainsi aboutir à de nouveaux matériaux fonctionnels.

Références

(1) Pucci, A.; Bertoldo, M.; Bronco, S. *Macromol. Rapid Commun.* **2005**, *26*, 1043.

(2) Pucci, A.; Ruggeri, G.; Bronco, S.; Bertoldo, M.; Cappelli, C.; Ciardelli, F. *Prog. Org. Coat.* **2007**, *58*, 105.

(3) Adachi, C.; Tsutsui, T.; Saito, S. *Appl. Phys. Lett.* **1990**, *56*, 799.

(4) Bischoff, P.; Hutter, C.; Puebla, C.; E.P. 1294846, **2001**.

(5) Bur, A. J.; Roth, S. C. *Polym. Eng. Sci* **2004**, *44*, 898.

(6) Irie, M. *Chem. Rev.* **2000**, *100*, 1685.

(7) Kim, J. S. Seo, B. W.; Gu, H. B. *Synth. Met.*, **2003**, *132*, 285.

(8) Kim, J. S.; Seo, B. W.; Han, E. M.; Gu, H. B. *Mol. Cryst. Liq. Cryst.* **2001**, *370*, 35.

(9) Liu, M.; Guo, B.; Zou, Q.; Du, M.; Jia, D. *Nanotechnology* **2008**, *19*, 205709.

(10) Liu, M. O.; Lin, H. F.; Yang, M. C.; Lai, M. J.; Chang, C. C.; Liu, H. C.; Shiao, P. L.; Chen, I. M.; Chen, J. Y. *Mater. Lett.* **2006**, *60*, 2132.

(11) Momotake, A.; Arai, T. *J. Photochem. Photobiol. C: Photochem., Rev* **2004**, *5*, 1.

(12) Nam, N. P. H.; Cha, S. W.; Kim, B. S.; Choi, D. S.; Jin, J. I. *Synth. Met.* **2002**, *130*, 271.

(13) Sing, C. E.; Kunzelman, J.; Weder, C. *J. Mater. Chem.* **2009**, *19*, 104.

(14) Wang, J.; He, Z.; Mao, H.; Du, Y.; Wang, Y. *J. Lumin.* **2007**, *122-123*, 268.

(15) Ward, I. M. *Structure and Properties of Oriented Polymers*; Applied Science Publishers: London, **1975**.

(16) Yamaguchi, R.; Moriyama, K.; Sato, S. *Mol. Cryst. Liq. Cryst.* **2008**, *488*, 210.

(17) Yang, J.; Gordon, K. C. *Chem. Phys. Lett* **2003**, *375*, 649.

(18) Yang, J.; Gordon, K. C.; Mc Quillan, A. J.; Zidon, Y.; Shapira, Y. *Phys. Rev. B* **2005**, *71*, 155209.

(19) Yang, J. H.; Gordon, K.; Robinson, B. H. *Synth. Met.* **2003**, *137*, 999.

(20) Zhang, R.; Zheng, H.; Shen, J. *Synth. Met.* **1999**, *105*, 49.

(21) Karstens, T.; Kobs, K. *J. Phys. Chem* **1980**, *84*, 1871.

(22) Bolduc, A.; Dufresne, S.; Hanan, G. S.; Skene, W. G. *Can. J. Chem.* **2010**, *88*, 236.

(23) Pucci, A.; Di Cuia, F.; Signori, F.; Ruggeri, G. *J. Mater. Chem.* **2007**, *17*, 783.

(24) Pucci, A.; Signori, F.; Bizzarri, R.; Bronco, S.; Ruggeri, G.; Ciardelli, F. *J. Mater. Chem.* **2010**, *20*, 5843.